

**Wave Transmission in  
Finite Dissipative Nonlinear Periodic Structures**

by

Behrooz Yousefzadeh

M.A.Sc., The University of British Columbia, 2010

B.Sc., University of Tehran, 2008

A THESIS SUBMITTED IN PARTIAL FULFILLMENT  
OF THE REQUIREMENTS FOR THE DEGREE OF

**Doctor of Philosophy**

in

THE FACULTY OF GRADUATE AND POSTDOCTORAL  
STUDIES

(Mechanical Engineering)

The University Of British Columbia  
(Vancouver)

December 2016

© Behrooz Yousefzadeh, 2016

# Abstract

Spatially periodic structures exhibit intriguing dynamic characteristics, contributing to their growing applications as phononic crystals, acoustic metamaterials and lightweight lattice materials. A striking feature, employed in many engineering applications, is their filtering effect, whereby waves can propagate only in specific frequency intervals known as pass bands. Other frequency components (stop bands) are spatially attenuated as they propagate through the structure.

This thesis studies nonlinear wave transmission in periodic structures of finite extent in the presence of dissipative forces and externally induced nonlinear forces. Perfectly periodic structures with identical units are considered, as well as nearly periodic structures with small deviations from periodicity extended throughout the structure.

At high amplitudes of motion, nonlinear forces gain significance, generating qualitatively new dynamic phenomena such as supratransmission. Supratransmission is an instability-driven transmission mechanism that occurs when a periodic structure is driven harmonically at one end with a frequency within its stop band. The ensuing enhanced transmission contrasts the vibration isolation characteristic of the same structure operating in the linear regime.

In the context of engineering applications, three factors play a significant role: dissipative forces, symmetry-breaking imperfections induced by manufacturing constraints (disorder) and the finite size of the structure. This thesis systematically investigates the influence of these parameters on supratransmission in a one-dimensional periodic structure, studying the competition between the effects of dispersion, dissipation, nonlinearity and disorder-borne wave localization (Anderson localization).

We identify the mechanism underlying supratransmission using direct numerical simulations and numerical continuation. Based on this insight, we obtain analytical expressions for the onset of supratransmission for weakly coupled structures using asymptotic analysis. Particularly, we highlight the non-trivial effects of damping on supratransmission in finite structures. We demonstrate that, regardless of the type of nonlinearity, dissipative forces can delay the onset of supratransmission, and high levels of damping can eliminate it.

Given that the spectral contents of transmitted energies fall within the pass band, we expect a competition between supratransmission and Anderson localization. Using direct numerical simulations and continuation techniques, we demonstrate that disorder reduces the transmitted wave energy in the ensemble-average sense. However, the average force threshold required to trigger supratransmission remains unchanged.

# Preface

Parts of the research described in this thesis have been published in peer-reviewed journals and conference proceedings. These publications report work carried out during my Ph.D. research under the supervision of Dr. A. Srikantha Phani. We are the only authors of all the publications and presentations. I was responsible for areas of concept formation, data collection and analysis, and manuscript composition. A.S. Phani was the supervisory author on the entire project and was involved throughout the work in concept formation and manuscript composition.

Portions of Chapters 2 and 3 are published in *Journal of Sound and Vibration* [133]. Parts of the same work, at various stages of completion, were also presented at the following conferences: (i) Conference on Nonlinear Vibrations, Localization and Energy Transfer, June 2014, Istanbul, Turkey; (ii) International Symposium on Optomechatronic Technologies, November 2014, Seattle, WA [132].

A version of Chapter 4 is published in *Journal of Sound and Vibration* [134]. Portions of the same work, at various stages of completion, were also presented at the following conferences: (i) ASME Applied Mechanics and Materials Conference, June 2015, Seattle, WA; (ii) SIAM Conference on Nonlinear Waves and Coherent Structures, August 2016, Philadelphia, PA; (iii) International Congress of Theoretical and Applied Mechanics, August 2016, Montreal, QC.

# Table of Contents

<b>Abstract</b> . . . . .	<b>ii</b>
<b>Preface</b> . . . . .	<b>iv</b>
<b>Table of Contents</b> . . . . .	<b>v</b>
<b>List of Figures</b> . . . . .	<b>viii</b>
<b>1 Introduction</b> . . . . .	<b>1</b>
1.1 Periodic Structures in Engineering . . . . .	1
1.2 Factors Influencing the Dynamic Response of Periodic Structures . . . . .	3
1.3 Energy Transmission in Nonlinear Periodic Structures . . . . .	5
1.3.1 Nonlinear Structures with Exact Periodicity . . . . .	6
1.3.2 Nonlinear Structures with Disorder . . . . .	9
1.4 Research Objectives and Methodology . . . . .	12
1.5 Thesis Outline . . . . .	14
<b>2 Supratransmission</b> . . . . .	<b>16</b>
2.1 A Periodic Structure with Tunable Nonlinearity . . . . .	16
2.1.1 Governing Equations for the Periodic Structure . . . . .	18
2.1.2 Tunability of the Nonlinear Forces . . . . .	20
2.2 Band Structure of Periodic Systems . . . . .	22
2.2.1 Forced Response of Linear Structures . . . . .	22
2.2.2 Free Wave Propagation in Linear and Nonlinear Structures . . . . .	23
2.3 Energy Transmission via Harmonic Excitation within a Stop Band . . . . .	26

2.4	Computing the Supratransmission Threshold . . . . .	33
2.4.1	Nonlinear Response Manifold (NLRM) . . . . .	33
2.4.2	Resonances with the Shifted Pass Band . . . . .	36
2.5	Analytical Prediction of the Onset of Supratransmission . . . . .	38
2.5.1	Analysis Based on Local Nonlinear Dynamics . . . . .	38
2.5.2	Comparison with Numerical Computations . . . . .	41
2.6	Concluding Remarks . . . . .	42
<b>3</b>	<b>Parametric Study . . . . .</b>	<b>44</b>
3.1	Type and Strength of Nonlinearity . . . . .	44
3.2	Number of Units . . . . .	45
3.3	Damping . . . . .	47
3.4	Strength of Coupling . . . . .	52
3.5	Forcing Amplitude: Hysteresis . . . . .	55
3.6	Forcing Frequency . . . . .	56
3.7	Strong Propagation Regime . . . . .	58
3.8	Concluding Remarks . . . . .	59
<b>4</b>	<b>Disorder Effects . . . . .</b>	<b>61</b>
4.1	Disorder-Borne Energy Localization in Linear Structures . . . . .	61
4.1.1	Localization Occurring within a Pass Band . . . . .	63
4.1.2	Quantifying the Degree of Localization . . . . .	64
4.1.3	Influence of Disorder on the Band Structure . . . . .	68
4.2	Combined Effects of Damping and Disorder Near a Pass Band . . . . .	69
4.3	Supratransmission in Disordered Nonlinear Periodic Structures . . . . .	74
4.3.1	Loss of Stability Leads to Enhanced Transmission . . . . .	75
4.3.2	Onset of Transmission Remains Unchanged on Average . . . . .	76
4.3.3	Energy Profiles of Transmitted Waves . . . . .	78
4.3.4	Average Frequency Spectra Above the Threshold . . . . .	79
4.3.5	Prediction of Transmitted Energies Based on Linear Theory . . . . .	82
4.4	Prediction of the Onset of Supratransmission in Disordered Structures . . . . .	83
4.4.1	Analytical Estimate of the Force Threshold . . . . .	83
4.4.2	Dependence of Threshold Curves on Nonlinearity . . . . .	86

4.4.3	Dependence of Locally-Nonlinear Behavior on Coupling .	89
4.5	Concluding Remarks . . . . .	91
<b>5</b>	<b>Conclusion . . . . .</b>	<b>93</b>
5.1	Summary of Contributions . . . . .	94
5.2	Limitations . . . . .	99
5.3	Future Directions . . . . .	101
	<b>Bibliography . . . . .</b>	<b>103</b>
<b>A</b>	<b>Numerical Continuation . . . . .</b>	<b>115</b>
<b>B</b>	<b>Derivations . . . . .</b>	<b>118</b>
B.1	Derivation of the Transfer Matrix Formulation . . . . .	118
B.2	Derivation of the Onset of Supratransmission . . . . .	119

# List of Figures

Figure 2.1	A schematic of the proposed periodic structure . . . . .	17
Figure 2.2	Tunability of the normalized restoring force . . . . .	22
Figure 2.3	Decay exponents for an infinitely long exactly periodic linear structure . . . . .	24
Figure 2.4	Tunability of linear dispersion curves . . . . .	25
Figure 2.5	The supratransmission phenomenon for the hardening system	30
Figure 2.6	The supratransmission phenomenon for the softening system .	31
Figure 2.7	Poincaré maps of the response above the onset of supratransmission . . . . .	32
Figure 2.8	Normalized amplitude profiles above the onset of supratransmission . . . . .	32
Figure 2.9	The NLRM for the structure with softening nonlinearity . . .	34
Figure 2.10	The NLRM and threshold curve for the structure with hardening nonlinearity . . . . .	35
Figure 2.11	Comparison of the threshold curve with the shifted pass band .	37
Figure 2.12	Computed versus predicted threshold curves for a weakly coupled structure . . . . .	42
Figure 3.1	Threshold curves for different values of $N$ (free-free boundary conditions) . . . . .	46
Figure 3.2	Threshold curves for different values of $N$ (fixed-fixed boundary conditions) . . . . .	47
Figure 3.3	Influence of damping on the NLRM in a hardening structure .	48
Figure 3.4	Influence of damping on threshold curves in a hardening structure	50

Figure 3.5	Influence of damping on the onset of supratransmission . . . .	51
Figure 3.6	Influence of the strength of coupling on threshold curves . . .	54
Figure 3.7	The hysteresis phenomenon for the hardening structure . . . .	56
Figure 3.8	Influence of forcing frequency on enhances nonlinear energy transmission . . . . .	57
Figure 4.1	Influence of disorder on response localization within the pass band . . . . .	64
Figure 4.2	Comparison of different decay exponents . . . . .	65
Figure 4.3	Influence of $N$ on the decay exponent . . . . .	67
Figure 4.4	Influence of disorder on spatial localization of mode shapes .	68
Figure 4.5	Influence of disorder on decay exponent and natural frequen- cies of the linear structure . . . . .	69
Figure 4.6	Threshold curve for the hardening ordered structure with $N = 10$	70
Figure 4.7	Influence of damping on supratransmission in the vicinity of a pass band . . . . .	71
Figure 4.8	Influence of damping on the NLRM in the vicinity of a pass band	72
Figure 4.9	Influence of disorder on the NLRM in the vicinity of a pass band	74
Figure 4.10	Influence of disorder on the onset of supratransmission at indi- vidual realizations . . . . .	76
Figure 4.11	Influence of disorder on the supratransmission force threshold	77
Figure 4.12	Influence of disorder on the threshold curve . . . . .	78
Figure 4.13	Average energy profiles below and above the onset of supra- transmission . . . . .	79
Figure 4.14	Average frequency spectra of the driven unit . . . . .	80
Figure 4.15	Average frequency spectra of the end unit . . . . .	80
Figure 4.16	Influence of disorder on normalized transmitted energy ratios .	83
Figure 4.17	The schematics of two adjacent units in a mono-coupled system.	84
Figure 4.18	Dependence of threshold curves on the nonlinear force in a softening structure . . . . .	87
Figure 4.19	Dependence of threshold curves on the nonlinear force in a hardening structure . . . . .	88

Figure 4.20	Dependence of the locally-nonlinear behavior on strength of coupling . . . . .	90
Figure B.1	The schematic of a unit cell . . . . .	118

# Chapter 1

## Introduction

### 1.1 Periodic Structures in Engineering

Any structure with some form of spatial periodicity, either in its constituent material properties, internal micro-architecture or boundary conditions is a periodic structure. In engineering applications, spatially periodic micro-architecture has been utilized in the design of cellular solids to develop *lattice materials* for multifunctional applications, where a mechanical function such as stiffness or strength is combined with some other property such as thermal insulation [33, 130]. Examples include lightweight structural applications with superior thermal insulation or superior impact and blast resistance [120], as well as ultralight materials (density below  $10 \text{ mg/cm}^3$ ) with superior specific stiffness and strength [118].

Spatially periodic structures exhibit intriguing wave transmission characteristics. Of particular interest in many engineering applications are the wave-filtering features of periodic structures in the frequency (temporal) domain and the wavenumber (spatial) domain. In the frequency domain [8], a periodic structure allows selective transmission of waves over certain frequency intervals known as *pass bands*. All other frequency components (belonging to *stop bands*) are spatially attenuated as waves propagate through the periodic structure. This filtering is attributed to *Bragg scattering*, the destructive interference of waves that are periodically scattered as they propagate through the structure. A consequence of this filtering is that vibration energy is localized to the source of excitation in stop bands. In the

wavenumber domain [72], periodic structures exhibit directional wave propagation characteristics. The band-pass filtering property of periodic structures has led to development of mechanical filters in electronics [58] and microelectromechanical systems for radio frequency applications [27]. The directional dependency of wave propagation enables steering and focusing of waves, with applications in energy harvesting [11] among others.

The wave-filtering characteristics and other unique properties of periodic structures, such as negative group velocity, have spurred an array of applications for these structures as *phononic crystals* and *acoustic or elastic metamaterials* – see [19, 24, 76] for recent monographs and reviews on this subject. Phononic crystals are composites with periodically distributed inclusions of high impedance contrast with the matrix (host) material. This periodic configuration allows for manipulation of wave propagation characteristics of the elastic medium, with applications in wave-filtering, wave-guiding and energy harvesting – see [55, 104] for recent reviews on this topic.

Bragg scattering is effective when the wavelength of the incident wave is on the same order as the characteristic spatial periodicity length scale of the structure. Thus, exploiting passive vibration isolation induced by Bragg scattering is challenging at low frequencies. By *low* we denote frequencies below the fundamental resonant frequency of the unit cell under free boundary conditions. This limitation can be overcome by coupling a periodic structure to local resonators and inertial amplifiers [34, 131] to gain additional control over the wave propagation characteristics. The interaction between the host dispersive medium and the dynamic properties of the local resonators allows the possibility to realize sub-Bragg stop bands. Periodic structures featuring the local-resonance mechanism are called acoustic or elastic metamaterials. Examples of such ‘meta’ characteristics include surpassing the mass-law limit of sound transmission [75], albeit in a narrow frequency band, and *cloaking* of acoustic waves [101]. See [20, 42, 79] for recent reviews of some other applications.

There are many other examples of periodic structures in engineering applications. In the context of aerospace structures, a wide body of literature already exists on the dynamic response of periodic structures such as rib-stiffened panels, plates used in the aircraft fuselage and tail, and sandwich panels with periodic

cores [77, 90]. Another example is bladed disk assemblies in turbomachinery, which are periodic structures with cyclic symmetry. Certain features of their vibration characteristics, such as fatigue failure due to mistuning, can be explained based on the dynamics of periodic structures [30, 102].

To conclude this section, we point to the fundamental contributions to waves in periodic structures by condensed matter and solid state physicists, particularly in the context of phonon and electron transport in solids [4, 8], inspired by pioneering works of Rayleigh [111] in the context of vibration response of a string (Melde's experiment) subjected to parametric excitation via variable tension.

## **1.2 Factors Influencing the Dynamic Response of Periodic Structures**

Although periodic structures have been studied extensively in solid-state physics, transfer of that body of knowledge to problems relevant in engineering applications is not a trivial task. As cases in point, the governing equations and boundary conditions in engineering can be different from those in other fields (nonlinear forces, in particular); damping often has a significant contribution in engineering while it is normally absent in solid-state physics; and the typical assumption of infinite systems in solid-state physics is often unrealistic in engineering applications. Accounting for these differences are therefore crucial in making the results directly applicable to engineering structures.

While the ultimate interest in solid-state physics is in three-dimensional systems, engineering problems often provide the luxury of structures in which periodicity is in one or two dimensions only [49]; e.g. bladed disk assemblies in turbomachinery and sandwich structures with periodic cores. Apart from this factor, there are common features among periodic structures relevant in engineering applications that set them apart from their classical counterparts in solid-state physics. These features can be divided into four main categories: (i) energy dissipation, (ii) finite length of the structure (iii) deviations from exact periodicity, and (iv) non-linearity. Qualitatively new phenomena may emerge when one or more of these conditions are present. These deviations often result in localization or confinement of macroscopic deformations or high sensitivity of the structure to changes in

parameters.

**(i) Damping:** Energy dissipation, however small, is *intrinsic* to engineering structures and may have significant influence on the dynamic response of a periodic structure. Addition of dissipative forces to a periodic structure results in a new spatial attenuation mechanism for the traveling waves. For a linear viscous dissipative force, the corresponding decay rate is exponential and uniform, and could influence all frequencies. In addition, dissipative forces (if they are strong enough) can result in appearance of *spatial* stop bands, corresponding to prohibited wavenumbers. For more details on this aspect see [54, 105].

**(ii) Finite length:** In many applications of periodic structures, the number of repeating unit cells is not large enough to warrant an infinite-length approximation. Finite length of a structure produces reflection of waves from its boundaries, leading to formation of standing waves with restricted wavenumbers [119]. The precise dispersive characteristics of finite periodic structures also depend on the type of the boundary conditions (e.g. fixed, guided or free) and can be analysed using phase closure principle [89, 119].

**(iii) Disorder:** Engineered periodic materials and structures possess inherent imperfections imposed by manufacturing constraints. Such small symmetry-breaking imperfections can lead to significant qualitative changes in the *global* dynamic response of the structure under certain conditions. These deviations from exact periodicity could be a result of either *defect* or *disorder*. A defect is normally a large deviation from periodicity that is concentrated at a certain location (or locations) within the structure, such as a crack. In a defective structure, the response localizes to the vicinity of the defect [92], typically enticing further damage to the structure. Disorder usually refers to small deviations from exact periodicity spread throughout the structure, such as the mistuning in a bladed disk assembly. Disorder results in spatial confinement of the dynamic response near the source of excitation, a phenomenon known as *Anderson localization*. This phenomenon is reviewed in more detail in Section 4.1.

**(iv) Nonlinearity:** Nonlinearities arising from large deformations (geometric nonlinearity), constitutive laws of the materials (material nonlinearity), boundary conditions or external forces are important considerations in many engineering applications. In the presence of nonlinearity, mechanical systems often exhibit dra-

matic changes in their response caused by a small change of some parameter or small-amplitude disturbances. Such sudden changes are often accompanied by a large amplitude discontinuity in the dynamic response of the structure, often leading to a rich bifurcation structure. In aerospace engineering, for example, there has been a trend to design slender and lightweight structures to decrease power consumption and increase performance. Accordingly, and from a practical viewpoint, there is an increasing demand for understanding the nonlinear behaviour of these structures and mitigating the corresponding vibration problems [129]. A similar situation exists in steel bridges and large marine structures [95]. In MEMS applications, it is also likely to trigger nonlinear phenomena due to coexistence of more than one source of nonlinearity [113]; for example, many microstructures undergo large deformations due to their high mechanical compliance; parallel-plate electrostatic forces that are very commonly used for actuation and detection are inherently nonlinear; and squeeze-film damping, the most common and dominant damping mechanism, is inherently nonlinear. Accordingly, there has been a recent surge of interest in studying nonlinear (periodic) arrays of micromechanical oscillators [116].

### **1.3 Energy Transmission in Nonlinear Periodic Structures**

This thesis is on energy transmission through nonlinear periodic structures with disorder. When the amplitudes of motion are small enough that nonlinear forces are negligible, wave transmission in periodic structures is dominated by three factors: dispersion, dissipation and disorder. Dispersion is responsible for the band-pass filtering feature of periodic structures, leading to the formation of pass bands and stop bands. If we add damping to a periodic structure, there will be a new attenuation mechanism acting on traveling waves via dissipation of energy. Disorder may lead to confinement of energy to a small spatial region within the structure (Anderson localization). If there is an external force acting in a spatially localized region of the structure, then energy is confined to that region. In contrast to this *point* excitation case, predicting the region of localization is not as straightforward in the *distributed* excitation case, as in base excitation of a structure or

convected boundary layer excitation of an aircraft panel.

Nonlinearities are typically avoided in the design and control of engineering systems. Nevertheless, exploiting the nonlinear response of structures can reveal hidden design opportunities and accommodate bolder design goals. The reason is that qualitatively new phenomena emerge when the requirement of linearity is relaxed. In this section, we review some of the literature pertaining to nonlinear periodic structures with and without disorder.

Throughout the thesis, we distinguish between periodic structures with exact periodicity and those with disorder by referring to them as ordered and disordered structures, respectively.

### 1.3.1 Nonlinear Structures with Exact Periodicity

It has been known for a long time, that localized wave packets (called *solitons*) exist in continuous nonlinear systems [22, 112]. Solitons maintain their shape when traveling at a constant speed, due to the balance between the nonlinear and dispersive properties of the continuum. In addition, when two solitons pass through each other, they retain their shapes and only a phase change occurs between them.

Continuous systems possess translational invariance in all directions, whereas discrete periodic structures are translationally invariant in certain directions only. Solitons cannot propagate in a discrete system due to this lack of an arbitrary translational invariance [31]. On the other hand, discreteness allows the existence of other types of localized waves that do not exist in a continuous system. These localized waves can propagate in a discrete system in the same manner a soliton propagates in a continuum. In contrast to solitons, however, collisions between such excitations result in energy transfer between them, with the more localized excitations gaining energy from the less localized ones [116]. These spatially localized, time-periodic and stable excitations in perfectly periodic, nonlinear, discrete systems are known as *discrete breathers* or *intrinsic localized modes*. Unlike solitons, discrete breathers could be either stationary (“pinned” to a specific spatial location) or mobile (traveling through the structure).

Two requirements are indispensable for discrete breathers to exist in a periodic structure [10]: discreteness and nonlinearity. Discreteness ensures that the

pass bands of the structure are bounded and do not extend to infinity like that of a continuum. Nonlinearity, on the other hand, allows propagating modes to have a fundamental frequency outside the pass bands. Therefore, the frequency of oscillations of discrete breathers lies inside the stop bands of the periodic structure. We emphasize that, strictly speaking, this discussion pertains primarily to the free response of an undamped nonlinear periodic structure.

Discrete breathers have been experimentally observed in many physical systems – see [32] for a detailed review of some applications. When damping forces are present (which is the case in engineering problems), an external harmonic force is required to sustain the discrete breathers in experiments. This is normally achieved through excitation of the base of the structure. As a case in point [25, 116], stationary and moving discrete breathers have been observed in micromechanical cantilever arrays. Such results are very important in paving the way for sensor applications in MEMS devices. Other mechanical experiments with harmonic base excitation include [29, 56, 63, 123, 124].

Discrete breathers provide a route to energy localization in nonlinear periodic structures. They are primarily investigated as either (i) the periodic orbits of an undamped (Hamiltonian) periodic structure or (ii) the limit cycles of a damped periodic structure subject to external harmonic base (uniform) excitation. Apart from these, there are two other classes of problems that are important in nonlinear periodic structures: (iii) pulse propagation and (iv) response to localized harmonic excitation. Although these four problems are intimately related to each other, a direct connection does not exist between them. This is because the principle of superposition does not generally hold in nonlinear systems.

The problem of pulse propagation in nonlinear periodic structures has been a topic of research for a long time. The majority of this literature, originating within the physics community, focuses on conservative and infinitely long systems. In that context, the main goal is to understand the spreading process of initially localized wave packets (an initial value problem); e.g. see [45] for a review of this topic. Within the nonlinear mechanics literature, many of the contributions on this topic are in the context of one-dimensional granular crystals [110]. Nonlinearity in these structures arises from the coupling *contact* forces between adjacent units (*inter-site* nonlinearity). Furthermore, there have been detailed theoretical studies

on the spectral and temporal characteristics of wave packet propagation through these structures [37, 38, 43]. Refer to [55, Section 4.2] for a review of other theoretical studies on nonlinear periodic structures pertaining to phononic structures and materials.

In this thesis, we focus on the problem of nonlinear wave transmission due to external *point* harmonic excitation applied to a single unit of the periodic structure. The starting point in this context is understanding the influence of nonlinearity on the dispersive characteristics of the periodic structure. While the dispersion properties (locations of the pass bands and stop bands) of a periodic structure are fixed in the linear operating regime, they become dependent on the amplitude of motion in the nonlinear regime. This is because nonlinearity makes the resonant frequencies of vibrations dependent on the total energy of the vibrating system, which is often characterized by the amplitudes of motion. As a result, the location and/or width of a pass band may vary based on the amplitudes of motion. This characteristic also depends on the nature of the nonlinear forces. For early works on this topic in the engineering literature refer to [14, 128]. Nonlinearity, therefore, can offer tunable filtering properties and opportunities to enhance the performance of linear periodic structures. See [97] for an example of such a tunable filter and [96] for an extension of this work to a two-dimensional problem. The same concept of amplitude-tunable filtering properties also applies to pass bands produced by local resonators within the unit cell of a periodic structure [74, 83]. This concept can be used in design of acoustic metamaterials with tunable properties.

In the situation where an external harmonic excitation is applied to one unit of a nonlinear periodic structure, nonlinearity offers a route to achieve enhanced energy transmission. This may happen due to instability of periodic solutions through either nonlinear resonances [78] or a saddle-node bifurcation [82, 122]. Nonlinear resonances occur due to internal or combination resonances with the external harmonic excitation [98] and may occur for frequencies inside or outside a pass band. The former mechanism, called *supratransmission*, occurs when the driving frequency lies within a stop band. For small values of the driving force, the amplitudes of motion are small and decay exponentially away from the driven end of the structure; i.e. energy transmission is not possible at low amplitudes of the driving force. When the driving force exceeds a certain threshold, energy transmission

becomes possible even though the forcing frequency remains within the stop band of the periodic structure. Supratransmission was first studied in discrete periodic structures by Geniet and Léon [39, 40].

The nonlinear supratransmission phenomenon emanates from the physics community. Accordingly, the majority of the existing studies on supratransmission consider non-dissipative and infinitely long systems [39, 62, 80, 82, 122]. In comparison, supratransmission in finite dissipative periodic structures have received little attention [16, 51, 61, 66]. Most notably, the hysteresis loops associated with the saddle-node bifurcation at the onset of supratransmission have been explored [51], and devices have been designed based on the sensitivity of the structure near the point of instability [16]. Also, supratransmission has been utilized in a defective granular chain to develop an acoustic switch [7]. Supratransmission has been observed in experiments on macro-scale mechanical systems [40, 51]. Nevertheless, there are no systematic studies on the influence of different system parameters (damping, strength of coupling, type of nonlinearity, etc.) on this phenomenon in finite structures. In particular, there is limited information about the influence of damping and strength of coupling on supratransmission [80, 82]. We note that these studies are purely numerical.

### **1.3.2 Nonlinear Structures with Disorder**

Nonlinearities can be introduced in an otherwise linear system to achieve qualitatively new dynamic phenomena. In this approach, nonlinearity can be regarded as a local disorder (similar to a defect). As a case in point, Cho et al. [18] have intentionally introduced strong stiffness nonlinearity in a microcantilever system by a nanotube coupling. Further, by changing the placement of the nanotube, they have been able to realize coupling forces with either softening or hardening types of nonlinearity. This led to a new tunable broadband resonator design [17].

A very interesting result of adding a single nonlinear attachment to a linear mechanical structure is that the vibration energy of the linear structure can be irreversibly and passively transferred to the nonlinear attachment [115, 127]. Such nonlinear attachments act as local energy sinks and can be used in the design of broadband vibration absorbers. Locating the local nonlinear component in a linear

periodic structure can also have practical significance in structural fault diagnosis [103]; in this context, the appearance of nonlinearity indicates a defect in the periodic structure.

In the examples given above, a single nonlinear element in an otherwise linear periodic structure breaks the periodicity of the entire structure. An opposite configuration is a nonlinear periodic structure with one or more defects [85]. Using the terminology introduced in Section 1.2, either of these configurations results in a defective periodic structure. In contrast, our interest in this work is in the case of a nonlinear periodic structure with disorder: deviations from periodicity spread *throughout* the structure. Within this framework, we are particularly interested in studying the scenarios in which there is a competition between supratransmission and Anderson localization.

Anderson localization manifests its significance within the pass band of the structure. At these frequencies, the (average) response of a disordered periodic structure decays exponentially away from the source of excitation. This is in contrast to the behavior of the same structure in the absence of disorder. This localization can have important consequences for the energies transmitted via the supratransmission mechanism. The reason is that the frequency components of these nonlinearly transmitted waves lie within the linear pass band of the structure [82]. It is therefore natural to expect a competition between nonlinearity and disorder (supratransmission and Anderson localization) with regards to the transmitted energies above the supratransmission threshold.

There is a myriad of papers on the interplay between nonlinearity and disorder in periodic structures. The majority of this literature, similar to the literature on ordered nonlinear periodic structures, originates from the physics community and focuses on pulse propagation through conservative and infinitely long systems. Recent reviews of this literature can be found in [73, 94].

Within the nonlinear mechanics literature, some of the earlier works on nonlinear disordered structures include [28, 64, 117]. These studies deal with the free response of conservative systems; thus, their results are not applicable to the case of supratransmission. Many of the remaining studies are concerned with the evolution of pulses as they propagate through nonlinear disordered structures [2, 52, 84, 109], particularly for granular chains [2, 84, 109]. The specific decay characteristics of

pulses (exponential or algebraic) is found to depend on the relative strengths of nonlinearity and disorder, as well as the specific form of nonlinear forces. Unfortunately, these results are not directly applicable to the case of continuous wave excitation in supratransmission because superposition does not generally hold in nonlinear systems.

Wave propagation due to continuous harmonic excitation has been studied in strings loaded with masses, both experimentally and numerically. It is reported in the experimental work [44, 53] that for forcing frequencies within the pass band, increasing the driving amplitude leads to a decrease in the transmitted energy. The reported results, though, are obtained for only one realization of disorder. Besides, the response regime is confined to driving amplitudes below the onset of anharmonic motion, which would be below the onset of supratransmission<sup>1</sup>. In the numerical work [114], transmitted energies were found to generally increase with the amplitudes of incident waves. Although anharmonic regimes were observed at high intensities, the corresponding increases in transmitted energies are surprisingly small in these regions (especially for an undamped structure). This is uncharacteristic of supratransmission in which case an energy increase of a few orders of magnitude is expected (see Section 2.3).

We are aware of two main studies that directly address the phenomenon of enhanced energy transmission in nonlinear disordered structures due to continuous harmonic excitation [57, 125]. These studies report the existence of transmission thresholds for undamped structures of long [57] and (relatively) short [125] lengths. In both studies, the excitation frequencies are limited to the pass bands of the corresponding ordered structures (this is the frequency range in which disorder prohibits energy transmission from a linear perspective). In [125], the statistical influence of disorder on the average response is studied for different structure lengths. It is further shown that the average threshold amplitude decreases with the number of units according to a power law. In the limit of an infinitely long structure, though, the average transmission threshold is expected to remain finite [57].

Despite the detailed studies in [57, 125], the case of supratransmission (excitation within a stop band) remains unexplored in disordered periodic structures.

---

<sup>1</sup>The nature of the post-threshold response is non-periodic in supratransmission. This is explained in Section 2.3.

So is the influence of system parameters (damping, in specific) on the mechanism leading to supratransmission. In the two studies [57, 125] mentioned above, energy dissipation occurs at the boundaries of the periodic structures, but there is no internal energy loss within the periodic structures themselves. Hence, the influence of damping forces remains to be investigated. Damping and finite-size effects are necessary to make the results applicable to engineering structures.

## 1.4 Research Objectives and Methodology

The goal of this thesis is to study the supratransmission phenomenon in a setting that is applicable to engineering problems. From the perspective of engineering applications, it is essential to incorporate three features in this study: (i) dissipative forces; (ii) small deviations from exact periodicity distributed throughout the structure (disorder); (iii) the finite size of the structure. This thesis systematically investigates the influence of these parameters on the supratransmission phenomenon in a one-dimensional periodic structure. Within this setting, we address the competition that takes place among the effects of dispersion, dissipation, nonlinearity and disorder-borne localization (Anderson localization).

Dispersion effects are inherently present in periodic structures and are responsible for the formation of stop bands. Dissipation effects are unavoidable in engineering structures and normally influence all frequencies. Finite-size effects lead to formation of standing waves and restrict the allowable wavenumbers for propagating waves. Nonlinearity counters these effects, most importantly those of dispersion, to give rise to supratransmission, which is an instability-induced transmission mechanism within a stop band. Finally, disorder effects become significant because the spectral contents of the waves transmitted above the supratransmission threshold fall within the pass band. This is the same frequency range where Anderson localization dominates dispersion effects, thus leading to vibration localization near the source of excitation. In this case, our goal is to investigate the statistical influence of linear disorder on (i) the supratransmission thresholds within a stop band, (ii) transmitted energies above the supratransmission threshold, and (iii) the spectrum of the nonlinearly transmitted waves. While some portions of this problem may only be tackled numerically, such as (ii) and (iii), we aim to

develop analytical estimates to be used in (i) in order to complement the numerical approach .

To this end, we study energy transmission through a discrete nonlinear periodic structure, subjected to continuous harmonic point excitation at one end. We propose a macro-mechanical periodic structure in this study that consists of coupled suspended cantilever beams. Within each unit cell, the linear restoring force of each beam is combined with a strong nonlinear magnetic force to produce on-site nonlinearity. The magnetic force can be tuned, thereby providing control over the strength of nonlinearity, as well as its type (softening or hardening). The idea of combining a strong magnetic force with the linear restoring force of a cantilever has been previously used in the literature, most notably by Den Hartog [23, Sec. 8.10], Moon and Holmes [93] and Kimura and Hikihara [63], among others. The proposed setup can be used to realize both ordered and disordered periodic structures.

Using the proposed mechanical structure, we review the mechanism responsible for the onset of nonlinear energy transmission. We use the appropriate computational methodology for calculation of the supratransmission thresholds and develop analytical estimates for predicting the onset of supratransmission. We study the influence of various system parameters on the supratransmission mechanism: type and strength of nonlinearity, number of units, damping, strength of coupling, forcing amplitude and frequency, and disorder. In disordered structures, we investigate the statistical behavior of the structure in an ensemble-average sense.

It is noted that the analytical approximations are developed using asymptotic analysis, which assumes that the nonlinear forces are comparable to linear forces. As we will explain in detail, this assumption may only be valid up to the onset of supratransmission for certain range of system parameters. The analytical approximations are not valid above the onset of supratransmission (where the response is no longer periodic) and accordingly cannot describe the response of the structure in that regime. Only direct numerical simulations can be used above the onset of supratransmission. Further details on the analyses are provided in Sections 2.5 and 4.4.

This thesis does not contain an experimental component. As outlined in Section 5.3, the long-term perspective of this research project (beyond the present

thesis) is to build the mechanical setup proposed here in order to validate the theoretical findings in this thesis.

## 1.5 Thesis Outline

The rest of this work is organized in four main chapters.

We start in Chapter 2 by presenting the proposed mechanical setup. We derive the governing equations of motion and explain the controls provided by the magnetic forces: (i) strength of nonlinearity, (ii) type of nonlinearity, (iii) disorder. In this chapter, we focus on an ordered periodic structure (no defect or disorder). The periodic structure is very short (6 unit cells), has light damping and weak coupling forces between adjacent units. We explain the supratransmission phenomenon and identify its underlying mechanism using direct numerical simulations and numerical continuation techniques. The onset of supratransmission is computed numerically by constructing the nonlinear response manifold of the system. The mechanism for nonlinear energy propagation is explained and its relevance to the resonances of the driving force with the shifted pass band of the structure is discussed. We then derive analytical expressions for predicting the onset of transmission based on the local nonlinear dynamics of the driven unit.

In Chapter 3, we investigate the influence of various system parameters on supratransmission in ordered structures. The following parameters are considered: type and strength of nonlinearity, number of units, damping and strength of coupling. We highlight the importance of forcing frequency by contrasting supratransmission with the case of harmonic excitation within a pass band. We also briefly address the hysteresis phenomenon accompanying supratransmission, as well as broadband energy propagation at very high driving amplitudes.

In Chapter 4, we study the influence of disorder on supratransmission. We start by an overview of the key features of the linear response of disordered structures (Anderson localization). We consider a periodic structure with 10 units in this chapter. The choice of other system parameters, such as strength of disorder, are motivated in this context. We highlight the non-trivial effects of damping and disorder on the transmission mechanism. We then discuss the statistical effects of linear disorder on supratransmission. The changes in threshold curves, transmitted

energies and transmitted wave spectra are discussed in an ensemble-average sense. Finally, we present an analytical formula for predicting the onset of supratransmission in ordered and disordered structures, and investigate its range of validity. In doing so, we investigate the influence of nonlinearity and strength of coupling on the average transmission threshold curves.

We conclude in Chapter 5 by summarizing the contributions and limitations of this work and providing suggestions for future research on this topic.

## Chapter 2

# Supratransmission

In this chapter, we review the supratransmission phenomenon in a short, damped periodic structure. We identify the instability mechanism underlying supratransmission and clarify its relation to resonances of the driving force with the shifted pass bands of the structure. Approximate analytical expressions are derived for predicting the onset of supratransmission using asymptotic analysis, and validated against results from numerical computations.

### 2.1 A Periodic Structure with Tunable Nonlinearity

Figure 2.1 shows the proposed periodic structure consisting of  $N$  repeating units. Each unit is made of a thin, suspended cantilever beam of length  $\ell$  with a tip mass (a permanent magnet). Two electromagnets (hatched rectangles in Figure 2.1) are fixed to the ground at a vertical distance  $h$  below the tip mass, and interact with the permanent magnet (black rectangles). The electromagnets are symmetrically placed from the beam axis at a horizontal distance  $d$ . This symmetric arrangement ensures that the vertical position of the cantilever is the equilibrium configuration. Direct current (DC) is passed through each electromagnet such that they have the same polarity facing the beam. The magnetic forces between the permanent magnet at the tip and the two electromagnets provide tunable nonlinear restoring force for each beam. The first beam is excited with a harmonic force  $\tilde{f}(\tilde{t}) = \tilde{F} \cos(\omega_f \tilde{t})$ , where  $\tilde{F}$  is the magnitude of the applied force,  $\omega_f$  is the driving frequency and  $\tilde{t}$

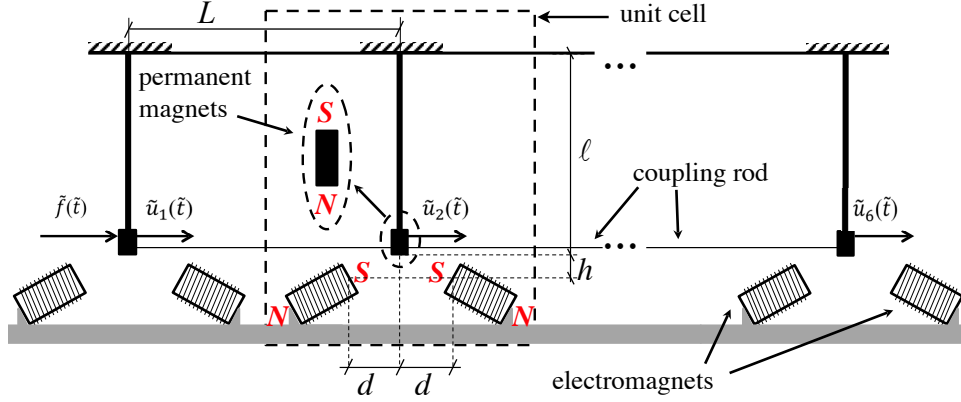


**Figure 2.1:** A schematic of the periodic structure made of  $N$  unit cells. The repeating unit is indicated by the dashed box. The external harmonic force,  $\tilde{f}(\tilde{t}) = \tilde{F} \cos(\omega_f \tilde{t})$ , is applied to the first unit only. Two electromagnets, operated by direct currents, are fixed to the ground under the beam in each unit. The currents are chosen such that the electromagnets have the same polarity facing the beam. We fix  $h = d/10$  throughout this work.

is time. A coupling rod of length  $L$  couples the displacements of adjacent beams. The spacing between adjacent beams ( $L$ ) is large compared to the separation between the magnets ( $2d$ ) in order to avoid magnetic interference effects between the magnetic fields in adjacent units.

The proposed mechanical setup has features that make it a good candidate for our study on nonlinear periodic structures. It can be easily manufactured compared to its counterparts, such as arrays of micromechanical resonators [116]. The instrumentation required for performing the tests are often available to researchers in mechanical vibrations (electrodynamic shaker and accelerometer). Furthermore, the tunable magnetic force makes it possible to control the form of nonlinearity, a feature that can be used to replicate different types of nonlinear forces and thereby different types of nonlinear periodic structures. This cannot be achieved with simpler setups such as arrays of coupled pendulums [40]. The limitation here is the form of the nonlinear force (described in Section 2.1.1). As cases in point, the results obtained in this thesis may not be readily extended to systems with nonlinear friction forces or saturable nonlinear forces without further investigation. As will

be demonstrated in this chapter, the nonlinear force provided via the electromagnetic interaction is appropriate for generating the supratransmission phenomenon. The strength of the coupling force between adjacent units may also be adjusted by placing the coupling rod at different heights along the cantilevers. The setup may also be used to realize disordered periodic structures. This can be done by adjusting the currents going through the electromagnets, as described in the following section.

### 2.1.1 Governing Equations for the Periodic Structure

The chain of coupled cantilever beams in Figure 2.1 is a continuous system with infinite degrees of freedom, with each individual cantilever beam having infinite number of vibration modes. Therefore, there will be infinitely many pass bands, extending to infinite frequency. In the first pass band, all cantilever beams vibrate in their fundamental mode with different phases. In the second pass band, the beams vibrate in their second deformation mode shape with different phases, and so on. We focus on energy transmission in frequency ranges within the first pass band of the structure so that a dynamical representation with  $N$  degrees of freedom is appropriate. Thus the governing system of partial differential equations reduces to a set of coupled ordinary differential equations. The equation governing the vibrations of a unit cell (before coupling to adjacent units) can be expressed as follows:

$$\ddot{\tilde{u}}_n + 2\tilde{\zeta}\dot{\tilde{u}}_n + \omega_0^2\tilde{u}_n + \tilde{F}_{M,n} = 0 \quad (2.1)$$

where overdot denotes time derivative,  $\tilde{u}_n(\tilde{t})$  is the lateral deflection of the tip of beam  $n$ ,  $\tilde{\zeta}$  is the coefficient of viscous damping,  $\omega_0$  is the first natural frequency of the beam when the electromagnets are removed and  $\tilde{F}_{M,n}$  is the horizontal component of the magnetic force acting on the tip of the beam resulting from the interaction of the permanent magnet and two electromagnets. The axial component of the force is ignored because the coupling between axial and lateral vibrations of the beams are negligible. If the displacements of the tip of the beam are small compared to its length, equal currents pass through the two electromagnets within the unit cell, and the magnets are modeled as magnetic poles, then the magnetic

force  $\tilde{F}_{M,n}$  can be written according to Coulomb's law:

$$\tilde{F}_{M,n} = \tilde{\mu}_n \frac{(d + \tilde{u}_n)}{((d + \tilde{u}_n)^2 + h^2)^{3/2}} - \tilde{\mu}_n \frac{(d - \tilde{u}_n)}{((d - \tilde{u}_n)^2 + h^2)^{3/2}} \quad (2.2)$$

This is the horizontal component of the magnetic force acting on the  $n$ th beam. The constants  $\tilde{\mu}_n$  depend on the strengths of the magnetic poles and contain the non-geometric dependencies of the magnetic force. The magnetic force can be tuned, thus providing control over the strength of nonlinearity, as well as its type (softening or hardening). This will be explained in detail in Section 2.1.2.

To normalize the governing equations, we use  $\omega_0$  for time and  $d$  for displacements. We consider a linear coupling force between adjacent units due to the coupling rod. Including this force and dividing all terms by  $\omega_0^2 d$ , we arrive at the non-dimensional form of the governing equations (2.1) for  $N$  units

$$\ddot{u}_n + 2\zeta \dot{u}_n + u_n + k_c \Delta^2(u_n) + F_{M,n} = f_n \cos(\Omega t), \quad 1 \leq n \leq N \quad (2.3)$$

Here,  $u_n \equiv \tilde{u}_n/d$  is the normalized displacement of each unit,  $k_c$  represents the normalized coupling force between adjacent units and  $\Delta^2(u_n) = 2u_n - u_{n+1} - u_{n-1}$  everywhere except at the boundaries, where  $\Delta^2(u_1) = u_1 - u_2$  and  $\Delta^2(u_N) = u_N - u_{N-1}$  (free boundary conditions). The normalized external force is given by  $f_n = F$  for  $n = 1$  and zero elsewhere, with  $F \equiv \tilde{F}/d \omega_0^2$  as the normalized forcing amplitude,  $\Omega \equiv \omega_f/\omega_0$  as the normalized forcing frequency and  $t \equiv \omega_0 \tilde{t}$  as normalized time.  $F_{M,n}$  represents the only nonlinear force in the model and is given by

$$F_{M,n} = \mu_n \left( \frac{(1 + u_n)}{((1 + u_n)^2 + r^2)^{3/2}} - \frac{(1 - u_n)}{((1 - u_n)^2 + r^2)^{3/2}} \right) \quad (2.4)$$

where  $r \equiv h/d$  is a fixed parameter and  $\mu_n \equiv \tilde{\mu}_n/d^3 \omega_0^2$  is a control parameter that can be changed. In the case of an ordered periodic structure, we have  $\mu_n = \mu_0$  for all  $n$ . For a disordered periodic structure,  $\mu_n = \mu_0 + \delta\mu_n$  where  $|\delta\mu_n| < |\mu_0|$ . Hereafter, all parameters used in the thesis, including time, are non-dimensional.

Expanding (2.4) about its trivial equilibrium point,  $u_n = 0$ , we obtain

$$F_{M,n} \approx -\mu_n(a_1 u_n + a_3 u_n^3 + \dots) \equiv k_1 u_n + k_3 u_n^3 + \dots \quad (2.5)$$

where  $a_1$  and  $a_3$  only depend on the (fixed) parameter  $r$  as follows:

$$a_1 = \frac{2(2-r^2)}{(1+r^2)^{5/2}} \quad (2.6a)$$

$$a_3 = \frac{8-24r^2+3r^4}{(1+r^2)^{9/2}} \quad (2.6b)$$

The constants  $k_j$  in (2.5) are defined as  $k_j \equiv -\mu_n a_j$  for  $j = 1, 3, 5, \dots$ .

We set  $r = 0.1$  throughout the work. Unless otherwise specified, we use  $k_c = 0.05(1+k_1)$  as the default value for the strength of coupling between adjacent units – the need for weak coupling will be motivated in Section 4.1. Furthermore, we consider lightly damped structures. The values of  $\mu_n$  change throughout the work to realize different nonlinear forces, and are reported in each case. The importance of the type of nonlinearity (determined by the sign of  $\mu_n$ ) is addressed in Section 3.1. The remaining two parameters are  $F$  and  $\Omega$ , which are typically free parameters. Throughout this chapter, we consider a periodic structure with six units,  $N = 6$ .

### 2.1.2 Tunability of the Nonlinear Forces

The source of nonlinearity in the proposed periodic structure is  $F_{M,n}$ , which acts as an on-site nonlinear force for each unit. The type and strength of nonlinearity can be tuned by changing the control parameter  $\mu_n$ . In particular, the strength of nonlinear terms increases when we increase the magnitude of  $\mu_n$ , as evident from (2.4). Moreover, the sign of  $\mu_n$  determines whether nonlinearity is of the hardening or softening type. If  $\mu_n < 0$ , then  $k_3 > 0$  in (2.5) and we have a hardening nonlinearity. Likewise, a softening nonlinearity can be realized by setting  $\mu_n > 0$ , thus obtaining  $k_3 < 0$  according to (2.5).

In order to show the tunability of nonlinear forces, we consider the normalized restoring force acting on a beam in a single unit. Denoted by  $P_n$ , the normalized restoring force is the sum of a normalized elastic force ( $u_n$ ) and a normalized magnetic force ( $F_{M,n}$ ),

$$P_n = u_n + F_{M,n} \quad (2.7)$$

The linear natural frequency of a unit is the first derivative of the restoring force at

the origin,

$$\omega_1^2 \equiv \left( \frac{\partial P_n}{\partial u_n} \right)_{u_n=0} = 1 + k_1 \quad (2.8)$$

Note that the linear part of the magnetic force (i.e.  $k_1 u_n$ ) has an influence on the natural frequencies of the system. The sign of  $k_1$  depends on  $\mu_n$  according to (2.5), such that the first natural frequency of the periodic structure ( $\omega_1$ ) is below 1 when  $\mu_n > 0$  (softening nonlinearity) and above 1 when  $\mu_n < 0$  (hardening nonlinearity).

The nonlinear force  $F_{M,n}$  can be adjusted within each unit by changing the currents passing through the electromagnets,  $I_n$ , thereby varying  $\mu_n$  in (2.4). The sign of  $I_n$  depends on the direction of the current passing through the electromagnets within that unit. Note that  $F_{M,n}$  also depends on the geometrical configuration of the setup through parameter  $r$ , though we fix  $r = 0.1$  in this work and only change  $\mu_n$ .

Following Kimura and Hikiyama [63], we have assumed  $\mu_n = \xi_0 + \xi_1 I_n$  for all  $n$ , where  $\xi_0$  corresponds to the normalized magnetic strength of the ferromagnetic core of the electromagnets, and  $\xi_0 = 0.0151$  and  $\xi_1 = 0.0029$ . Due to the presence of ferromagnetic cores ( $\xi_0 \neq 0$ ), the magnetic coefficients  $\mu_n$  do not depend symmetrically on the currents; i.e.  $\mu_n(I_n) \neq \mu_n(-I_n)$ . If the electromagnets had non-ferromagnetic cores, then we would have  $\xi_0 = 0$ .

Figure 2.2 shows the variation of  $P_n$  as a function of  $u_n$  for a single unit. We can see that when both electromagnets are removed ( $\mu_n = 0$ ), the restoring force is linear as expected. By placing the electromagnets with the polarity shown in Figure 2.1 and setting  $I_n = 15$  mA, we get a nonlinear restoring force of the softening type. A hardening nonlinear force is realized when the direction of the currents passing through both electromagnets is reversed ( $I_n = -15$  mA). Notice that the restoring forces for the hardening and softening systems are not symmetric with respect to the restoring force of the linear system. This is due to the presence of ferromagnetic cores in the electromagnets, as explained in the previous paragraph. Because of the same reason, the case of  $I_n = 0$  does not correspond to  $\mu_0 = 0$  and is therefore different from the linear case ( $P_n$  is not shown for  $I_n = 0$  here).

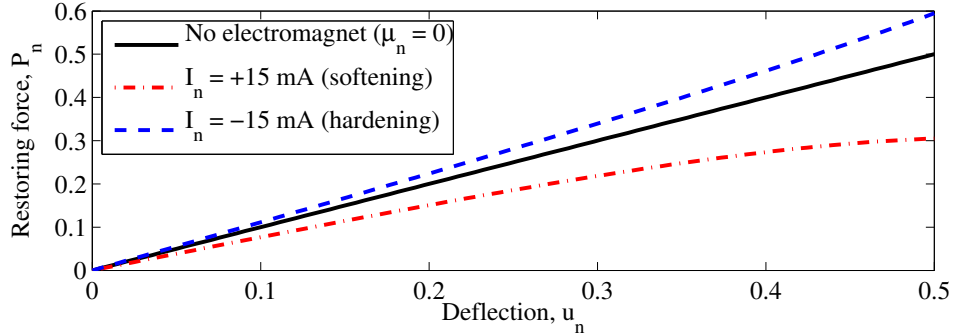


**Figure 2.2:** The dependence of the normalized restoring force,  $P_n = u_n + F_{M,n}$ , on the currents passing through the two electromagnets,  $I_n$ . Notice that the restoring forces for the hardening (blue dashed curve) and softening (red dash-dotted curve) systems are not symmetric with respect to the restoring force of the linear system (black solid line). This is due to the presence of ferromagnetic cores in the electromagnets.

## 2.2 Band Structure of Periodic Systems

### 2.2.1 Forced Response of Linear Structures

For small-amplitude vibrations, we can linearize (2.3) to get

$$\ddot{u}_n + 2\zeta\dot{u}_n + \omega_1^2 u_n + k_c \Delta^2(u_n) = f_n \cos(\Omega t), \quad f_n = 0 \text{ for } 2 \leq n \leq N \quad (2.9)$$

where  $\omega_1$  is defined in (2.8). The solutions to the linear system (2.9) can be written as follows

$$u_n(t) = u_1(t) e^{-i\kappa(n-1)} e^{-\gamma_0(n-1)} \quad (2.10)$$

where  $i = \sqrt{-1}$ ,  $\kappa$  is normalized wavenumber,  $u_1(t)$  denotes the response of the first unit as a function of time, and  $\gamma_0 \geq 0$  is a real-valued decay exponent.  $u_1(t) = U_1 \exp(i\Omega t)$ , in which  $U_1$  is the complex-valued amplitude of motion. When  $\gamma_0 > 0$ , amplitudes of vibration attenuate exponentially through the periodic structure and energy propagation is not possible over long distances. We get complete transmission when  $\gamma_0 = 0$ . Substituting solution (2.10) into the governing equations (2.9),

we arrive at the following

$$\cosh(\gamma_0) \cos(\kappa) = 1 + (\omega_1^2 - \Omega^2)/(2k_c) \quad (2.11a)$$

$$\sinh(\gamma_0) \sin(\kappa) = (2\zeta\Omega)/(2k_c) \quad (2.11b)$$

In the absence of damping ( $\zeta = 0$ ), we have  $\gamma_0 = 0$  (complete transmission) for  $\omega_1^2 \leq \Omega \leq \omega_1^2 + 4k_c$ , which is the pass band of the structure. Outside this frequency range,  $\gamma_0 > 0$  and waves will attenuate exponentially away from the source ( $n = 1$ ). This can be seen in Figure 2.3 where  $\gamma_0$  is plotted as a function of  $\Omega$ , for different values of damping. The area with a white background indicates frequencies for which  $\gamma_0 = 0$  in the undamped system. We can see that the presence of damping results in spatial decay of response at all frequencies, even within the pass band. In particular, the influence of damping on the decay exponent is mostly significant within the pass band. We note that the analysis in this section is exact for an infinitely long exactly periodic linear structure.

To conclude this section, we point out that viscous damping, if it is high enough, can result in emergence of stop bands in the wavenumber domain; i.e. spatial stop bands corresponding to imaginary wavenumbers. See [54] for more details on the influence of high levels of damping on the band structure of (ordered) linear periodic structures.

### 2.2.2 Free Wave Propagation in Linear and Nonlinear Structures

For small displacements around the vertical equilibrium position, we can write the following equations for free vibrations of the unforced, undamped periodic structure

$$\ddot{u}_n + \omega_1^2 u_n + k_c(2u_n - u_{n-1} - u_{n+1}) = 0 \quad (2.12)$$

where  $\omega_1$  is defined in (2.8). In an infinitely long periodic structure, the linear equations (2.12) admit plane wave solutions

$$u_n(t) = U \cos(\omega t - qn) \quad (2.13)$$

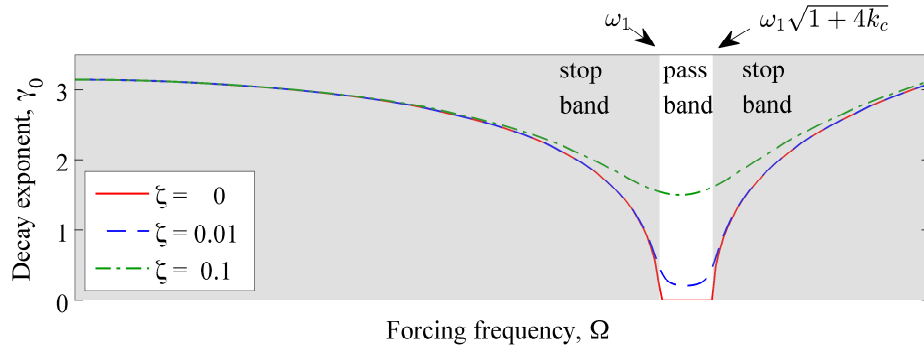


**Figure 2.3:** Decay exponent  $\gamma_0$  for an infinitely long exactly periodic linear structure. The white and grey backgrounds indicate the pass and stop bands, respectively. When  $\zeta > 0$ , the decay exponent is always positive, even within the pass band. Anderson localization is relevant for frequencies within the pass band, whereas supratransmission occurs within the stop band – we will discuss these phenomena in subsequent chapters.

where  $U$  is the wave amplitude and  $q$  is the normalized wave number, with  $0 \leq q \leq \pi$ . Using this solution, the linear dispersion relation is found to be:

$$\omega^2 = \omega_1^2 + 4k_c \sin^2(q/2). \quad (2.14)$$

The above dispersion relation describes the first pass band of the system, which starts at a finite frequency,  $\omega_1$ . The upper frequency of the pass band edge (denoted by  $\omega_u$ ) is associated with the wave number  $q = \pi$ . Therefore, from (2.14), we have

$$\omega_u^2 = \omega_1^2 + 4k_c \quad (2.15)$$

Notice that the width of the pass band ( $\omega_u^2 - \omega_1^2$ ) is directly proportional to the strength of coupling,  $k_c$ . We can also conclude from (2.14) and (2.8) that the location of the pass band (but not its width) depends on  $\mu_n$ , and thereby on the currents passing through the electromagnets. This can be verified from Figure 2.4, where the dispersion curve (2.14) is plotted for the softening ( $I = 15$  mA) and hardening ( $I = -15$  mA) realizations of the magnetic force. If the electromagnets were removed ( $\mu_n = 0$ ), then the pass band would start from the first natural frequency of

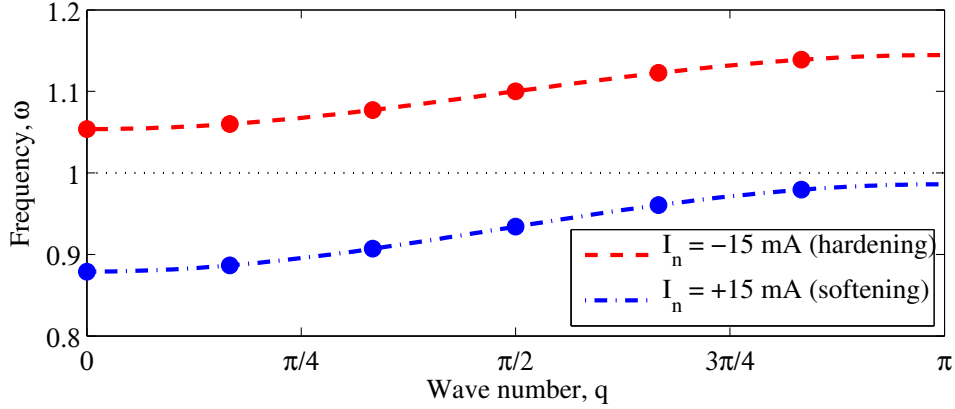


**Figure 2.4:** The dependence of the linear dispersion curve, (2.14), on the currents passing through the electromagnets. The red dashed curve corresponds to the hardening structure ( $I = -15$  mA) and the blue dash-dotted curve to the softening structure ( $I = 15$  mA). The six dots along each curve correspond to the natural frequencies of the finite structure with free boundary conditions. The horizontal dotted line depicts the first natural frequency of the structure when the electromagnets are removed. See (2.8) and its foregoing explanation regarding the dependence of linear dispersion curves on the type of nonlinearity.

the beams ( $\omega_1 = 1$ ).

The finite periodic structure shown in Figure 2.1 is symmetric, has symmetric unit cells and has open (free-free) boundary conditions. Therefore, the first natural frequency of the finite structure coincides with the the lower edge of the pass band of the infinite system [87]. The remaining natural frequencies of the finite structure distribute within the pass band of the infinite system with a uniform wave number spacing of  $\pi/N$ , where  $N$  is the number of the units [119]. As a result, the highest natural frequency of the finite system increases with the number of units and, in the limit of infinite units, it reaches  $\omega_u$ . Again, we emphasize that these conclusions pertain to our model of the infinite degrees of freedom system reduced to frequencies within the first pass band region. The six computed natural frequencies of the finite periodic structure studied in this work are shown as dots in Figure 2.4. As expected, all of them lie within the first pass band of the infinite system, with the lowest one coinciding with the lower edge of the pass band.

For finite amplitudes of motion, the dispersion relation naturally becomes dependent on the amplitude of motion. To obtain the dispersion relation for a weakly nonlinear system (small but finite amplitudes of motion), we need to account for the dependence of the natural frequencies on the amplitudes of motion; i.e.  $\omega = \omega(U)$  in (2.13). A standard asymptotic analysis, such as the Lindstedt-Poincaré or multiple-scale method, can be performed for this purpose – e.g. see [97, 128] for similar analyses. To the leading order (i.e. for weak nonlinearity), the amplitude-dependent correction to the linear dispersion relation results in the following dispersion relation

$$\omega^2 = \omega_1^2 + 4k_c \sin^2(q/2) + 3/4k_3U^2 \quad (2.16)$$

where  $U$  represents the amplitude of motion. According to the amplitude-dependent dispersion relation (2.16), nonlinearity can shift the pass band, but cannot change its width. This is not surprising because the width of the pass band depends on the coupling force between the units, which is linear in this case. We note that this approximation is valid for finite but small amplitudes of motion. Higher-order corrections would be needed to improve the approximation.

For the infinite system, we can readily study the edges of the pass band in more detail. At the lower edge, adjacent units move in phase with each other ( $q = 0$ ) and we have  $u_{n\pm 1} = u_n$ . At the upper edge, adjacent units move out of phase ( $q = \pi$ ) and  $u_{n\pm 1} = -u_n$ , as a result. We can therefore decouple the equations at the two edges of the pass band as follows:

$$\ddot{u}_n + u_n + F_{M,n} = 0 \quad (2.17a)$$

$$\ddot{u}_n + (1 + 4k_c)u_n + F_{M,n} = 0 \quad (2.17b)$$

where the natural frequencies of (2.17a) and (2.17b) correspond to the lower and upper edges of the pass band, respectively.

### 2.3 Energy Transmission via Harmonic Excitation within a Stop Band

Consider the hardening system with  $I = -15$  mA, which has its upper linear natural frequency at  $\omega_6 \approx 1.139$ . We choose  $\zeta = 0.004$ . The forcing frequency is fixed

above the linear pass band of the infinite system; i.e.  $\Omega > \omega_u \approx 1.145$  – we will see in Section 3.1 that supratransmission occurs above the pass band in a structure with hardening nonlinearity. We choose a small driving amplitude  $F$  and numerically integrate the governing equations (2.3) for a large number of periods,  $T = 2\pi/\Omega$ , starting from zero initial displacements and velocities. We then repeat this procedure for increasing values of  $F$ . For a given  $F$ , we increase the forcing amplitude smoothly from zero to  $F$  to avoid formation of shocks in the numerical solution. This is done by replacing  $F$  with  $F(1 - \exp(-t/\tau_1))$ , and is particularly important for undamped systems. After the initial transient part of the solution is passed, we calculate the energy in each unit, denoted by  $E_n$  (normalized), as follows:

$$E_n = \frac{1}{(m_2 - m_1)T} \int_{m_1 T}^{m_2 T} \left( \frac{u_n(t)}{F} \right)^2 dt \quad (2.18)$$

We have used  $\tau_1 = 50$ ,  $m_1 = 500$  and  $m_2 = 3500$  in this chapter. Notice that energy is normalized to compensate for the linear increase in response amplitudes,  $u_n(t)$ , due to increase in  $F$ .

Figure 2.5(a) shows the time-averaged energy in the last unit,  $E_6$ , as a function of  $F$ , for a fixed forcing frequency of  $\Omega = 1.25$  above the linear pass band (hardening nonlinearity). We can see a threshold around  $F = 0.116$  above which there is a sudden large increase in the energy that reaches the end of the structure. The frequency components of the response at the first and last units are also shown for two cases: (1)  $F = 0.114$ , below the transmission threshold in Figure 2.5(b), (2)  $F = 0.116$ , above the threshold in Figure 2.5(c). The frequency spectrum for each oscillator is obtained by taking the Fast Fourier transform (FFT) of the corresponding time series after the initial transient has passed; no additional windowing or scaling is used. We can see in Figure 2.5(b) that the driving frequency ( $\Omega = 1.25$ ) is the predominant frequency component throughout the structure below the threshold. Therefore, the response of the system remains harmonic below the threshold. Above the threshold, see Figure 2.5(c), the driven unit moves with a high amplitude and its response is broadband and highly nonlinear. Figure 2.5(c) shows that the frequencies of the transmitted waves are predominantly within the linear pass band of the structure. The amplitude of waves with frequencies within the stop band attenuate due to dispersion effects. Notice that the amplitudes of waves within the

pass band also decrease due to dissipation.

We observe the same phenomenon in the case of a softening system ( $I = 15$  mA). In this case, the lower linear natural frequency of the structure is at  $\omega_1 \approx 0.88$ . We fix the forcing frequency below this value, at  $\Omega = 0.85 < \omega_1$ , and follow the same procedure as before to observe supratransmission. Figure 2.6(a) shows  $E_6$  as a function of  $F$ . We observe the onset of supratransmission occurring between  $F = 0.019$  and  $F = 0.021$ . We show the frequency components of the response at  $F = 0.019$  in Figure 2.6(b). As expected, the response is harmonic with the same frequency as the driving force ( $\Omega = 0.85$ ). Because this frequency is within the stop band, we observe a large decrease in the amplitudes of motion as we go from  $n = 1$  to  $n = 6$ . At  $F = 0.021$  (above the transmission threshold), we see in Figure 2.6(c) that the response at the first unit is highly nonlinear. As we go through the periodic structure to its other end, the frequency components within the linear stop band are highly attenuated by dispersion. Accordingly, the spectrum of the transmitted waves lies mainly within the pass band of the linear structure. Thus supratransmission is a band-limited transmission phenomenon.

It is worth mentioning that the nature of the post-threshold response in supratransmission can vary based on system parameters (driving frequency, type of nonlinearity, etc). There does not seem to be a reliable methodology that can predict the nature of the post-threshold response a-priori. We will see in Section 2.4.1 that supratransmission occurs as long as the post-threshold response is non-periodic. Accordingly, classification (from a dynamical-systems viewpoint) of the post-threshold non-periodic attractors is not of primary interest in this context.

To indicate this point, we consider the post-threshold responses of structures with hardening and softening nonlinearities in Figures 2.5(c) and 2.6(c), respectively. The response of the hardening system appears to be chaotic, while that of the softening systems appears to be quasi-periodic – a quasi-periodic motion consists of two or more incommensurate frequencies. To confirm this observation, we construct the Poincaré map of the two responses above the supratransmission threshold. Because of the external harmonic force applied to the structure, the Poincaré map can be constructed by (stroboscopically) recording the displacement and velocity of the response at a fixed phase of the driving force – see [70, Ch. 1] for more details. Figure 2.7 shows the projection of this Poincaré map (obtained

at zero phase) onto the phase space of the last unit,  $(u_N, v_N)$ . The Poincaré map of the response for the hardening system, Figure 2.7(a), consists of a cloud of scattered points. This implies that the response is chaotic – note that a rigorous proof of chaos (and its classification) is immaterial in the current discussion. We see in Figure 2.7(b) that the Poincaré map of the response for the softening system is a closed curve. This confirms that the post-threshold response of the softening system is quasi-periodic.

Figure 2.8 shows the normalized amplitude profiles of the structures, below and above the supratransmission threshold. For each unit, the amplitude  $U_n$  is computed as half the difference between the maximum and minimum values,  $U_n = (\max\{u_n(t)\} - \min\{u_n(t)\})/2$ , after the initial transient part of the response is passed. This is equal to the amplitude of the motion in the phase space. For the hardening system, we see in Figure 2.8(a) that the amplitude profile shows exponential decay below the threshold. This is a characteristic of the linear behavior of periodic structures when the forcing frequency is within the stop band. Above the threshold, on the other hand, the decay in amplitude is no longer exponential. This suggests that above the threshold, the energy injected in the stop band transmits to distant units with less attenuation. Qualitatively, we make the same observation in Figure 2.8(b) for the softening system. It is important to note that attenuation over large distances is always present in a damped structure. In this sense, damping prevails over nonlinearity.

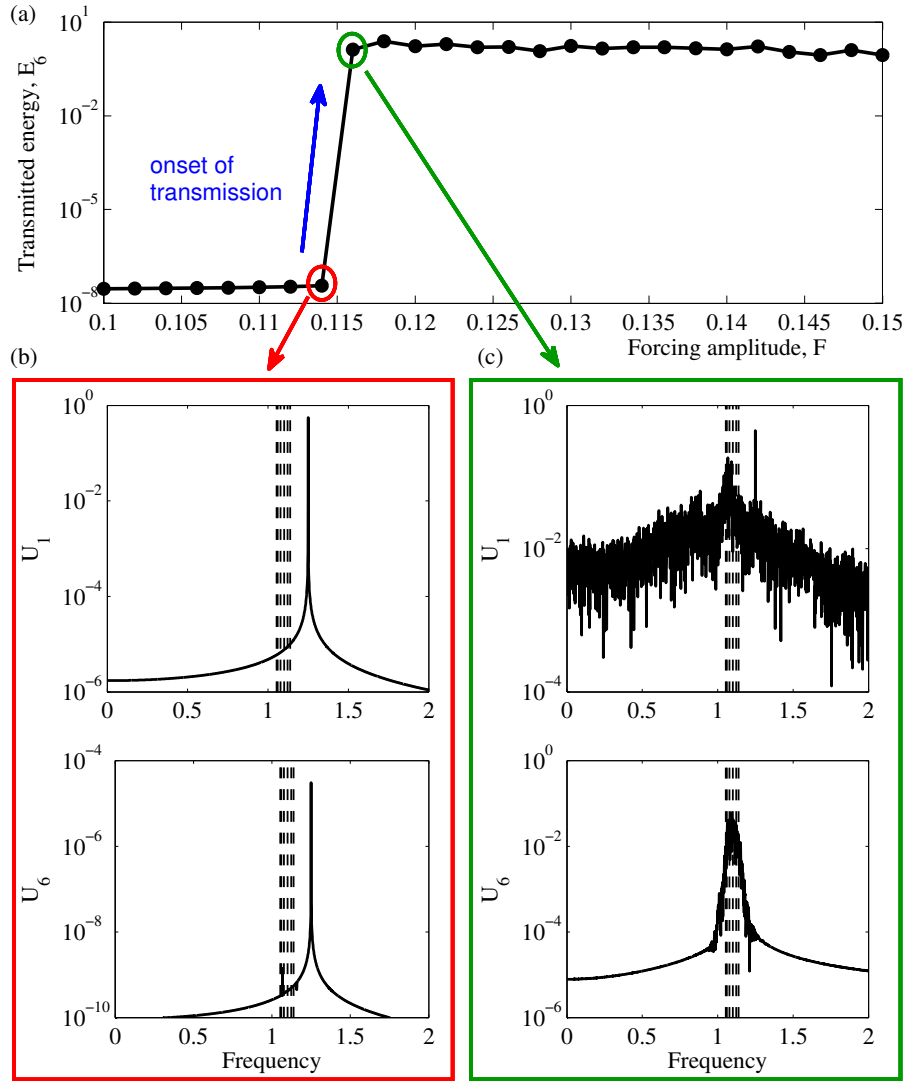


**Figure 2.5:** The supratransmission mechanism for the hardening system ( $I = -15$  mA). (a) Energy transmitted to the end of the chain,  $E_6$ , as a function of the driving amplitude,  $F$ , at  $\Omega = 1.25$ . The blue arrow indicates the onset of transmission. (b) Frequency components of the first unit ( $U_1$ ) and last unit ( $U_6$ ) for  $F = 0.114$ , below the transmission threshold at  $\Omega = 1.25$ . (c) Frequency components of the first unit ( $U_1$ ) and last unit ( $U_6$ ) for  $F = 0.116$ , above the transmission threshold at  $\Omega = 1.25$ . The six vertical lines in (a) and (b) indicate the linear natural frequencies of the structure.

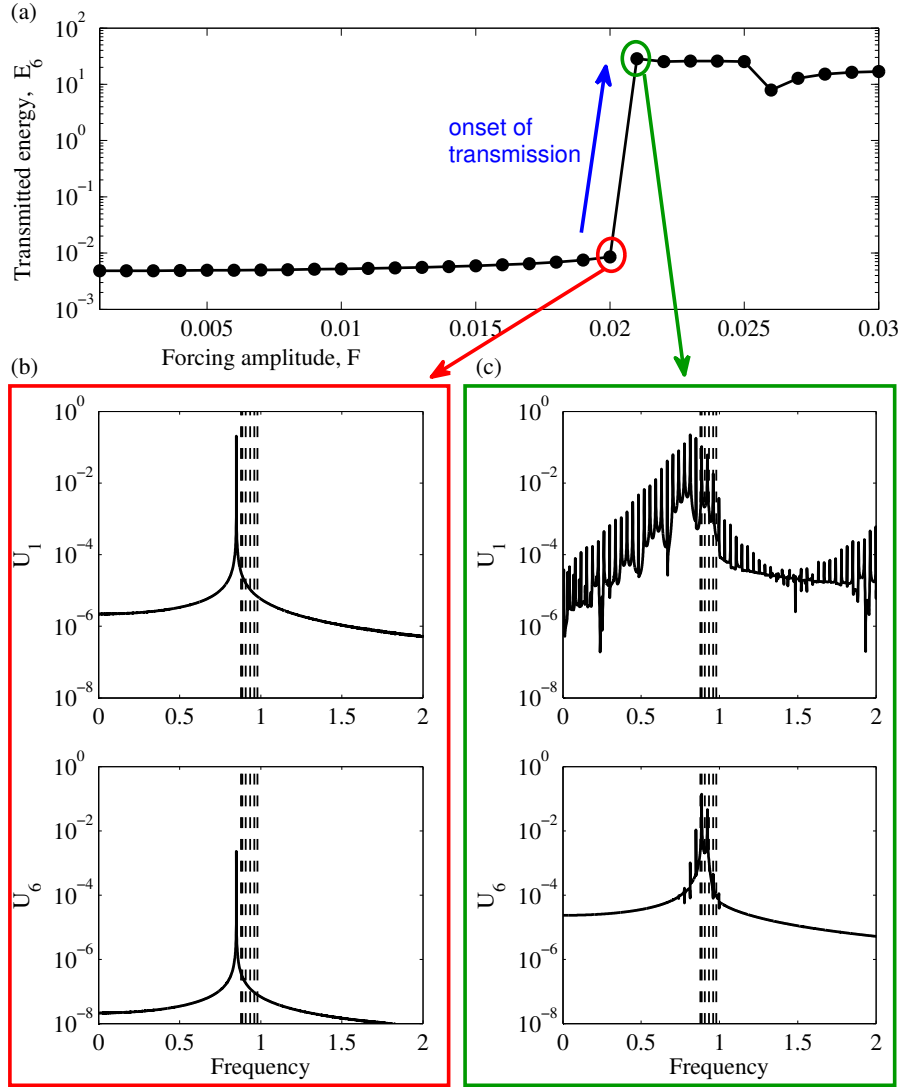


**Figure 2.6:** The supratransmission mechanism for the softening system ( $I = 15$  mA). (a) Energy transmitted to the end of the chain,  $E_6$ , as a function of the driving amplitude,  $F$ , at  $\Omega = 0.85$ . The blue arrow indicates the onset of transmission. (b) Frequency components of the first unit ( $U_1$ ) and last unit ( $U_6$ ) for  $F = 0.020$ , below the transmission threshold at  $\Omega = 0.85$ . (c) Frequency components of the first unit ( $U_1$ ) and last unit ( $U_6$ ) for  $F = 0.021$ , above the transmission threshold at  $\Omega = 0.85$ . The six vertical lines in (a) and (b) indicate the linear natural frequencies of the structure.

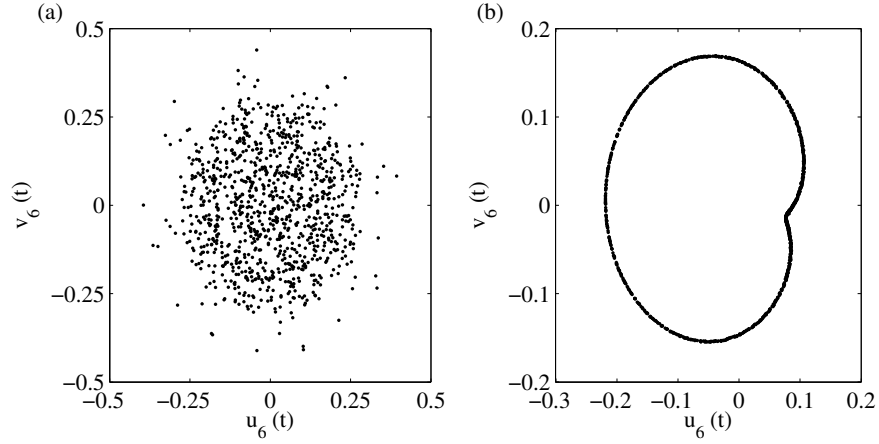


**Figure 2.7:** The projection of the Poincaré map of the response just above the transmission threshold onto the phase space of the last unit. (a) the hardening system at  $F = 0.116$ , (b) the softening system at  $F = 0.021$ . Notice that the post-threshold response of the hardening system is chaotic, while that of the softening system is quasi-periodic.

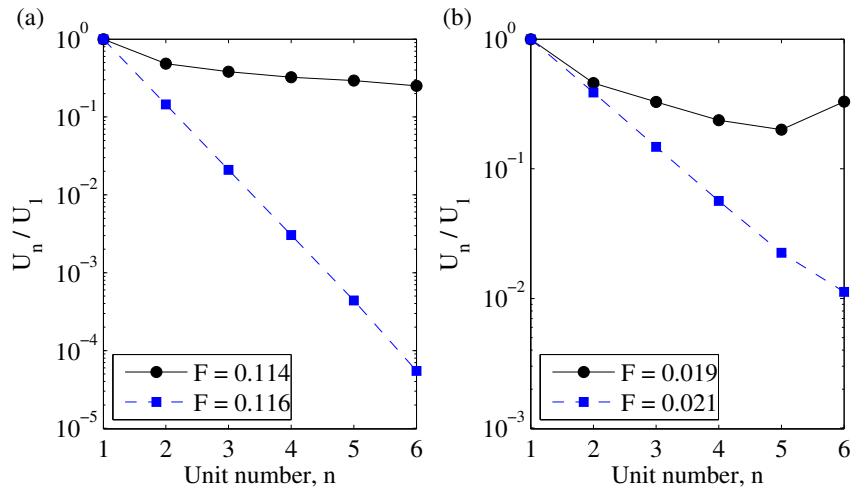


**Figure 2.8:** Normalized amplitude profiles ( $U_n/U_1$ ) for (a) the hardening system and (b) the softening system. In each case, the amplitude profiles below and above the transmission threshold are shown respectively with blue squares and black circles. The amplitude profiles show exponential decay below the threshold, which is a characteristic of linear behavior.

## 2.4 Computing the Supratransmission Threshold

### 2.4.1 Nonlinear Response Manifold (NLRM)

In contrast to the existing literature on supratransmission, we are concerned with periodic structure with damping and finite length. For undamped and infinitely long periodic structures, Maniadis et al. [82] have observed that as the forcing amplitude is increased, transmission starts when the periodic solutions lose their stability. They show that the onset of transmission coincides with the first turning point of the *nonlinear response manifold* (NLRM). This is defined as the manifold of initial conditions with zero initial velocities that give a time-reversible periodic solution at a given driving amplitude [67, 82]. At the first turning point of the NLRM for a non-dissipative system, the stable periodic solution that continues from the linear regime (passing through the trivial equilibrium) collides with another unstable periodic solution that continues from a discrete breather (a non-zero solution corresponding to zero driving amplitude)<sup>1</sup>. The NLRM possesses a turning point at a given forcing frequency provided that the free system supports breather solutions at that frequency [82]. The collision between the continuations of the trivial equilibrium and the discrete breather corresponds to a saddle-node bifurcation, where one of the Floquet multipliers of the dynamical system exits the unit circle on the positive real axis. Further technical details about bifurcations of periodic orbits can be found in [70, Ch. 5].

We compute the NLRM using numerical continuation techniques as implemented in AUTO [26]. This numerical approach allows us to follow the evolution of the steady-state periodic response of the structure as a function of the forcing amplitude, without the need to directly integrate the governing equations at each step. In order to perform this computation, the governing equations are first recast as a boundary value problem and then continuation methods are used to follow the branches of periodic solutions and their subsequent bifurcations; refer to Appendix A for an explanation of this process. Note that there is no need to impose a phase condition to the NLRM in a damped system (as opposed to Hamiltonian

---

<sup>1</sup>Discrete breathers are spatially localized, time-periodic solutions in discrete nonlinear periodic systems; see [5, 10] for more details.

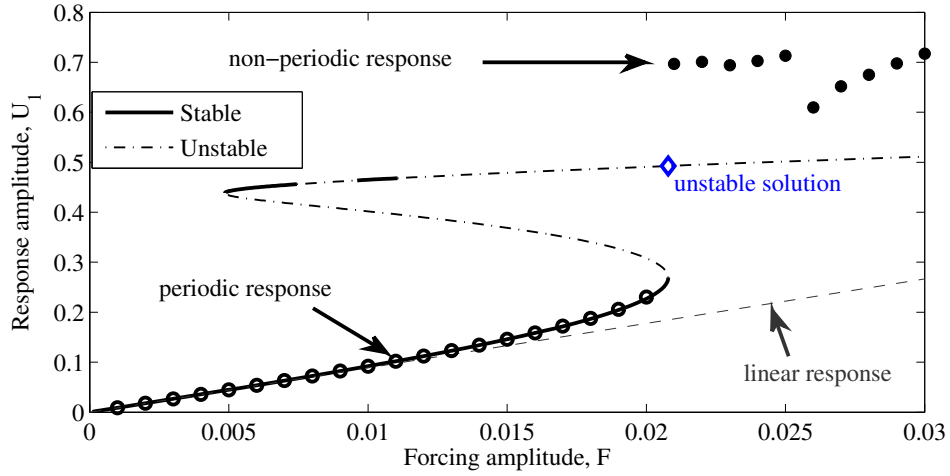


**Figure 2.9:** The projection of the NLRM of the softening system onto the  $U_1 - F$  plane for  $\Omega = 0.85$ . The NLRM is shown using the black curve. The solid section of this curve represents stable solutions and the dashed section represents unstable solutions. The grey dash-dotted line shows the linear response of the structure. The results of direct numerical integration (DNI) are shown using the circle markers. Periodic responses are shown by empty markers and aperiodic responses are shown by filled markers. The blue diamond indicates an unstable periodic solution at the same  $F$  as the first turning point.

systems) because the response frequency and phase are fixed by the external force – we have limit cycles. In fact, the NLRM can be redefined in this case as the manifold of initial conditions on a limit cycle at a given driving amplitude. This definition is trivial, but to keep the connection with the undamped case, we will refer to the response of the forced and damped system as the NLRM as well.

Figure 2.9 shows the NLRM for the softening system at  $\Omega = 0.85$ , along with results from direct numerical integration of the governing equations (2.3). The response is harmonic below the transmission threshold (empty markers) and follows the linear response for small values of driving amplitude. At the first turning point of the NLRM, this harmonic response becomes unstable (through a saddle-node bifurcation) and the response inevitably jumps to another basin of attraction for another attractor, which is aperiodic (filled markers). This jump is accompanied by

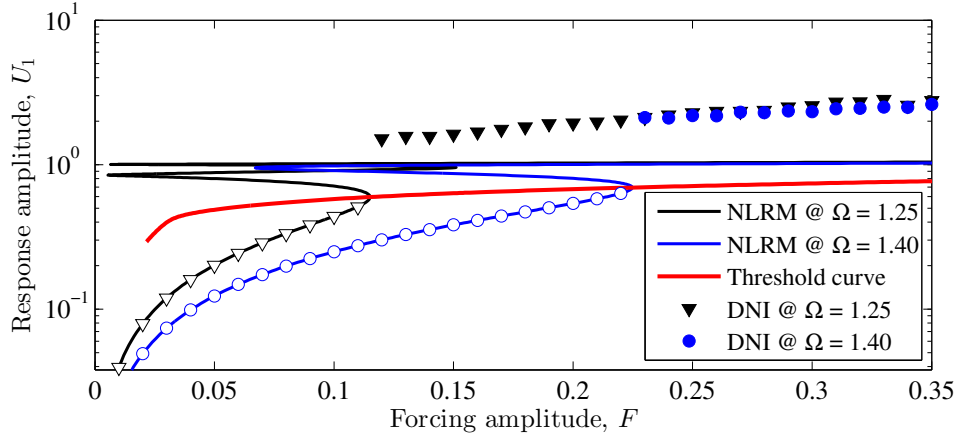


**Figure 2.10:** Evolution of the response (represented by  $U_1$ ) as a function of the driving amplitude for the hardening system. Solid black curve: NLRM at  $\Omega = 1.25$ ; dashed blue curve: NLRM at  $\Omega = 1.40$ . The dash-dotted red curve shows the locus of the first turning points of the NLRM as  $\Omega$  varies. The results of direct numerical integration (DNI) at each driving frequency are shown using the markers: triangles for  $\Omega = 1.25$  and circles for  $\Omega = 1.40$ . Periodic responses are shown by empty markers and aperiodic responses by filled markers. We see that the first turning point in each NLRM coincides with the onset of supratransmission. At the threshold, the response jumps to a different (non-periodic) branch.

a large increase in the energy transmitted to the end of the structure. Note that there is another periodic solution branch right above the first turning point, indicated in Figure 2.9 by the blue diamond. This solution is unstable. If the upper branch were stable, the solution would have jumped to that branch instead, accompanied by a modest increase in energy transmitted, but not an increase of an order of magnitude. It is important to note that the instability of this upper solution branch is a necessary requirement for supratransmission. We are not aware of any other work that highlights this requirement.

Figure 2.10 shows the NLRM for the hardening system at two different forcing frequencies above the linear pass band. Similar to the case of the softening system, the response is harmonic below the transmission threshold (empty markers) and jumps to an aperiodic branch (filled markers) at the first turning point of the NLRM.

Figure 2.10 also shows the transmission threshold curve of the hardening system (red dashed curve). The threshold curve shows the locus of the first turning points of different NLRMs as the driving frequency  $\Omega$  varies. It is worth noting that the threshold curve is a codimension-two manifold, meaning that it is parameterized by two free variables ( $F$  and  $\Omega$  in this case). We see its projection onto the  $U_1 - F$  plane in Figure 2.10. Also, notice that the threshold curve terminates (in a cusp) at a finite value of  $F$ . This is due to the presence of damping, and will be discussed in detail in Section 3.3.

#### 2.4.2 Resonances with the Shifted Pass Band

Repeating the numerical analysis for different values of  $\Omega$  reveals that as the driving frequency is varied within the linear stop band (away from the edge of the pass band), the transmission threshold increases. Moreover, supratransmission occurs above the pass band in the hardening case and below the pass band in the softening case – see Section 3.1 for more details. Also, it is known [14, 128] that nonlinearity can alter the dispersion relation of periodic structures and may shift the location of the pass band depending on the total energy level of the system<sup>2</sup>. Putting all this together, one might be inclined to explain the nonlinear supratransmission phenomenon occurring due to the resonance of the driving force with the shifted pass band of the structure: due to increased amplitudes of motion, the pass band shifts to lower frequencies in the case of softening nonlinearity and the driving force resonates with the shifted pass band. The same argument can be made for frequencies above the pass band in the case of a hardening nonlinearity.

We show here that the true mechanism is indeed the saddle-node bifurcation described in Section 2.4, and the resonance of the driving force with the shifted pass band merely provides a qualitative explanation of the phenomenon. Figure 2.11 compares the edge of the pass band with the transmission threshold for the softening system ( $I = 15$  mA). The lower edge of the pass band is computed as the nonlinear normal mode of (2.17a). The transmission threshold is computed for an undamped system ( $\zeta = 0$ ) as described in Section 2.4.1, and corresponds to the

---

<sup>2</sup>This shift is towards lower frequencies in a structure with softening nonlinearity and towards higher frequencies in the case of a hardening nonlinearity. We can also see this in the amplitude-dependent dispersion relation in (2.16).

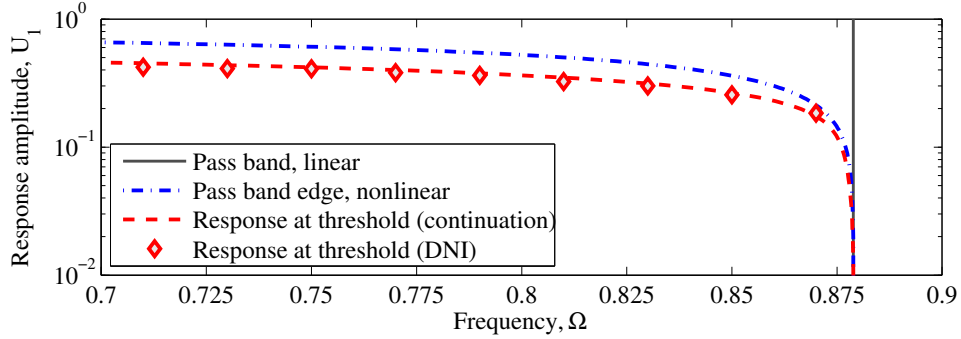


**Figure 2.11:** Comparison of the transmission threshold and the edge of the pass band for the structure with softening nonlinearity. The vertical line shows the lower edge of the pass band for the linear system ( $\omega_1$ ). The dash-dotted blue curve shows the lower edge of the pass band for the nonlinear system, which is computed as the nonlinear normal mode of (2.17a). The dashed red curve shows the amplitude of the first unit,  $U_1$ , at the onset of transmission as a function of the driving frequency. The empty diamond markers show  $U_1$  at the driving amplitude just below the onset of transmission. They are obtained from direct numerical integration (DNI) of the equations of motion (2.3).

point where the periodic solutions lose stability through a saddle-node bifurcation. The onset of transmission is also obtained from direct numerical integration (DNI) of (2.3) at separate driving frequencies. The amplitudes of the first unit,  $U_1$ , at the driving amplitudes just below the threshold are shown for each driving frequency with empty markers. We can see in Figure 2.11 that the results from DNI agree well with the threshold curve. Notice that the threshold curve and the edge of the pass band show a similar trend: they both increase as we move farther into the linear stop band. More importantly, however, we see that the two curves do not match. This is not a surprising feature after all: the threshold curve traces the locus of saddle-node bifurcations while the pass band edge is a nonlinear normal mode (backbone curve) of the structure. These two curves are not expected to coincide. The distinction between these two loci in single forced oscillators is indeed among the early topics discussed in typical textbooks on nonlinear vibrations such as [99, 121].

In conclusion, Figure 2.11 and the accompanying explanation indicate that the

resonance of the driving force with the shifted pass band is not a correct predictor of the onset of transmission from either a quantitative or phenomenological perspective. Similar observations are made for damped structures or in the case of hardening nonlinearity, but the results are not shown here. We will further see in Chapter 3 that the onset of supratransmission is a function of damping, strength of coupling and other system parameters.

## 2.5 Analytical Prediction of the Onset of Supratransmission

### 2.5.1 Analysis Based on Local Nonlinear Dynamics

To find the force threshold for the onset of supratransmission, we look for the onset of instability for the harmonic solutions of the dynamical system. To this end, we first derive the equations governing the evolution of the envelope of harmonic waves using multiple-scale analysis; see [99, Ch. 6] for details of the methodology. We seek solutions to (2.3) of the following form:

$$u_n(t_1, t_2) = \varepsilon \psi_n(t_2) e^{-i\Omega t_1} + c.c. \quad (2.19)$$

where *c.c.* denotes the complex conjugate terms and  $\varepsilon$  is a small parameter. There are two time scales,  $t_1 \propto 1$  and  $t_2 \propto \varepsilon^2$ . The strength of coupling and damping coefficient are small,  $k_c \propto \varepsilon^2$  and  $\gamma \propto \varepsilon^2$ . Because we are looking for the small-amplitude wave envelope, we take the driving amplitude to be small,  $F \propto \varepsilon^2$ . The balance of equations at  $O(\varepsilon)$  is trivial. The same applies to the next order due to the odd nature of the nonlinear force; i.e. only odd orders appear in (2.5). From the balance of equations at  $O(\varepsilon^3)$ , we obtain the following equation for  $\psi_n$ :

$$-2i\Omega \psi_n' - i\beta \psi_n + \sigma_1 \psi_n - 3\alpha \psi_n^2 \psi_n^* + k_c \Delta^2(\psi_n) = f_n/2 \quad (2.20)$$

where an uppercase asterisk denotes complex conjugate, prime denotes differentiation with respect to the slow time scale,  $t_2$ , and  $\Delta^2(\cdot)$  is the same as in (2.3). The

following new parameters have been introduced in (2.20) for ease of reference

$$\beta \equiv 2\zeta\Omega \quad (2.21a)$$

$$\sigma_1 \equiv \omega_1^2 - \Omega^2 \quad (2.21b)$$

$$\alpha \equiv \mu_n a_3 \quad (2.21c)$$

Also,  $\beta = O(\varepsilon^2)$ ,  $\sigma_1 = O(\varepsilon^2)$  and  $\alpha = O(1)$ . Note that because the periodic system is very short (a few number of units) and the coupling between adjacent units is small, a spatial homogenization scheme, as often used in the literature [62, 66, 126], is not appropriate here.

We know that the amplitudes of motion decay rapidly along the structure away from the driven unit. As a first approximation, therefore, we decouple the first unit from the rest of the periodic structure, and look in the reduced system for points where the stability of motion changes (through a saddle-node bifurcation). It is expected that these points can be used to estimate the onset of instability and, therefore, the supratransmission force threshold for the entire structure. We note that this approximation may only be valid in the limit of very weak coupling, also known as the *anti-continuum limit*. See [82] for a similar approach.

The dynamic reduction of the periodic structure to a single unit depends on the location of the driving frequency relative to the linear pass band. In a system with softening type of nonlinearity, supratransmission occurs below the lower edge of the pass band. In hardening systems, on the other hand, supratransmission occurs above the upper edge of the pass band. Adjacent units move in phase with each other at the lower edge and out of phase at the upper edge. Therefore, before truncating (2.20) at  $n = 1$ , we take  $\Delta^2(\psi_n) = 0$  in the softening case and  $\Delta^2(\psi_n) = 4\psi_n$  in the hardening case. We note that this argument is valid for an infinite periodic structure. In a finite structure, as discussed in Section 2.2.2, only one of the edges of the pass band coincides with those of the infinite structure. As a result, taking  $\Delta^2(\psi_n) = 4\psi_n$  above the pass band is an approximation in our periodic structure because of the free-free boundary conditions.

With these considerations in mind, the wave envelope equation (2.20) reduces

to the following:

$$-2i\Omega\psi_1' - i\beta\psi_1 + \sigma\psi_1 - 3\alpha\psi_1^2\psi_1^* = F/2 \quad (2.22)$$

where  $\sigma$  represents the distance of the driving frequency from the closest edge of the pass band, defined differently based on the type of nonlinearity:

$$\sigma \equiv \begin{cases} \omega_1^2 - \Omega^2 = \sigma_1, & \text{softening} \\ \omega_1^2 + 4k_c - \Omega^2 = \sigma_1 + 4k_c, & \text{hardening} \end{cases} \quad (2.23)$$

We take the solution of (2.22) to be  $\psi_1 = A_1 \exp(i\theta_1)$ . Using this solution and looking for the steady-state response, we arrive at the following equations for  $A_1$  and  $\theta_1$ :

$$\beta A_1 = (F/2) \sin \theta_1 \quad (2.24a)$$

$$3\alpha A_1^3 + \sigma A_1 = (F/2) \cos \theta_1 \quad (2.24b)$$

We eliminate  $\theta_1$  from (2.24) to get the response curve for  $\psi_1$ :

$$(\beta A_1)^2 + (3\alpha A_1^3 + \sigma A_1)^2 - (F/2)^2 = 0 \quad (2.25)$$

which can be used to plot the approximate NLRM at a given  $\Omega$ . Notice that (2.25) depends on  $\Omega$  through the parameter  $\sigma$ , defined in (2.23).

Equation (2.25) can be rearranged as a cubic equation in  $A_1^2$ . For the NLRM to have turning points, it is required that this cubic equation have three real roots. The onset of supratransmission, where there is a turning point (saddle-node bifurcation) in the NLRM, corresponds to points where the cubic equation has three real roots with two of them being equal [50]. To satisfy this condition, a certain relation should hold between the coefficients of the cubic equation [1, Ch. 3]. This results in the following relation for the value of driving amplitude that corresponds to loss of stability:

$$F_{th,1}^2 = \frac{-8}{81\alpha} \left( \sigma(\sigma^2 + 9\beta^2) \pm (\sigma^2 - 3\beta^2)^{3/2} \right) \quad (2.26)$$

The subscript 1 has been used to emphasize that one unit is used in the approx-

imation. Supratransmission is possible (i.e. the NLRM possesses a saddle-node bifurcation) provided that the right-hand side of (2.26) is real and positive; otherwise, the NLRM does not have a turning point.

It is worth emphasizing that (2.26) traces (within the approximation limits) the locus of the first saddle-node bifurcation of the NLRM. Any other bifurcation of the NLRM will go unnoticed by this formulation.

## 2.5.2 Comparison with Numerical Computations

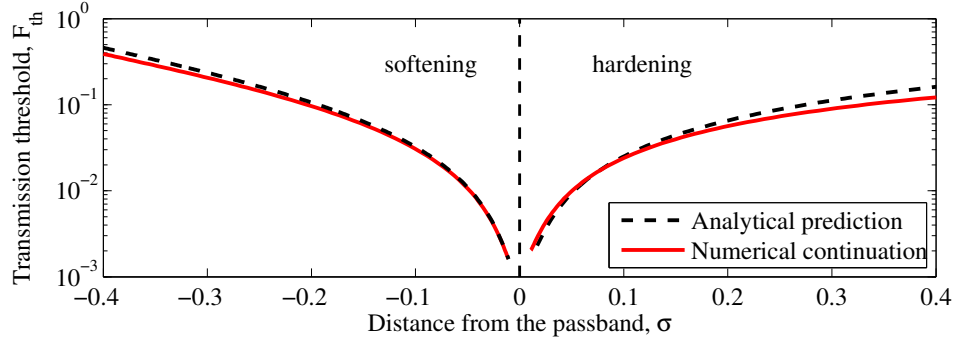
To validate the analytical estimate of the supratransmission force threshold, we compare the threshold curves predicted by (2.26) with numerical results obtained using continuation methods. Given that the analysis is performed assuming very weak coupling between adjacent units, our immediate goal is to show that the results are valid in the parameter range where they were derived. Accordingly, we use a value of  $k_c = 0.001$  for coupling in this section. We will further explore (and update) the validity of the locally nonlinear analysis throughout Chapter 3 and in Section 4.4.

Figure 2.12 shows the supratransmission threshold curves as a function of  $\sigma$ , the distance from the pass band edge. The red solid curves are obtained numerically from the governing equations (2.9), and threshold curves predicted by (2.26) are shown using the black dashed curves. Using  $\sigma$  allows us to compare the softening and hardening systems on the same plot. We see for the structure with softening nonlinearity that the analytical estimate predicts the threshold curve accurately, especially close to the pass band edge ( $\sigma = 0$ ) where the force threshold is lower. A similar observation is made for the structure with hardening nonlinearity. Compared to the softening system, the onset of transmission for the hardening system is predicted less accurately. This discrepancy between analytical and computational results occurs due to the finite size of the structure, as anticipated during the derivation<sup>3</sup>. Figure 2.12 also shows that as the forcing frequency moves farther into the stop band (as  $|\sigma|$  increases) the accuracy of the analysis decreases. This is because the force threshold increases with  $|\sigma|$ , making contributions from higher nonlinear

---

<sup>3</sup>Recall that the analysis in Section 2.5.1 is based on an infinite periodic structure. Because we are dealing with a finite structure, one of the lower or upper edges of the pass band is inevitably predicted inaccurately.

terms more significant.



**Figure 2.12:** The supratransmission threshold curves for a weakly coupled structure as a function of  $\sigma$ , the distance from the pass band edge.  $\sigma < 0$  for the structure with softening nonlinearity ( $I = 15$  mA) and  $\sigma > 0$  for the structure with hardening nonlinearity ( $I = -15$  mA). The solid curves are obtained using numerical continuation and dotted curves are obtained from (2.26) based on the local nonlinear dynamics of the driven unit. The vertical line denotes the pass band edge, where  $\sigma = 0$  for both the hardening and softening structures.

In summary, prediction of the onset of supratransmission based on the local nonlinear dynamics of the driven unit can be used to explain the supratransmission phenomenon for very weak values of coupling. The results from this analysis are more reliable from a *qualitative perspective* as opposed to a quantitative point of view.

## 2.6 Concluding Remarks

In this chapter, we studied the supratransmission phenomenon in a discrete nonlinear periodic structure with damping and finite length. This essentially nonlinear phenomenon occurs when the periodic structure is harmonically forced at one end with a forcing frequency lying within its linear stop band. Beyond a certain threshold of forcing amplitude, supratransmission occurs due to loss of stability of the periodic solutions that are initially localized to the driven unit. At the onset of supratransmission, the response of the system moves from the basin of attraction of a limit cycle to that of a non-periodic attractor – this non-periodic attractor may

be either quasi-periodic or chaotic. Supratransmission is accompanied by a very large increase (orders of magnitude) in the energy transmitted through the periodic structure. The frequency spectra of the nonlinearly transmitted waves lie inside the linear pass band of the periodic structure.

We reviewed the instability mechanism leading to supratransmission using direct numerical simulations and numerical continuation techniques. We showed that the onset of supratransmission coincides with the first turning point (saddle-node bifurcation) of the nonlinear response manifold (NLRM) of the damped, finite structure. This is the same mechanism that leads to supratransmission in infinite-dimensional Hamiltonian systems. We also highlighted that the onset of supratransmission does not necessarily coincide with the resonance of the driving force with the shifted pass band at higher amplitudes of motion.

Furthermore, based on the local nonlinear dynamics of the driven unit, we obtained closed-form analytical expressions for predicting the onset of supratransmission in weakly coupled periodic structures. This approximate formulation is based on finding the saddle-node bifurcations of the NLRM. For both hardening and softening types of nonlinearity, we verified the validity of the analytical estimates by comparing them with results obtained from numerical continuation for a weakly coupled periodic structure.

## Chapter 3

# Parametric Study

Supratransmission is a generic instability-driven transmission phenomenon in discrete nonlinear periodic structures. In this chapter, we explore how supratransmission depends on various system parameters. The following parameters are considered: type and strength of nonlinearity, number of units, damping and strength of coupling. We highlight the importance of forcing frequency by contrasting supratransmission with the case of harmonic excitation within a pass band. We also briefly address the hysteresis phenomenon accompanying supratransmission, as well as broadband energy propagation at very high driving amplitudes. The influence of structural irregularities (disorder) is addressed separately in Chapter 4.

### 3.1 Type and Strength of Nonlinearity

The most significant role of the type of nonlinearity (softening or hardening) is to determine on which side of the pass band supratransmission may occur. Supratransmission may be observed below the pass band for a structure with softening nonlinearity, and above it for a structure with hardening nonlinearity. The reason is that the NLRM possesses a turning point (saddle-node bifurcation) only on one side of the pass band<sup>1</sup>.

We can use the formula (2.26) to determine the dependence of supratransmission on the type of nonlinearity. To exclude the influence of damping, we consider

---

<sup>1</sup> We cannot rule out the possibility that the NLRM may lose stability through other bifurcations on the other side of the pass band. We are not aware of any work addressing this aspect.

the undamped structure ( $\beta = 0$ ). For the undamped case, (2.26) reduced to the following:

$$F_{th,1} = \frac{4}{9} \sqrt{\frac{\sigma^3}{-\alpha}} \quad (3.1)$$

In order to get a positive real value on the right-hand side of (3.1),  $\sigma$  and  $\alpha$  should have opposite signs. In the case of softening nonlinearity, we have  $\alpha < 0$  and supratransmission occurs when  $\sigma > 0$ ; i.e. for  $\Omega < \omega_1$ , below the linear pass band. Likewise, we have  $\alpha > 0$  for a hardening nonlinear force and supratransmission may occur when  $\sigma < 0$ , which is above the pass band. A similar observation has been made based on the symmetries of the the wave envelope equations in [122].

Regarding the strength of nonlinearity, we see from (3.1) that increasing  $|\alpha|$  reduces the force threshold at the onset of supratransmission for both softening and hardening types of nonlinearity. The same observation can be made using (2.26) for the onset of supratransmission in damped structures.

## 3.2 Number of Units

The question we are addressing in this section is whether the number of units ( $N$ ) has a qualitative effect on the supratransmission phenomenon. To this end, we focus on the undamped structure ( $\zeta = 0$ )<sup>2</sup>. For an undamped structure, we already know from the literature [39, 82, 122] that supratransmission exists for infinitely long periodic structures. We showed in Chapter 2 that supratransmission also exists in a very short periodic structure with  $N = 6$ . Here, we explore the influence of  $N$  on the threshold curves for small and moderate  $N$ , with  $N \in \{5, 10, 15, 20\}$ . We consider both softening and hardening types of nonlinearity, with the nonlinear force in (2.5) adjusted such that the coefficient of its cubic term is  $k_3 = \pm 0.2$ . The default value of  $k_c = 0.05$  is used for the strength of coupling.

Figure 3.1 shows the threshold curves as a function of  $\sigma$  for different values of  $N$ . These threshold curves are obtained using numerical continuation, as explained in Section 2.4. We see that for both types of nonlinearity, the influence of  $N$  is

---

<sup>2</sup>In the presence of damping, energy dissipation will prevail nonlinearity (as well as disorder) for large  $N$ . No information thus reaches the end of the chain; i.e.  $E_N$  from (2.18) is exponentially small. From that perspective, it would not matter whether supratransmission occurs for large  $N$  or not.

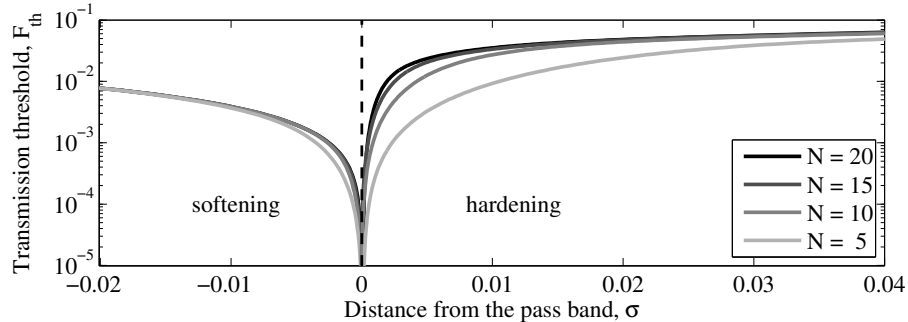


**Figure 3.1:** Threshold curves as a function of  $\sigma$  for different values of  $N$ . The periodic structure has free-free boundary conditions.  $\sigma < 0$  for the structure with softening nonlinearity ( $k_3 = -0.2$ ) and  $\sigma > 0$  for the structure with hardening nonlinearity ( $k_3 = +0.2$ ). For both structures, the transmission threshold  $F_{th}$  increases with  $N$ , but only at driving frequencies very close to a pass band edge. The hardening system is more sensitive to  $N$  than the softening system.

significant only in the close vicinity of the edge of the pass band (near  $\sigma = 0$ ). As expected, this difference decreases by increasing the number of units.

Furthermore, we see in Figure 3.1 that the structure with hardening nonlinearity is more sensitive to  $N$  than the softening structure; in fact, the structure with softening nonlinearity is almost insensitive to  $N$ . We explain this based on the boundary conditions of the entire periodic structure. Recall from Section 2.1 that the periodic structure studied in this work is subject to free boundary conditions at both ends (Figure 2.1). For the finite structure, this means that the lower edge of the pass band does not change with  $N$ . Thus, varying  $N$  has a minimal effect on the dynamics of the softening periodic structure below the pass band. To support our claim, we repeat the computations of Figure 3.1 for the same periodic structure, but with fixed boundary conditions at both ends. We show the results of these computations in Figure 3.2. We see that the dependence of threshold curves on  $N$  is now similar for both types of nonlinearity. For both boundary conditions, the influence of  $N$  on threshold curves is significant only for very small values of  $|\sigma|$ .

In summary, increasing the number of units can increase the force threshold at the onset of supratransmission at driving frequencies very close to the edge of a pass band.

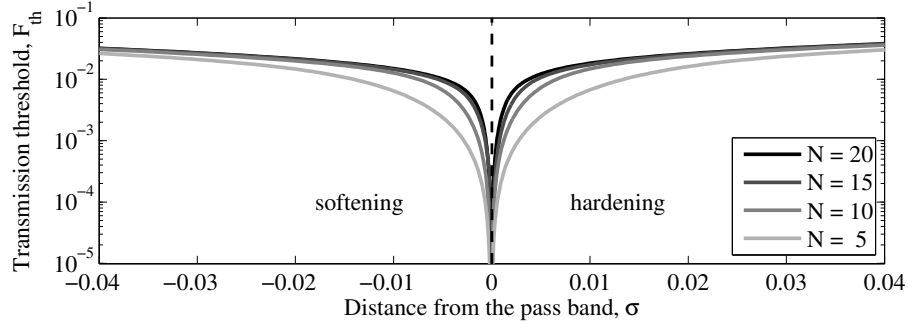


**Figure 3.2:** Threshold curves as a function of  $\sigma$  for different values of  $N$ . The periodic structure has fixed-fixed boundary conditions; c.f. Figure 3.1. The number of units plays a significant role only in the close vicinity of the edge of the pass band (near  $\sigma = 0$ ).

Note that Figure 3.2 is the only instance where we consider a fixed-fixed boundary condition throughout the thesis. In all other analyses, based on the mechanical structure of Figure 2.1, we use free-free boundary conditions. In the remainder of this chapter, in accordance with Chapter 2, we use a structure with six units.

### 3.3 Damping

As we have already seen in Figure 2.10, the first turning point of the NLRM occurs at a higher driving amplitude as the forcing frequency moves farther from the linear pass band. For an undamped structure, the force threshold goes to zero when the forcing frequency reaches the pass band. In other words, the threshold curve has a vertical asymptote in the  $(F - \Omega)$  plane, coinciding with the edge of the pass band (at  $\sigma = 0$ ). Therefore the NLRM for an undamped structure has a turning point for all forcing frequencies in the stop band – this only happens on one side of the pass band as already explained in Section 3.1.

The topology of the NLRM depends on the amount of damping in the structure. Figure 3.3 shows the NLRM at  $\Omega = 1.25$  for  $I = -15$  mA (hardening) and different values of damping. We can see that the structure of the undamped NLRM is qualitatively different from that of a damped NLRM. In the undamped case, the NLRM crosses the zero-force axis ( $F = 0$ ) after the first turning point. These crossing points correspond to discrete breathers, which are non-zero harmonic solutions in

the unforced undamped periodic structure that are spatially localized to the driven unit<sup>3</sup>. The amplitude profiles of the two discrete breathers are shown in Figure 3.3 in the insets. The damped NLRMs do not cross the zero-force axis because the damped structure cannot sustain steady-state motion with non-zero amplitude. The damped NLRM will have a second turning point for non-zero values of damping below a certain threshold – see also [81]. The existence of subsequent turning points or other bifurcations of the NLRM depends strongly on the nature of the nonlinear force among other parameters.

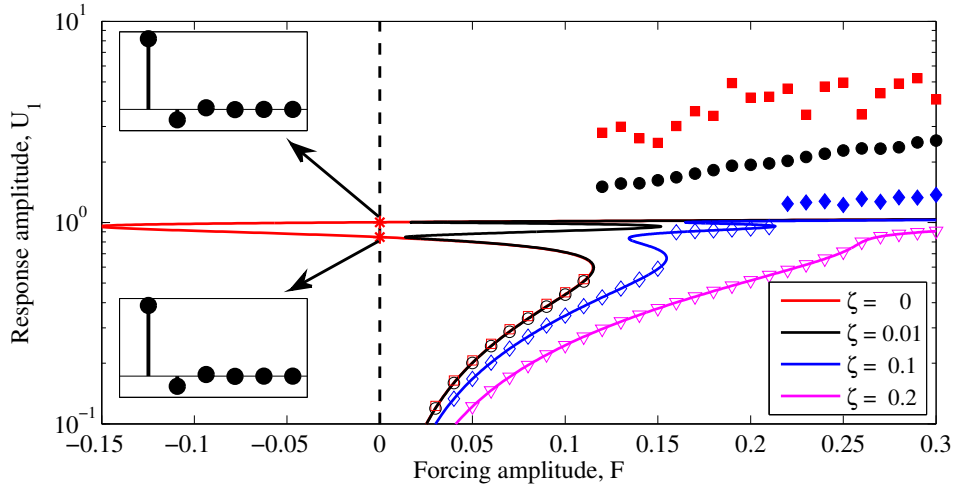


**Figure 3.3:** The NLRM of the hardening system at  $\Omega = 1.25$  and different values of damping are shown by the curves without markers. The results of direct numerical integration at each damping value are shown using the markers: red squares,  $\zeta = 0$ ; black circles,  $\zeta = 0.01$ ; blue diamonds,  $\zeta = 0.1$ ; magenta triangles,  $\zeta = 0.2$ . Periodic responses are shown by empty markers and non-periodic responses are shown by filled markers. Increasing the damping ratio eventually eliminates the turning point of the NLRM. We also observe an intermediate stage ( $\zeta = 0.1$ ) where the onset of supratransmission is delayed until the third turning point of the NLRM. The intersections of the undamped NLRM with the zero-force axis, shown by red stars, correspond to discrete breathers. The insets show the amplitude profiles of these discrete breathers.

<sup>3</sup>The NLRM of the undamped structure may cross the zero-force axis many times. We show only two of these crossings in Figure 3.3. See [82] for more details about the zero-crossings and the associated discrete breathers.

Comparing the NLRMs at non-zero damping values, we see in Figure 3.3 that as damping increases the first turning point occurs at a higher driving amplitude. Moreover, the second turning point moves to the right (higher driving amplitudes) at a higher rate than the first turning point and the distance between the two turning points decreases. Eventually, there exists a threshold for the damping coefficient ( $\zeta = 0.160$  in this case) above which the two turning points merge and disappear. The NLRM above this threshold does not have a turning point.

There is an intermediate stage during this transition,  $\zeta = 0.1$  in Figure 3.3, where the low-amplitude periodic solution jumps to a secondary (stable) periodic branch before supratransmission occurs. In this case, in contrast to the behavior of undamped structures, supratransmission does not occur at the first turning point of the NLRM. Instead, it is delayed until subsequent turning points<sup>4</sup>. We conclude that damping changes the topology of the NLRM and may effectively delay or completely eliminate the onset of supratransmission.

We can use (2.26) to study the influence of damping on the transmission threshold in more detail. In an undamped system ( $\beta = 0$ ), the transmission threshold goes to zero at the edge of the linear pass band; i.e.  $F_{th} = 0$  if  $\sigma = 0$ . In order to obtain a real value for  $F_1$  in the damped case ( $\beta \neq 0$ ), it is required that  $\sigma^2 - 3\beta^2 > 0$  in (2.26). There is therefore a frequency range in the immediate vicinity of the pass band in which the NLRM does not have a turning point and supratransmission cannot occur. The critical value  $\sigma_{cr}$  at which transmission starts can be obtained by setting  $\sigma^2 - 3\beta^2 = 0$ . Recalling the definition of  $\sigma$  from (2.22), this can be written in terms of the critical forcing frequency, denoted by  $\Omega_{cr}$ , as follows:

$$\Omega_{cr} = \begin{cases} \sqrt{\omega_u^2 + 3\zeta^2} + \sqrt{3}\zeta \approx \omega_u + \sqrt{3}\zeta, & \alpha > 0 \\ \sqrt{\omega_l^2 + 3\zeta^2} - \sqrt{3}\zeta \approx \omega_l - \sqrt{3}\zeta, & \alpha < 0 \end{cases} \quad (3.2)$$

where the approximations are made for small damping ( $\zeta \ll 1$ ). We see in (3.2) that as damping increases, the onset of supratransmission occurs at a forcing frequency farther from the pass band. Accordingly, the value of forcing amplitude required at

---

<sup>4</sup> In Section 4.2, we further elaborate on this non-trivial effect of damping, where we also highlight the additional role played by disorder in this context.

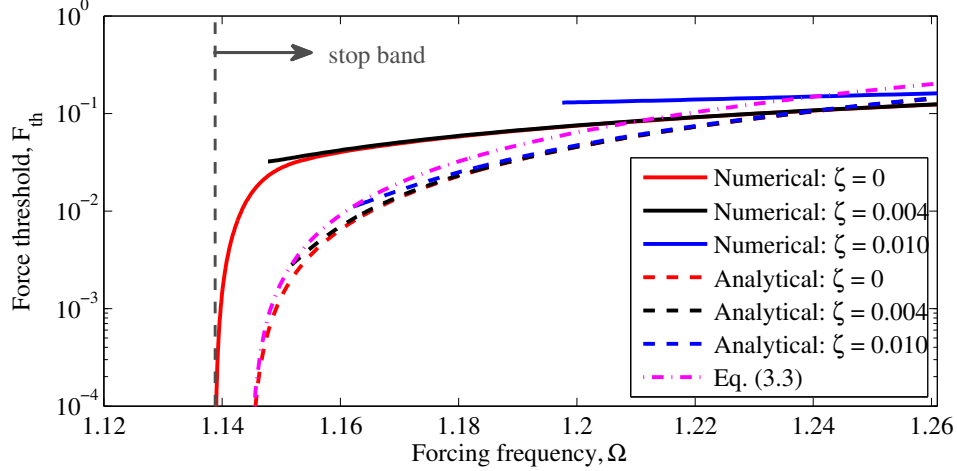


**Figure 3.4:** The transmission threshold curves for the structure with hardening nonlinearity at different values of damping. Solid curves are obtained using numerical continuation and dashed curves are from the analytical solution (2.26). Red:  $\zeta = 0$ ; black:  $\zeta = 0.004$ ; blue:  $\zeta = 0.010$ . The magenta dash-dotted curve, obtained from (3.3), shows the locus of the critical values of  $F$  and  $\Omega$  at the onset of supratransmission. The vertical grey line shows the upper edge of the pass band ( $\omega_6 \approx 1.139$ ).

$\Omega_{cr}$  for the onset of supratransmission, denoted by  $F_{cr}$ , can be obtained from (2.26):

$$F_{cr} = \begin{cases} \sqrt{\frac{32}{81|\alpha|}(\Omega_{cr}^2 - \omega_u^2)^3}, & \alpha > 0 \\ \sqrt{\frac{32}{81|\alpha|}(\omega_1^2 - \Omega_{cr}^2)^3}, & \alpha < 0 \end{cases} \quad (3.3)$$

This is the minimum force required in a damped periodic structure to trigger the supratransmission phenomenon. This behavior is in contrast to that of undamped structures where the minimum force amplitude required approaches zero as the forcing frequency approaches the pass band (notice that  $F_{cr} = 0$  for  $\zeta = 0$ ).

Figure 3.4 shows the threshold curves of the structure with hardening nonlinearity for different values of damping. The solid curves are obtained using numerical continuation, and threshold curves predicted by (2.26) are shown by the

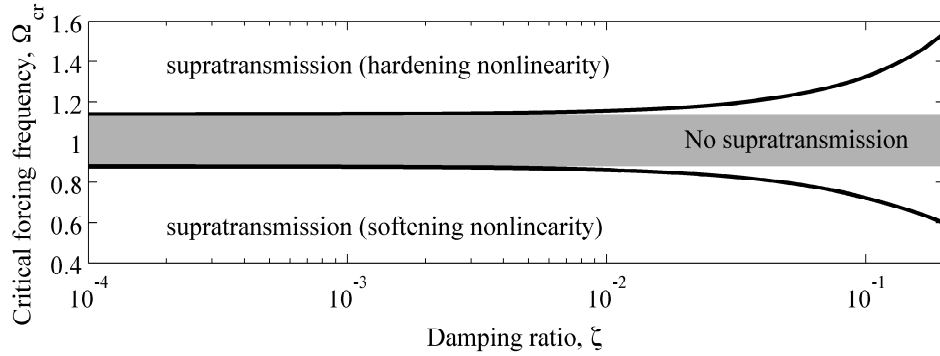


**Figure 3.5:** The dependence of supratransmission on damping ratio for hardening and softening types of nonlinearity. The solid curves, obtained from (3.2), depict the boundaries between regions where supratransmission may exist and where supratransmission does not exist. The grey area corresponds to the linear pass band of the structure.

dashed curves. We see that the threshold force goes to zero at the edge of the linear pass band in the undamped structure (the red solid curve). We also observe a discrepancy between numerical computations and analytical predictions (for example, compare the two red curves). This is because the analysis is based on an infinite periodic structure, in which the upper edge of the pass band is at  $\omega_u$ . The upper edge of the pass band in the finite system is slightly lower than  $\omega_u$ , as explained in Section 2.2.2. For nonzero values of damping, the minimum forcing amplitude required for supratransmission to occur is nonzero and occurs at a forcing frequency away from the linear pass band. The locus of the critical forcing frequency and amplitude at the onset of transmission is given by (3.3), which is shown by the dash-dotted curve in Figure 3.4. This locus is the upper envelope of the threshold curves. All transmission threshold curves lie between the undamped threshold curve and the locus of the critical value; i.e. (3.1) and (3.3), respectively.

Figure 3.5 shows the critical frequency at the onset of supratransmission,  $\Omega_{cr}$ , as a function of damping ratio,  $\zeta$ , for both types of nonlinearity. The two solid curves split the  $(\Omega - \zeta)$  plane into areas where supratransmission may occur, divided by an area where supratransmission does not exist. The boundaries are obtained from (3.2). For very low values of damping, the prohibited region is mostly

comprised of the linear pass band. As damping increases, the critical forcing frequencies moves away from the edges of the pass bands. It is crucial to note that derivation of (3.2) is based on the locus of the first turning point (saddle-node bifurcation) of the nonlinear response manifold – recall the analysis in Section 2.5.1. We cannot definitively rule out the possibility that once the first turning point is eliminated by damping, the NLRM will remain stable for all values of forcing amplitude. Nevertheless, we have not observed this in our numerical investigations, nor has such behavior been reported in the literature.

In summary, damping (i) introduces a threshold on the minimum forcing amplitude required for supratransmission to occur (ii) may delay the onset of supratransmission until the third turning point of the NLRM, (iii) may eliminate a range of frequencies from the stop band in which supratransmission occurs. Although the predicted critical values of forcing amplitude and frequency are only fairly accurate, we can still use (2.26) and (3.3) to qualitatively explain the influence of damping on the supratransmission phenomenon.

### 3.4 Strength of Coupling

The strength of coupling,  $k_c$ , is directly related to the width of the pass band, as shown in (2.15). Increasing the strength of coupling widens the linear pass band of the structure, in particular by moving the upper edge of the pass band to higher frequencies. Therefore, if the driving frequency is fixed above the pass band and  $k_c$  is increased, the linear pass band eventually reaches the driving frequency and energy transmission occurs through resonance with the linear modes of the structure. This essentially linear phenomenon may occur in a nonlinear system as well, and is not further discussed here. Instead, we study the influence of the strength of coupling on the (nonlinear) supratransmission phenomenon.

The analysis in Section 2.5.1 is based on reducing the dynamics of the periodic structure to that of a single unit (the driven unit). That analysis is therefore unable to account for the strength of coupling. We begin this section by updating our prediction of the onset of instability to account for the strength of coupling. To improve our reduced model, we truncate the periodic structure at the second unit instead of the first one. In this new reduced model, the first unit is taken to be

the same as that of the original periodic structure and the second unit is assumed to be linear. This approximation is appropriate for small but non-zero values of coupling; note that (2.26) is only valid for  $k_c = 0$ .

For the reduced system with two degrees of freedom, we can proceed in the same way as in Section 2.5.1 for the one-unit approximation to obtain the response curve. The equation describing the loci of turning points (saddle-node bifurcation) of the NLRM of the reduced system can then be obtained in the same way that (2.26) was derived from (2.25). Thus, the value of force threshold that corresponds to loss of stability of periodic solutions is found to be:

$$F_{th,2}^2 = \frac{-8}{81\alpha} \left( S(S^2 + 9T^2) \pm (S^2 - 3T^2)^{3/2} \right) \quad (3.4)$$

where the subscript 2 is used to emphasize that two units are used in the approximation, and  $S$  and  $T$  are defined as below:

$$S \equiv (\sigma + k_c)(1 - R) \quad (3.5a)$$

$$T \equiv \beta(1 + R) \quad (3.5b)$$

$R$  denotes the ratio of the amplitudes of the two units:

$$R \equiv \left( \frac{A_2}{A_1} \right)^2 = \frac{k_c^2}{\beta^2 + (\sigma + k_c)^2} \quad (3.6)$$

where  $A_1$  and  $A_2$  are the amplitudes of the driven unit ( $n = 1$ ) and the linear unit ( $n = 2$ ), respectively. As expected, we obtain  $F_{th,2} = F_{th,1}$  for  $k_c = 0$ .

Figure 3.6 shows the supratransmission threshold curves at three different strengths of coupling as a function of  $\sigma$ , the distance from the pass band edge. Using  $\sigma$  allows us to compare the softening system ( $I = 15$  mA) and hardening system ( $I = -15$  mA) on the same plot. The solid curves are obtained using numerical continuation, as described in Section 2.4. For both the structures with softening and hardening nonlinearities, we see that increasing the strength of coupling does not have a significant influence on the critical frequency at which supratransmission starts. The minimum forcing amplitude for the onset of supratransmission, however, increases with the strength of coupling. In fact, the supratransmission thresh-

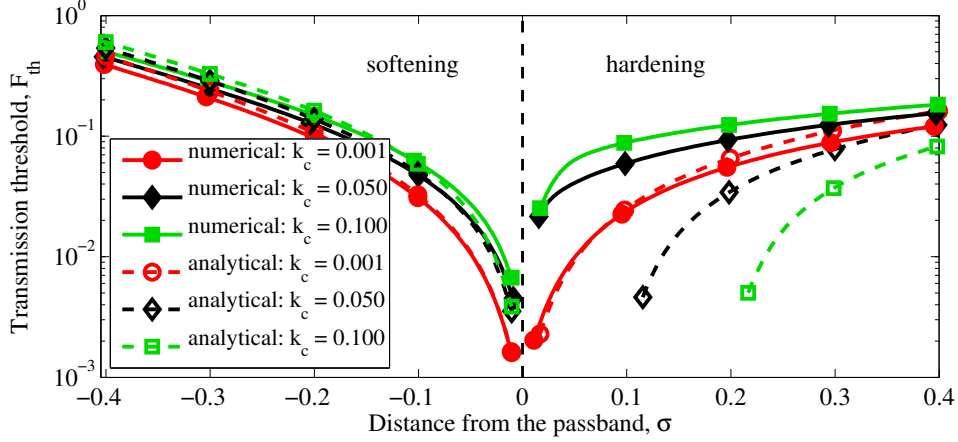


**Figure 3.6:** The transmission threshold curves at different strengths of coupling as a function of  $\sigma$ .  $\sigma < 0$  for the softening system and  $\sigma > 0$  for the hardening system. Three coupling coefficients are used in each case; red:  $k_c = 0.001$ , black:  $k_c = 0.050$ , green:  $k_c = 0.100$ . Solid curves are obtained using numerical continuation and dashed curves are from the analytical solution (3.4). The vertical line denotes the pass band edge.

old is increased at all forcing frequencies if the coupling becomes stronger. This is true even in an undamped structure for which the threshold curve approaches zero at the edge of the pass band [82].

The dashed curves in Figure 3.6 show predictions of the threshold curves based on (3.4). We see that the reduced model can capture the behavior of the threshold curves only at very weak coupling,  $\kappa = 0.001$ . For higher strengths of coupling, the reduced model can still capture the qualitative behavior of the softening system, but not that of the hardening system. Specifically, it fails in predicting the critical forcing frequency and amplitude at the onset of supratransmission in the structure with hardening nonlinearity. Two reasons contribute to this: (a) reducing the periodic structure to two units only works in the limit of weak coupling; (b) the upper linear natural frequency of the reduced model (two degrees of freedom) is lower than that of the full model (six degrees of freedom). While the former is an intrinsic limitation of the reduced model, the latter can be improved by offsetting the threshold curves with respect to their corresponding edge of the pass band (not shown here).

In summary, increasing the strength of coupling (i) increases the minimum force amplitude required for the onset of supratransmission; (ii) does not change the frequency location of the onset of supratransmission significantly with respect to the nearest edge of the pass band.

### 3.5 Forcing Amplitude: Hysteresis

Associated with a saddle-node bifurcation, one normally expects to observe the hysteresis phenomenon. This results from the co-existence of two (or more) stable solutions near the bifurcation point. As expected, hysteresis can also be observed near the supratransmission threshold.

In order to observe the hysteresis effect, a different numerical approach is required than the one used in Section 2.3. The approach we use here is based on sweeping the driving amplitude back and forth near the supratransmission threshold; this method can also be used in experiments. We start from a small forcing amplitude below the threshold,  $F = 0.09$  in Figure 3.7. Once the steady state is reached, the forcing amplitude is smoothly increased in small increments, and a new steady state is obtained at each step (black circle markers). Once we pass the supratransmission threshold, we reverse this procedure and decrease the forcing amplitude stepwise (blue square markers). Figure 3.7 shows the results of this computation for the structure with hardening nonlinearity ( $I = -15$  mA) at  $\Omega = 1.25$ . We can clearly observe the hysteresis phenomenon.

The hysteresis associated with supratransmission has been previously studied both theoretically and experimentally; e.g. see [51, 62, 66]. Further discussion of the hysteresis effect, such as the influence of sweeping parameters on the observed width of the hysteresis gap, is not within the scope of the present work.

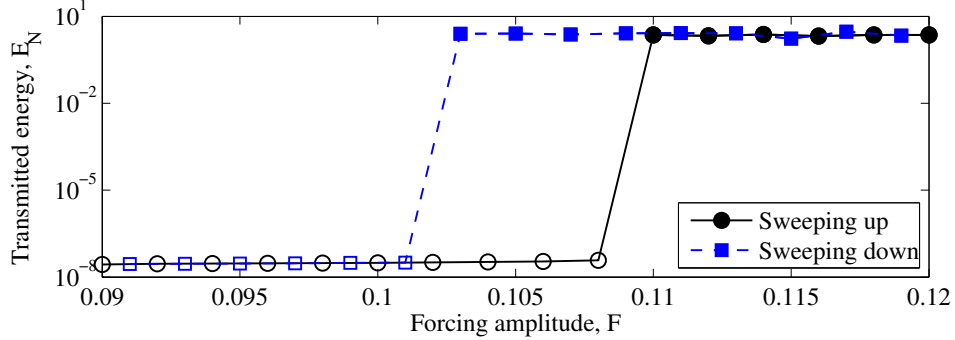


**Figure 3.7:** The hysteresis effect at  $\Omega = 1.25$  for the structure with hardening nonlinearity. Black circle markers correspond to up-sweep of  $F$  and blue square markers correspond to sweeping  $F$  down. Empty markers denote periodic solutions and filled markers denote non-periodic response.

### 3.6 Forcing Frequency

The driving frequency plays a crucial role in determining the energy transmission characteristics of a nonlinear periodic structure. To highlight this, we compare supratransmission (driving within a stop band) to the case in which a periodic structure is driven within its pass band. When the driving frequency lies within the pass band, energy transmission occurs in a linear fashion at low driving amplitudes, with a small decay occurring due to dissipative forces – see Figure 2.3. These linear solutions eventually lose their stability if the driving amplitude is increased. This loss of stability is not usually accompanied by a large increase in the transmitted energy, in strong contrast with what happens for stop band excitation. We show this for a periodic structure with the following parameters:  $k_c = 0.05$ ,  $\zeta = 0.005$ ,  $k_3 = +0.2$  (hardening) and  $N = 10$ . Figure 3.8 shows the energy transmitted through this structure as a function of  $F$  at different forcing frequencies near the upper edge of the pass band ( $\omega_N \approx 1.149$ ).

In all forcing frequencies shown in Figure 3.8, loss of stability is accompanied with an increase in the transmitted energy. At  $\Omega = 1.16$ , excitation is within the stop band and we see an increase in the transmitted energy over a few orders of magnitude (supratransmission). In comparison, the increase in transmitted energies

is not as significant for the driving frequencies within the pass band, namely at  $\Omega = 1.13$  and  $\Omega = 1.14$ . At  $\Omega = 1.15$ , which is on the edge of the pass band, loss of stability leads to enhanced transmission, but not as significant as what happens at higher forcing frequencies within the stop band. Within the pass band, the location of  $\Omega$  with respect to the linear natural frequencies changes the onset of transmission ( $F_{th}$ ), yet the qualitative behavior explained here remains the same; i.e. eventual loss of stability and an increase in  $E_N$ . If the structure were undamped, then the onset of transmission would have approached zero at the linear natural frequencies of the structure.

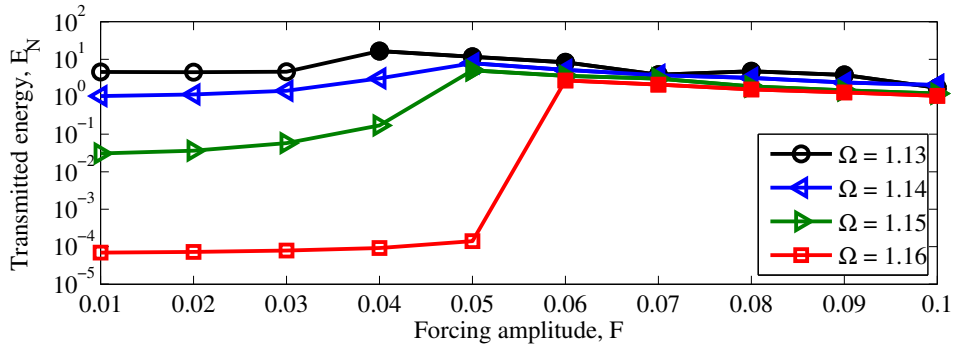


**Figure 3.8:** The influence of forcing frequency ( $\Omega$ ) on enhanced nonlinear energy transmission in a damped periodic structure. Energy at the end of the structure ( $E_N$ ) is plotted as a function of driving amplitude ( $F$ ) for different forcing frequencies. The upper edge of the pass band is at  $\omega_N \approx 1.149$ .  $\Omega = 1.13$  and  $\Omega = 1.14$  are inside the pass band,  $\Omega = 1.15$  is at the edge of the pass band, and  $\Omega = 1.16$  is above the pass band. Filled markers indicate periodic responses and empty markers indicate non-periodic responses. In all four cases, loss of stability leads to an increase in  $E_N$ . This increase is most significant when excitation is within the stop band (supratransmission).

Although loss of stability leads to enhanced transmission within both pass and stop bands, the increase in transmitted energies is much smaller within the pass band. One explanation is that the response is already extended throughout the structure within the pass band, thus waves can reach the end of the structure without much attenuation – compare the transmitted energies in Figure 3.8 at low forcing amplitudes. Another factor could be the instability mechanism. Linear solu-

tions lose their stability through saddle-node bifurcation at  $\Omega = 1.16$  (and driving frequencies above it), whereas loss of stability occurs through a Neimark-Sacker bifurcation [70, Ch. 5] at  $\Omega = 1.15$ . The latter is also the typical instability mechanism inside the pass band. We have found damping to play a major role in determining the behavior of the Floquet multipliers and consequently the mechanism leading to loss of stability within and in the vicinity of a pass band. A detailed analysis of the influence of damping on the bifurcation structure of the NLRM within a pass band is very interesting from a nonlinear-dynamics perspective but lies outside the framework of this thesis. This is also not a pressing study from a practical point of view because supratransmission is most significant when the driving frequency is away from the pass band. The additional role played by disorder in this context will be discussed in Section 4.2.

### 3.7 Strong Propagation Regime

The nonlinear transmission phenomenon discussed in the preceding sections of this work occurs above a certain driving amplitude threshold. If the driving amplitude is increased further, a second threshold may exist in the case of undamped structures (possibly for driving frequencies on both sides of the pass band) above which there is another large increase in the transmitted energy through the chain [82]. In this context, the operating range between the first and second thresholds is referred to as the weak propagation regime, and the range above the second threshold is known as the strong propagation regime. The strong energy propagation is due to large-amplitude chaotic motions of the structure, and the transmitted wave is characterized by a broad frequency spectrum extending beyond the linear pass band. Also, the increase in the transmitted energy at the second threshold is much larger than the increase at the first threshold.

To the best of our knowledge, the strong propagation regime has only been reported in a semi-infinite Hamiltonian system with an on-site Morse potential [82]. Further investigation of the strong propagation regime and the possible influence of damping on the existence of the second threshold is beyond the scope of the present work.

### 3.8 Concluding Remarks

We studied the influence of various system parameters on the supratransmission phenomenon for a perfectly periodic structure. Our main findings are summarized here:

1. The *type of nonlinearity* determines on which side of the pass band supratransmission can occur. This is above the pass band for a hardening system and below it for a softening system. Increasing the *strength* of the nonlinear force lowers the force threshold for the onset of supratransmission.
2. Increasing the *number of units* can shift the threshold curves towards higher forcing thresholds at driving frequencies very close to the edge of a pass band.
3. In general, *damping* increases the force required for the onset of supratransmission at all forcing frequencies (away from the pass band). More significantly, damping may eliminate supratransmission within a frequency range in the immediate vicinity of the linear pass band, introducing a non-zero threshold on the minimum force amplitude required for transmission to occur. Increasing damping widens this frequency range and increases the minimum force. Furthermore, damping may delay the onset of supratransmission by stabilizing the periodic solutions. Supratransmission may occur in this case at higher forcing amplitudes.
4. Increasing the *strength of coupling* increases the minimum force required for the onset of supratransmission for all driving frequencies, but does not alter the location of the onset of transmission with respect to the nearest edge of the pass band.

Using the analytical estimates of the supratransmission threshold from Section 2.5.1, we explained the effects of nonlinearity and damping from a phenomenological viewpoint. Moreover, we updated the existing analysis in order to include the influence of the strength of coupling on the onset of supratransmission. The improved analysis is based on the local nonlinear dynamics of the driven unit, with the second unit included in the analysis but assumed to be linear (the rest of the

structure is truncated after the second unit). The updated approximate formulation can account for the strength of coupling, though it is still limited to weak coupling strengths.

We also briefly discussed the hysteresis phenomenon associated with supratransmission, and explained one methodology for observing it numerically. Furthermore, we briefly considered the instability-driven increase in energy transmission when the driving frequency is within the pass band (not supratransmission). We showed that the increase in transmitted energies in this situation is not significant when compared to the energy increase via supratransmission.

## Chapter 4

# Disorder Effects

We explore the influence of linear disorder on supratransmission in this chapter. We start by an overview of the key features of the linear response of disordered structures (Anderson localization), and highlight the combined influence of damping and disorder on supratransmission near a pass band. We then discuss the statistical effects of disorder on the transmission mechanism. In particular, we investigate the statistical influence of linear disorder on (i) the supratransmission thresholds within a stop band, (ii) transmitted energies above the supratransmission threshold, and (iii) the spectrum of the nonlinearly transmitted waves. We then present an approximate analytical formulation for predicting the onset of supratransmission in disordered structures and investigate its range of validity.

### 4.1 Disorder-Borne Energy Localization in Linear Structures

Wave propagation within a linear periodic structure may be significantly influenced by the presence of small disorder. In a disordered structure, waves scatter differently at the boundaries between adjacent units because the units are no longer identical. This can result in spatial decay of the response amplitude at frequencies within (and particularly near the edges of) the pass band of the underlying ordered structure. If we average the response over many different realizations of a prescribed disorder, then the response becomes localized to the source of excitation

and decays exponentially away from it. This statistical phenomenon is known as *Anderson localization*, after the seminal work of Philip W. Anderson in solid-state physics [3] – see also [47, 71, 86].

Disorder in engineering structures usually means small variations in spatially distributed (extended) structural parameters such as stiffness, mass, damping, or support conditions. These small irregularities can lead to significant *qualitative* changes in the global dynamic response. This spatial confinement of energy, or localization, is called *strong localization* [108], and occurs when the strength of coupling between adjacent units is weak in comparison to the strength of disorder. In *weak localization*, the coupling force is strong and damping effects dominate over disorder [12, 108]. Even in undamped structures, weak localization effects are only significant over very long distances (at least a few hundred units [108]). Given that engineering structures always have damping and do not typically consist of such large number of units, only strong localization is relevant in the majority of engineering applications. Accordingly, we study a damped finite periodic structure with weak coupling – we define the strength of coupling in (4.2). We consider a lightly damped structure and use a linear viscous damping model with a mass-proportional damping matrix. Refer to [106, 107] for a comprehensive review of general non-proportional and non-viscous damping models. An overview of simultaneous effects of damping and disorder in linear periodic structures can be found in [12]. See [13] for an extension of this work to structures with finite length.

It is important to note that disorder-borne confinement of energy only occurs *in an ensemble-average sense* and that individual realizations of disorder may behave differently. In particular, it is possible that the normal modes of a disordered structure are localized away from the driving point for a particular realization. These anomalous realizations can have a significant influence on the average response of the ensemble, to the extent that using a linear average may not necessarily give the typical value (statistical *mode*) of the ensemble [12, 48]. This is important in the case of weak localization [13], where localization length scales are large. For a damped structure, the contributions from anomalous realizations are much less significant because of the uniform decay caused by damping [12, 48].

Anderson localization can occur as a result of disorder that is present in either the grounding springs (on-site potential), coupling springs (inter-site potential) or

masses within the periodic structure [65]. It is argued [108] that random masses and grounding springs influence the degree of localization in a similar manner, while random coupling springs have a weaker influence in comparison. Here, we only consider disorder that is applied to the linear grounding springs of the system. This type of disorder is sufficient to capture strong localization in our system. In presence of such disorder, the linear governing equations of (2.9) are replaced with

$$\ddot{u}_n + 2\zeta\dot{u}_n + \omega_1^2(1 + \delta k_n)u_n + k_c \Delta^2(u_n) = f_n \cos(\Omega t), \quad f_n = 0 \text{ for } 2 \leq n \leq N \quad (4.1)$$

where  $\delta k_n$  are random numbers with a uniform probability density function. We assume that  $\delta k_n$  are distributed independently around a zero mean,  $\langle \delta k_n \rangle = 0$ , such that  $|\delta k_n| \leq D$ . We refer to  $D$  as the *strength of disorder*. We further introduce a parameter  $C$  that denotes the *strength of coupling* between units

$$C \equiv k_c / \omega_1^2 \quad (4.2)$$

Our earlier assumption of weak coupling can be expressed as  $C < 1$ . The value of  $C$  represents the ratio of coupling to grounding spring stiffness, and does not depend on the mass (coefficient of  $\ddot{u}_n$ ). With the exception of Section 4.4.3, we use  $C = 0.05$  in this chapter, which is the same strength of coupling used in Chapters 2 and 3. We use a periodic structure with  $N = 10$  units in this chapter.

#### 4.1.1 Localization Occurring within a Pass Band

A crucial parameter that determines the degree of localization is  $D/C$ , the ratio of the strengths of disorder to coupling [47]. As this ratio increases, the degree of localization within the pass band increases as well. This is shown in Figure 4.1 where we plot the normalized amplitude profile ( $U_n/U_1$ ) for different strengths of disorder. The results for the disordered structures are obtained after averaging over an ensemble of  $10^5$  realizations to ensure convergence of the average values at all forcing frequencies considered. We see in Figure 4.1 that the response of the ordered structure ( $D/C = 0$ ) is extended through the system, and the small overall attenuation in response amplitudes is due to damping. The oscillations in the response of the ordered structure near the end of the structure are caused by the

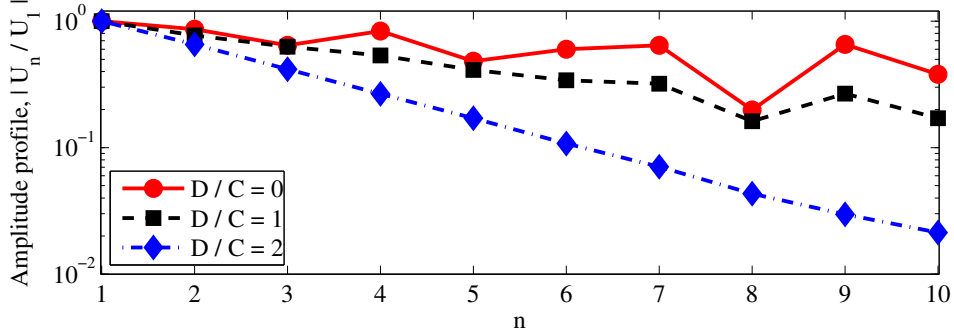


**Figure 4.1:** The influence of disorder on response localization at  $\Omega = 1.12$ , near the middle of the pass band. The average response becomes localized to the driven unit ( $n = 1$ ) as the value of  $D/C$  increases. The strength of coupling is kept constant,  $C = 0.05$ . An ensemble of  $10^5$  realizations are used for each non-zero value of  $D$  (namely  $D = 0.05$  and  $D = 0.10$ ). Other system parameters are  $N = 10$ ,  $\zeta = 0.005$  and  $\omega_1^2 = 1.05$ .

waves reflected at the free boundary at the end of the structure ( $n = 10$ ). Adding disorder results in smaller response amplitude in comparison with the ordered case. As the strength of disorder increases, the response becomes localized to  $n = 1$ , where the external force is applied. In addition, disorder effects eventually subdue wave reflections at the boundaries, which is why the boundary effects at  $n = 10$  become insignificant for high values of  $D/C$ .

#### 4.1.2 Quantifying the Degree of Localization

When there is exponential spatial decay of the response due to disorder, we expect

$$|U_n| \propto \exp(-\gamma_n n) \quad (4.3)$$

in an average sense.  $\gamma_n$  is the localization factor or decay exponent and describes the average rate of exponential amplitude decay per unit. As the length of the periodic structure extends to infinity (equivalently, when averaged over many realizations), expression (4.3) yields the correct decay rate [49]. Calculation of the decay exponent merely based on (4.3) involves solving for all response amplitudes

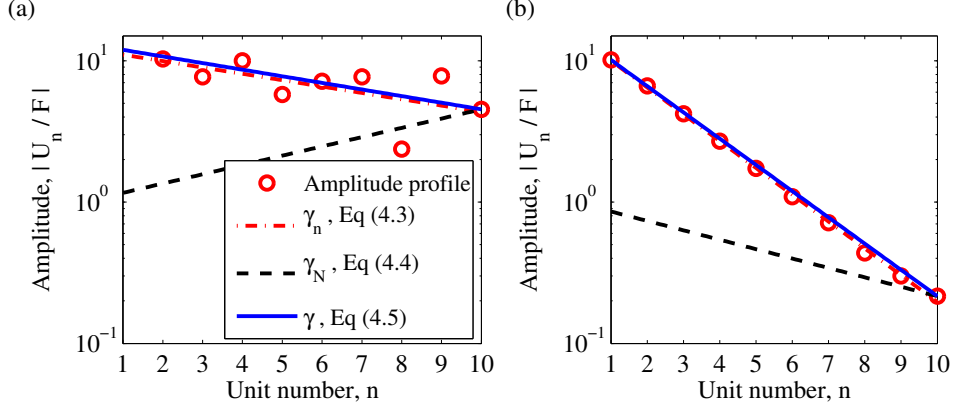


**Figure 4.2:** Comparison of the three decay exponents in describing amplitude profiles; (a) an extended response, (b) a localized response. The red circles denote the actual response at each unit, red dash-dotted lines are obtained based on  $\gamma_n$  (curve fit), black dashed lines are based on  $\gamma_N$  and blue solid lines are based on  $\gamma$ .

and fitting an exponential curve to the data.

There exist different approaches for studying the decay exponent analytically, such as using transfer-matrix [108] or receptance-matrix [91] formulations. In the former case, one could make use of the properties for products of random matrices [36] and obtain asymptotic estimates for decay exponents [12]. Alternatively, one could replace (4.3) with

$$|U_N| \equiv F \exp(-\gamma_N N) \quad (4.4)$$

and use the properties of tridiagonal matrices to obtain expressions for  $\gamma_N$  [46, 49]. It is important to note that (4.4) is true for any finite linear system and does not mean that the response is exponentially decaying. Nevertheless, if the response is exponentially decaying (as anticipated in Anderson localization), then the value of  $\gamma_N$  obtained from averaging (4.4) represents the average decay rate in the limit of a very long structure (as  $N \rightarrow \infty$ ).

Based on the value of  $\gamma_N$  alone one cannot draw any conclusions about the response of the periodic structure. In addition, because we are dealing with rela-

tively short periodic structures in this work ( $N = 10$ ), the boundary effects will have an influence on  $\gamma_N$ . These make the interpretation of the decay factor, as defined in (4.4), somewhat ambiguous. An alternative is to redefine the decay exponent by replacing  $|U_N|$  in (4.4) with  $|U_N/U_1|$ ; i.e. normalizing the response at the end of the chain with that of the driven unit. Then (4.4) is replaced by

$$\left| \frac{U_N}{U_1} \right| \equiv e^{-\gamma(N-1)} \quad (4.5)$$

Notice that the multiplier for the decay exponent is now  $(N - 1)$  because a wave goes through  $N - 1$  units from  $n = 1$  to  $n = N$ . Based on definition (4.5), we obtain  $\gamma > 0$  whenever the response has decayed through the structure; i.e.  $|U_N| < |U_1|$ . A negative value of the decay exponents is obtained whenever  $|U_N| > |U_1|$ ; we have observed this only at resonance frequencies for structures with few number of units and very light damping. We emphasize that definition (4.5) does not imply that the spatial decay envelop is exponential.

We use two different amplitude profiles to compare the performance of the three decay exponents  $\gamma_n$ ,  $\gamma_N$  and  $\gamma$  in describing amplitude profiles of finite structures. These two amplitude profiles are the (ensemble-) average response of the linear structure considered in Section 4.1.1 at  $\Omega = 1.12$  for  $D/C = 0$  (extended response) and  $D/C = 2$  (localized response). We reproduce these amplitude profiles in Figure 4.2, along with the estimates obtained based on  $\gamma_n$ ,  $\gamma_N$  and  $\gamma$ . We see that the proposed definition of the decay exponent ( $\gamma$ ) describes the actual amplitude profile better than the classical definition ( $\gamma_N$ ). The advantage of using  $\gamma$  over a decay exponent based on curve fitting (i.e.  $\gamma_n$ ) is that the former can be used for obtaining analytical estimates of the response. Since we do not make use of these analytical expressions in this work, we do not further elaborate on them.

Figure 4.3 shows the influence of the number of units on the decay exponent  $\gamma$  in an ordered structure. We see that as  $N$  increases, the results for a finite system approach those for the infinite system based on  $\gamma_0$  defined in (2.11). It is possible to show analytically for an ordered structure that in fact  $\gamma \rightarrow \gamma_0$  as  $N \rightarrow \infty$ . Based on the foregoing discussions in this section, we use the decay exponent defined in (4.5) in this work.

Another important characteristic of disorder-borne localization is that the mode

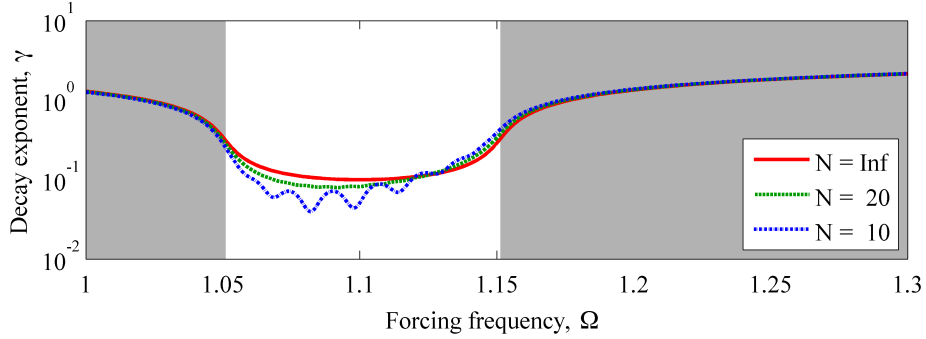


**Figure 4.3:** The dependence of the decay exponent on the number of units,  $N$ , for a linear ordered structure. As the size of the structure increases, the decay exponent of the finite structure approaches that of the infinite structure; i.e.  $\gamma \rightarrow \gamma_0$  as  $N \rightarrow \infty$ . The grey area corresponds to the stop band.

shapes of a disordered structure become spatially localized [47, 68]. This can be quantified using the inverse participation ratio (IPR), defined by

$$IPR = \frac{\sum_{n=1}^N (U_n^2)^2}{(\sum_{n=1}^N U_n^2)^2} \quad (4.6)$$

where  $U_n$  are the steady-state amplitudes of the  $n$ -th mode shape of the system; e.g. see [68] for more details. The IPR is a scalar with a value between  $1/N$  and 1. If all the units are moving with the same amplitude (uniform response), then  $IPR = 1/N$ . If only one unit is moving (absolute localization), then  $IPR = 1$ .

For the same ensemble used for Figure 4.1, we have computed the average IPR for the first and last mode shapes. We show this in Figure 4.4, along with a typical mode shape of the ensemble at three values of  $D/C$ . We can see that the mode shapes become spatially localized as disorder becomes stronger. One can also use a modal expansion to express the response of the forced structure in terms of its mode shapes; in this light, the response localization we observed in Figure 4.1 can be explained based on spatial localization of the mode shapes [49].

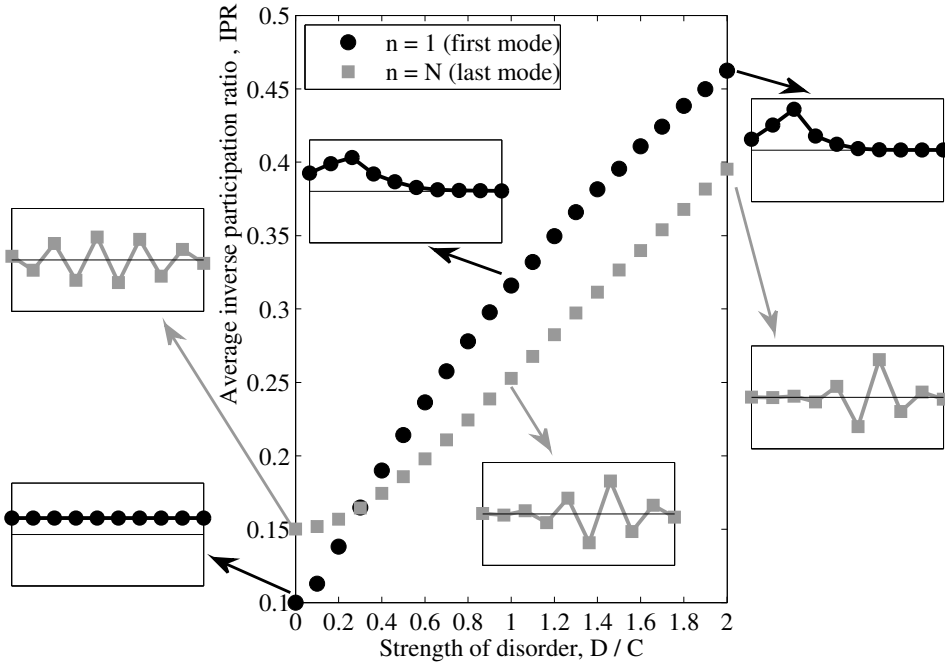


**Figure 4.4:** The influence of disorder on spatial localization of the mode shapes of the structure. IPR, defined in (4.6), is plotted as a function of  $D/C$  for the first and last mode shapes. The insets show the mode shape of a typical realization of disorder within the ensemble at  $D/C = 0, 1, 2$ . The result for  $n = 1$  are shown in black and those for  $n = N$  are shown in grey.

### 4.1.3 Influence of Disorder on the Band Structure

The frequency of excitation plays a major role in determining the influence of disorder on the dynamic response of periodic structures. On average, less energy is transmitted to the end of a disordered structure at frequencies lying within the pass band – recall Figure 4.1. Figure 4.5(a) shows the average decay exponent  $\gamma$  as a function of driving frequency  $\Omega$  for different values of disorder. We can see that disorder results in increased values of decay exponent within the pass band of the ordered structure. Within the stop band, however, the decay exponent has a larger value for the ordered structure. Similar observations have been made in infinite undamped structures [35]. In addition, Figure 4.5(a) shows that disorder

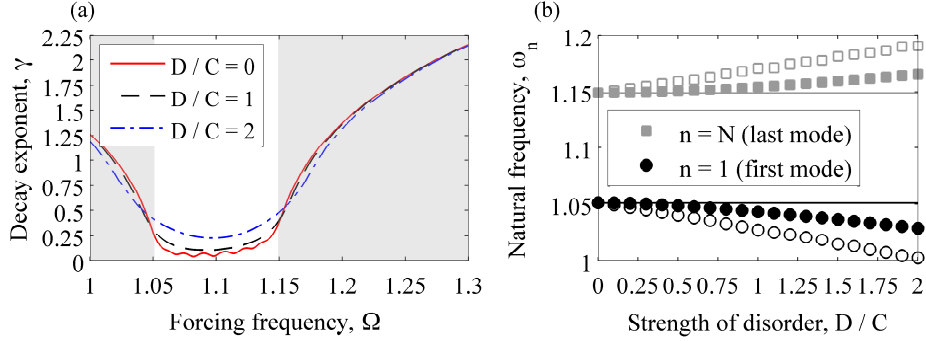


**Figure 4.5:** The influence of disorder on the linear response of the structure. (a) The average decay exponent  $\gamma$ , defined in (4.5), is plotted for different values of disorder. The grey area corresponds to the stop band. (b) The average natural frequencies of the first ( $\omega_1$ ) and last ( $\omega_N$ ) modes are plotted as a function of  $D/C$ . The black circles correspond to  $\omega_1$  and grey squares to  $\omega_N$ . The empty markers correspond to the minimum and maximum values of each natural frequency within the ensemble. The horizontal lines indicate the natural frequencies of the ordered structure.

has the overall effect of slightly widening the pass band of a periodic structure. As a result, the transmitted energy is much smaller in a disordered structure but covers a wider frequency range in comparison to an ordered structure. The same conclusion can be made based on Figure 4.5(b), where we show the first and last natural frequencies of the structure as a function of the strength of disorder. We can see that as  $D/C$  increases,  $\omega_1$  decreases and  $\omega_N$  increases on average.

## 4.2 Combined Effects of Damping and Disorder Near a Pass Band

We explained in Section 3.3 that, in general, the force threshold at the onset of supratransmission ( $F_{th}$ ) increases if the value of damping is increased. Close to the edge of a pass band, however, damping can play a more significant role. To illustrate this, we compare the transmitted energies in a damped ( $\zeta = 0.005$ ) and an undamped ( $\zeta = 0$ ) ordered structure with  $N = 10$ . Figure 4.6 shows the threshold curve for the damped structure studied in this chapter in the absence of disorder.

Given the low value of damping, we expect  $F_{th}$  to be very similar for the damped and undamped structures considered here. Thus, Figure 4.6 gives a good estimate for values of  $F_{th}$  in the undamped structure.

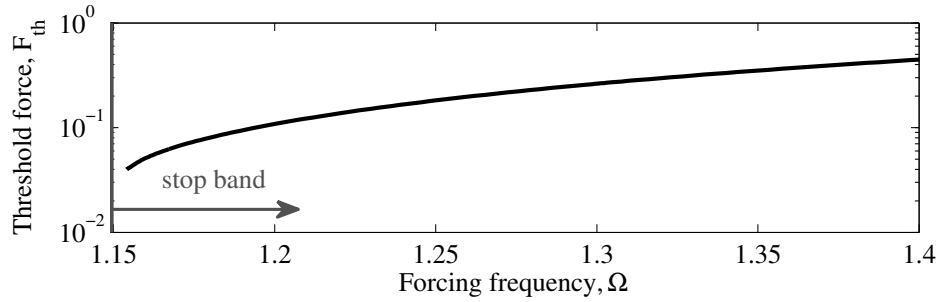


**Figure 4.6:** The threshold curve for the ordered structure ( $D = 0$ ), showing the dependence of the driving amplitude at the onset of transmission,  $F_{th}$ , as a function of the driving frequency,  $\Omega$ . Other system parameters include  $N = 10$ ,  $\zeta = 0.005$ ,  $C = 0.05$  and  $k_3 = 0.2$ . The upper edge of the pass band is at  $\omega_N \approx 1.149$ . As explained in Section 3.3, the threshold curve terminates near the pass band in a cusp.

Figure 4.7 shows  $E_N$  as a function of  $F$  at different values of  $\Omega$  close to the pass band – recall that the upper edge of the pass band is located at  $\omega_N \approx 1.149$ . In Figure 4.7, we see that at  $\Omega = 1.16$  the onset of supratransmission occurs near  $F_{th} \approx 0.05$  for both the damped and undamped structures. The transmitted energies above the threshold are lower for the damped structure, which can be easily attributed to energy loss through damping. At  $\Omega = 1.18$ , we see that supratransmission occurs at the expected value of  $F_{th} \approx 0.08$  for the undamped structure. In contrast, the damped structure has a relatively insignificant increase in  $E_N$  between  $F = 0.075$  and  $F = 0.100$  (indicated as weak jump in Figure 4.7). The response of the damped structure is periodic below and above  $F = 0.08$ , though with different amplitudes. Above  $F = 0.350$ , supratransmission occurs in the damped structure as well. A similar difference between the damped and undamped structures is observed at  $\Omega = 1.22$ . At  $\Omega = 1.26$  (and driving frequencies above it), supratransmission occurs around the same forcing thresholds for the damped and undamped structures, as initially expected.

To understand the unexpected behavior of the damped structure when  $1.18 \lesssim$

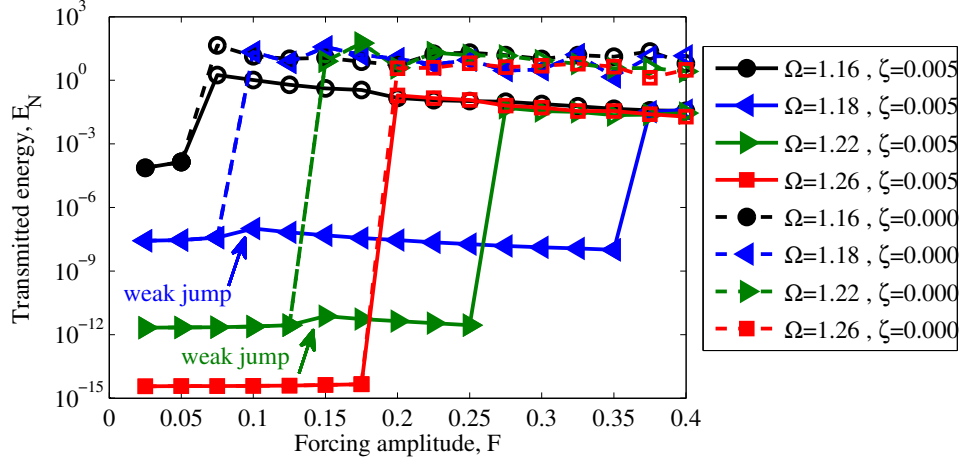


**Figure 4.7:** The influence of damping on supratransmission in the vicinity of a pass band for an ordered structure. Transmitted energy ( $E_N$ ) is plotted as a function of driving amplitude ( $F$ ) for different driving frequencies ( $\Omega$ ). The upper edge of the pass band is at  $\omega_N \approx 1.149$ . Filled markers indicate periodic response and empty markers indicate non-periodic response. Because damping is small, the threshold force ( $F_{th}$ ) of the undamped structure is expected to be very close to that of the damped structure. At  $\Omega = 1.16$  and  $\Omega = 1.26$ , supratransmission occurs at the expected force threshold based on Figure 4.6. At  $\Omega = 1.18$  and  $\Omega = 1.22$ , the response of the damped structure jumps to another stable periodic branch at the expected value of  $F$  (indicated as ‘weak jump’). In contrast, supratransmission occurs for the undamped structure at the expected value of  $F$ .

$\Omega \lesssim 1.26$ , we consider the evolution of the periodic solutions of the damped and undamped structures at different values of  $\Omega$  as a function of  $F$ . This information can be obtained from the nonlinear response manifold (NLRM), as discussed in Section 2.4. Figure 4.8 shows the projection of the NLRMs on the  $U_N - F$  plane for the same four values of  $\Omega$  that are used in Figure 4.7.

At  $\Omega = 1.16$ , shown in Figure 4.8(a), we see that the two NLRMs start from the origin and follow the linear solution (i.e.  $U_N \propto F$ ) for small values of  $F$ . At the first turning point (TP1), the periodic solutions lose their stability through a saddle-node bifurcation. Because neighboring periodic solutions either do not ex-

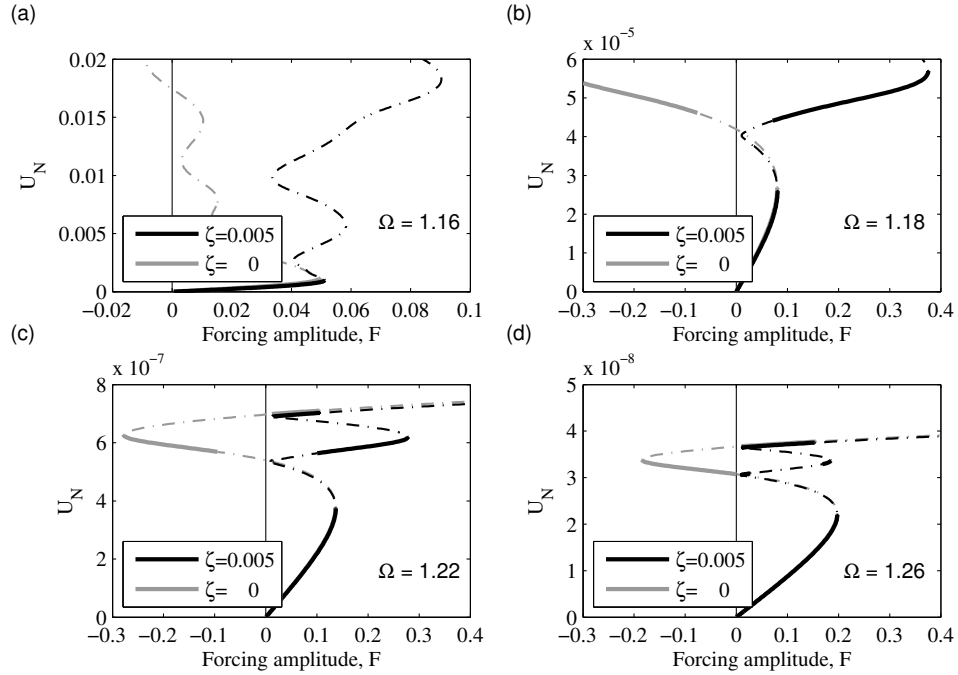


**Figure 4.8:** The influence of damping on the NLRM of the structure at different forcing frequencies: (a)  $\Omega = 1.16$ , (b)  $\Omega = 1.18$ , (c)  $\Omega = 1.22$ , (d)  $\Omega = 1.26$ . In each plot, the projection of the NLRM is plotted in the  $U_N - F$  plane for  $\zeta = 0.005$  (black curve) and  $\zeta = 0$  (grey curve). For each NLRM, the thick solid sections represent stable solutions and thin dash-dotted portions represent unstable solutions.

ist or are unstable at this point, the solution jumps to a non-periodic branch. This is accompanied by the large increase in transmitted energies shown in Figure 4.7. After TP1, the undamped response normally crosses the zero-force axis ( $F = 0$ ) multiple times. These zero-crossings correspond to non-zero time-periodic solutions in the undamped system that are spatially localized to the driven unit – these solutions are called discrete breathers (DB). See [82] for more details about the zero-crossings and the associated DBs. For a damped structure, it is important to note that the NLRM does not cross the zero-force axis because the structure can no longer sustain steady-state motion with non-zero amplitude.

At  $\Omega = 1.18$ , shown in Figure 4.8(b), we see that another stable periodic so-

lution exists at TP1 for the damped structure. As a result, the solution jumps to that solution branch when  $F$  is increased beyond its value at TP1. The response at this upper periodic branch is dominantly harmonic (with frequency  $\Omega$ ) and has a higher value of  $E_N$  than the linear solution – see Figure 4.7. Nevertheless, supratransmission does not occur until the third turning point (TP3) of the NLRM around  $F \approx 0.375$ . For the undamped structure, other solutions at TP1 are unstable and the solution jumps to a non-periodic branch.

At  $\Omega = 1.22$ , shown in Figure 4.8(c), the situation is similar to what happens at  $\Omega = 1.18$ . The main difference is the range over which the upper periodic branch is stable: compared to  $\Omega = 1.18$ , TP3 occurs at a lower value of  $F$ . Although the undamped NLRM has stable portions, we have not observed any situation in which the stable branch extends to TP1 – the same observation is made in [82]. Thus, supratransmission occurs at TP1 for the undamped structure. By  $\Omega = 1.26$ , shown in Figure 4.8(d), the damped NLRM has changed such that TP3 occurs again at a lower value of  $F$  than TP1. Accordingly, supratransmission occurs at TP1 for both the damped and undamped structures.

Figure 4.8 clearly shows that the stability of the upper branch of NLRM at the TP1 depends on the existence of damping. We have found that disorder can also play a role here. We show this in Figure 4.9 for two different realizations of disorder at  $\Omega = 1.22$ . We see in Figure 4.9(a) that increasing the strength of disorder has a stabilizing effect on the upper branch of periodic solutions. We observe the opposite effect for the other realization in Figure 4.9(b).

Investigating the necessary/sufficient conditions for the stability of the upper solution branch at the first turning point of the NLRM sets forth a very interesting problem. Knowing the location of TP3 or subsequent turning points would not suffice for this purpose because the upper branch can change stability between turning points (via Neimark-Sacker bifurcation), as seen in Figures 4.8(b-d). A systematic investigation of the influence of damping and disorder on the stability of the upper branch at TP1 can be done using numerical continuation. This study, however, falls outside the scope of our present work – it is also of less relevance in applications based on supratransmission because supratransmission is significant at frequencies away from a pass band. Consequently, we will only consider driving frequencies for which supratransmission occurs via jump to an anharmonic branch

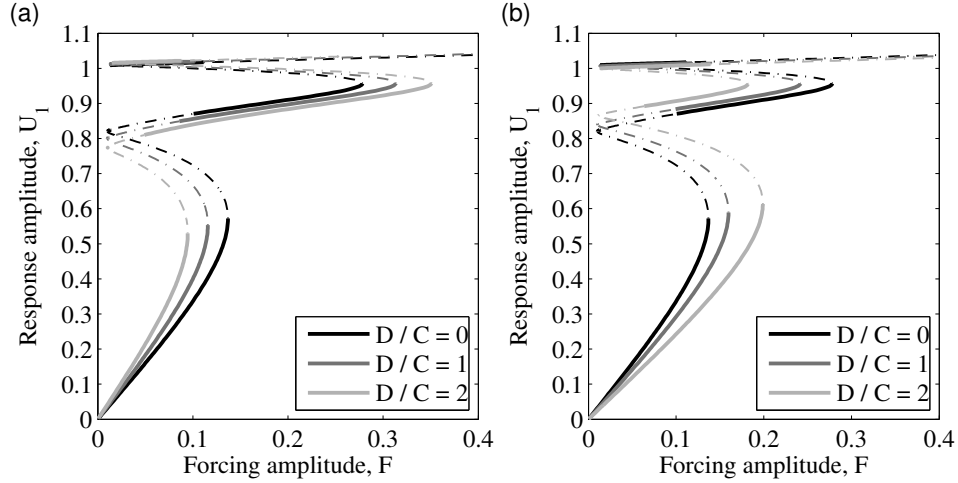


**Figure 4.9:** The influence of disorder on the NLRM of the damped structure at  $\Omega = 1.22$ . Two different realizations of disorder are considered in panels (a) and (b), with increasing the strengths of disorder ( $D/C$ ). The results for  $D/C = 0$  are reproduced from Figure 4.8(c). Notice that increasing  $D/C$  has opposing effects on the stability of the upper branch of periodic solutions in (a) and (b).

at the first turning point of the nonlinear response manifold [57, 82]. In this light, we will consider  $\Omega \geq 1.25$  in Section 4.3.

### 4.3 Supratransmission in Disordered Nonlinear Periodic Structures

We investigate the influence of disorder on supratransmission in this section. With the exception of Section 4.3.1, the results presented here are pertinent in an ensemble-average sense, meaning that they describe the behavior of a typical disordered structure; i.e. the statistical mode of the ensemble.

Similar to Section 4.1.1, we consider disorder as random linear spring constants taken from a uniform distribution, with  $-D \leq \delta k_n \leq D$ . We consider a disorder range of  $0 \leq D/C \leq 2$ . This range of deviation from periodicity captures the expected physical effects of disorder, as explained in Section 4.1. This provides sufficient justification for stopping at  $D/C = 2$ . Keeping  $C = 0.05$  constant, we

vary the strength of disorder by changing  $D$ . Thus, we are studying a disordered periodic structure with weak coupling and weak disorder ( $0 \leq D \leq 10\%$ ). Strictly speaking, a disorder value of 50% (for example) would not violate any physical law, but at that point we would be getting closer to a random structure as opposed to a disordered *periodic* structure.

Throughout this section, the nonlinear force in (2.5) is adjusted such that the coefficient of its cubic term is  $k_3 = +0.2$  (hardening nonlinearity). Accordingly, we only consider forcing frequencies above the pass band because supratransmission occurs above the pass band in a structure with hardening nonlinearity (recall Section 3.1). The upper edge of the pass band is located at  $\omega_N \approx 1.149$  in this case. As explained in Section 4.2, we only consider  $\Omega \geq 1.25$  to focus on supratransmission occurring at the first turning point of the nonlinear response manifold. Qualitatively similar results are expected if a softening nonlinearity is chosen and forcing frequencies are below the pass band. We will consider both hardening and softening types of nonlinearity in Section 4.4.2.

### 4.3.1 Loss of Stability Leads to Enhanced Transmission

For a given forcing frequency, the onset of transmission in a disordered structure may occur at a different value of the driving amplitude when compared with the corresponding ordered structure. The change in threshold force amplitude, and whether it occurs or not, depends on the particular realization that is being considered. We have shown this in Figure 4.10 for two different realizations of disorder with  $D/C = 2$ .

Figure 4.10(a) shows the evolution of the periodic solutions as a function of the driving amplitude,  $F$ . For low driving amplitudes (near the origin), the response amplitude increases linearly with  $F$ , as expected from linear theory. As  $F$  increases, there is a turning point in the response (saddle-node bifurcation). The solution then jumps to a non-periodic branch. Depending on the realization being considered, the onset of transmission may be lower or higher than the onset for the ordered structure. Results from direct numerical integration of (2.3) are shown in Figure 4.10(b). We can see that there is a significant decrease in the decay exponent that occurs at a value of  $F$  consistent with the turning points in Figure 4.10(a).

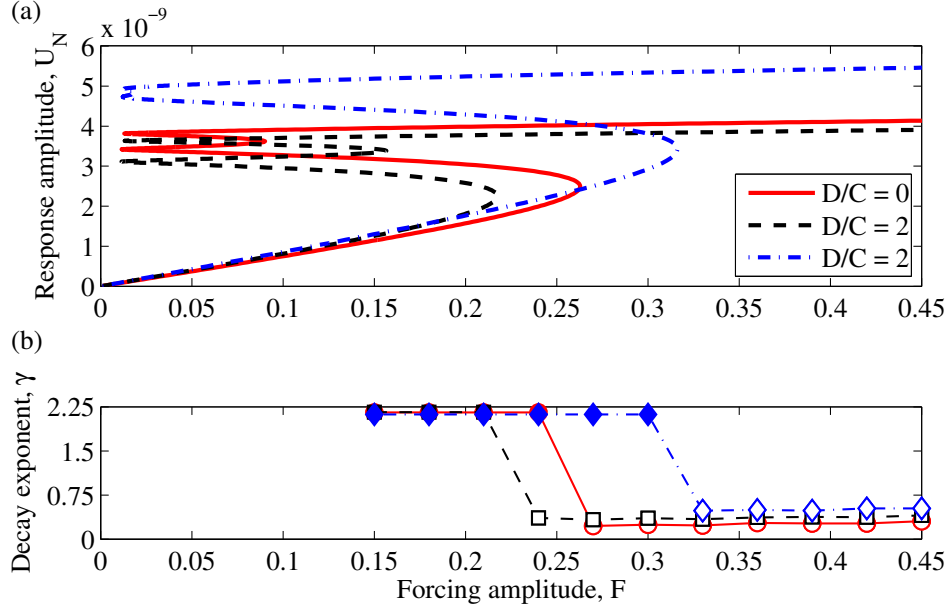


**Figure 4.10:** The influence of disorder on the onset of supratransmission at  $\Omega = 1.30$ . (a) the locus of periodic solutions in the  $U_N - F$  plane, the first turning point corresponding to loss of stability; (b) decay exponent as a function of  $F$  obtained from direct numerical integration (DNI) of the governing equations. Solid red curve corresponds to the periodic structure ( $D = 0$ ), black dashed curve and blue dash-dotted curve correspond to two different realizations of the disordered structure, both with  $D/C = 2$ . For both realizations,  $\sum \delta k_n \approx 0$ . Apart from the presence of disorder, all other system parameters are the same as in Section 4.2. The two plots (a) and (b) have the same horizontal axis.

### 4.3.2 Onset of Transmission Remains Unchanged on Average

Knowing that the onset of transmission occurs at different forcing amplitudes depending on the specific realization of a given disorder, we want to know the average value of the onset of transmission in an ensemble-average sense. To find the answer, we have computed the exact numerical value of the threshold force  $F_{th}(\Omega)$  using numerical continuation. Figure 4.11(a) shows the values of  $F_{th}$  at  $\Omega = 1.30$  for an ensemble of 1500 realizations with  $D/C = 2$ . Comparing the cumulative average with the total average indicates that the results have converged. The rel-

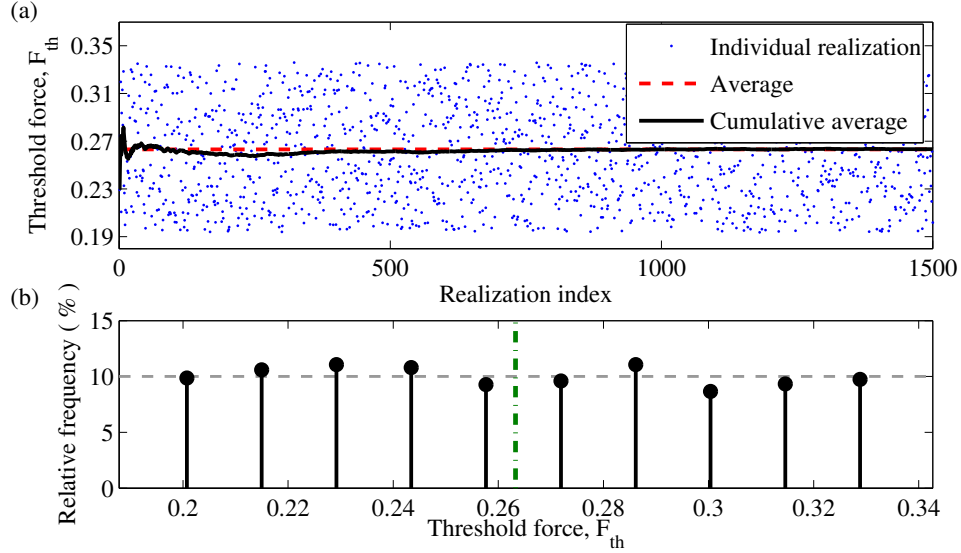


**Figure 4.11:** The influence of disorder on the supratransmission force threshold  $F_{th}$  at  $\Omega = 1.30$  for an ensemble of 1500 realizations with  $D/C = 2$ . The value of  $F_{th}$  for each realization is obtained by numerical continuation. (a) Individual values of  $F_{th}$  for each realization are shown by dots, the cumulative average is shown by the black solid curve and the total average is shown by the red dashed line. (b) The relative frequency of occurrence of  $F_{th}$  is shown by solid back lines. The value of  $F_{th}$  for the ordered system is shown using the vertical dash-dotted line. The horizontal dashed line indicates relative frequency of 10%. The results suggest that on average the onset of transmission is the same for ordered and disordered system.

ative frequency of occurrence of  $F_{th}$  within the same ensemble is shown in Figure 4.11(b). The average value of  $F_{th}$  for the disordered system was found to be the same as that of the ordered system. Moreover, we can see in Figure 4.11(b) that individual values of  $F_{th}$  for the disordered system are spread uniformly around the onset of transmission for the ordered system. We have made similar observations at other values of  $\Omega$  as well (not shown here).

Figure 4.12 shows the average values of  $F_{th}$  and their standard deviations for  $D/C = 2$  at different values of  $\Omega$  away from the linear pass band. The average values show that, *in an ensemble-average sense*, the onset of supratransmission is

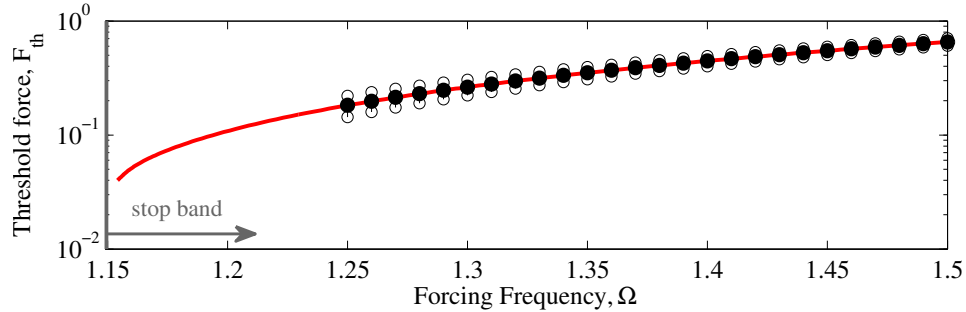


**Figure 4.12:** The influence of disorder on the average threshold force for the structure with hardening nonlinearity. The red solid curve shows the threshold curve for an ordered structure (cf. Figure 4.6). At each forcing frequency, the filled circles show the average value of  $F_{th}$  and the empty circles show the corresponding value of standard deviation. We see that the average threshold curve for a disordered system is the same as the threshold curve for an ordered system. The standard deviation of  $F_{th}$  decreases as we move away from the pass band.

the same in ordered and disordered systems. For a fixed strength of disorder, we observe that the standard deviation of  $F_{th}$  decreases as  $\Omega$  moves away from the pass band. This implies that as  $\Omega$  moves farther into the stop band, dispersion (due to Bragg scattering) is more dominant than disorder effects. This is in fact similar to how disorder affects the linear response of the system. As we showed in Section 4.1.3, the most significant influence of disorder occurs at frequencies within and near the pass band of the system. We found similar results for  $D/C = 1$ .

### 4.3.3 Energy Profiles of Transmitted Waves

We explore how disorder changes the average response above the transmission threshold for two strengths of disorder,  $D/C = 1$  and  $D/C = 2$ . For each disorder strength, we consider an ensemble of 1500 disordered structures; this ensemble is large enough that energies converge to their average values. For every realization within an ensemble, we compute the energy for each unit ( $E_n$ ) at a forcing amplitude 5% above the onset of transmission –  $E_n$  is defined in (2.18). Average energies at each strength of disorder are then obtained by averaging energies over the entire ensemble. The results presented here are for  $\Omega = 1.30$ .

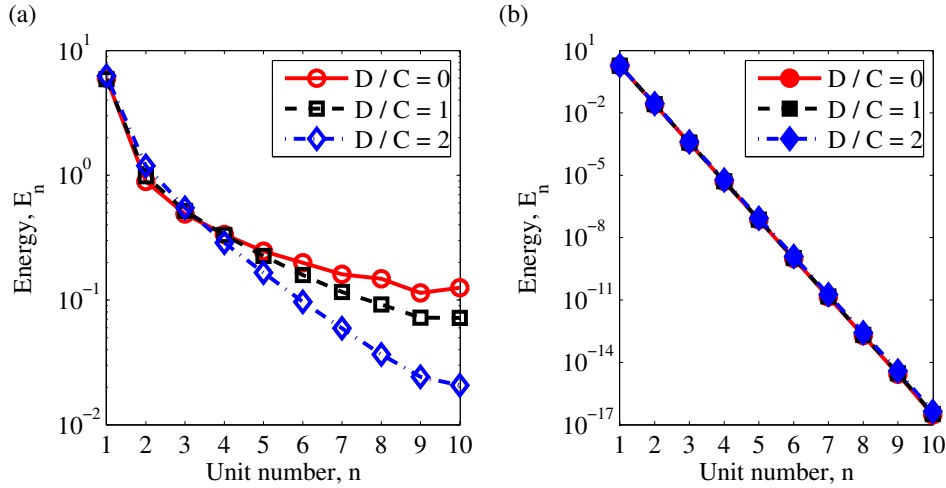


**Figure 4.13:** Average energy profiles at  $\Omega = 1.30$  for (a) the nonlinear structure above the onset of supratransmission, (b) the linear structure. Notice the difference between the vertical axes in (a) and (b). Above the threshold, disorder results in localization of energy to the driven unit.

Figure 4.13(a) shows the average energy profiles for the nonlinear system above the onset of transmission. We see that energies decay exponentially through the structure, particularly between  $n = 2$  and  $n = N - 1$  (away from the boundaries). Moreover, energy becomes more localized to the driven unit as the strength of disorder is increased. These energy profiles are drastically different from the energy profiles below the threshold, where the response is very similar to the linear response shown in Figure 4.13(b) – given that the response below the threshold is very similar to the linear response, we have used the linear energy profiles in Figure 4.13(b). We notice in Figure 4.13 that disorder effects are more significant above the transmission threshold (Figure 4.13(a)) than below it (Figure 4.13(b)). We explain this in more detail in the following section.

#### 4.3.4 Average Frequency Spectra Above the Threshold

For the system parameters used in this work, we have found that the post-threshold branch within the stop band is chaotic, with a frequency spectrum similar to Figure 2.5(c). To understand the average influence of disorder on the transmitted

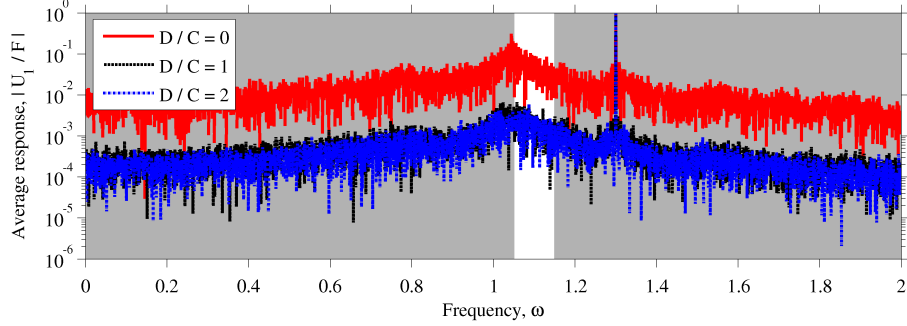


**Figure 4.14:** Average frequency spectra of the driven unit for the ordered and disordered structures. The common peak at 1.30 corresponds to the forcing frequency ( $\Omega = 1.30$ ). The grey area denotes the linear stop band.

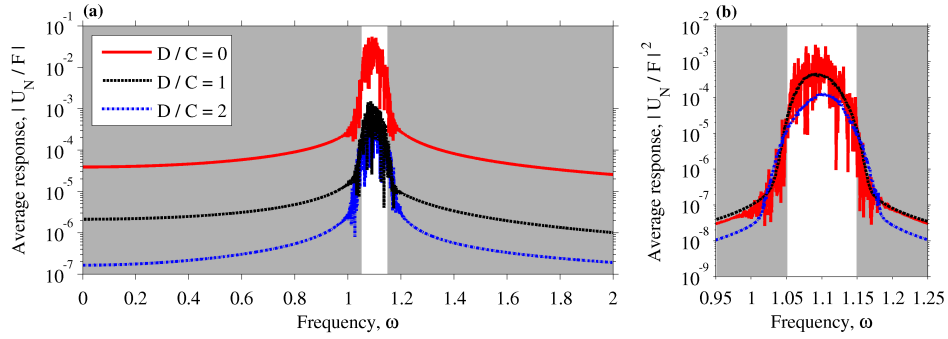


**Figure 4.15:** Average transmitted spectra (at  $n = N$ ) for the ordered and disordered structures; (a) average spectra based on complex-valued amplitudes, (b) average squared spectra in the vicinity of linear pass band. The average transmitted spectra lie within the linear pass band. Less energy is transmitted above the supratransmission threshold as we increase the strength of disorder. The grey area denotes the linear stop band.

waves above the threshold, we compare average frequency spectra of the first and last units in the structure. These results are obtained for the same ensembles as in Section 4.3.3. For disordered systems, the frequency spectrum of each individual realization is obtained as explained in Section 2.3. Before averaging the frequency spectra within each ensemble, the individual complex-valued spectra for each re-

alization is normalized with its forcing amplitude. This is because the threshold force is different for each individual realization (recall Figure 4.10).

Figure 4.14 shows the average frequency spectra of the driven unit ( $n = 1$ ) for the ordered and disordered structures. The three spectra have a common pronounced peak at 1.30, which corresponds to the forcing frequency ( $\Omega = 1.30$ ). This is the only dominant frequency component for the two disordered structures. At other frequencies, it is not easy to distinguish between the two disordered spectra, though they both have much lower amplitudes than those of the ordered structure. Based on the dominant peak in the average spectra of the disordered structures, it is tempting to infer that the response of the driven unit is harmonic on average. This is not correct, however; the frequency component for a given realization is similar to that of the ordered structure in terms of overall magnitude. When averaging over an entire ensemble, the phases are incoherent for any given frequency component (other than 1.30). As a result, the average spectrum of an ensemble will have a much lower amplitude than its individual realizations.

Figure 4.15(a) shows the average frequency spectra at the end of the structure ( $n = N$ ) for the ordered and disordered structures. The most notable feature of the transmitted spectra is that frequency components within the linear stop band (the area with grey background) have significantly decreased compared to  $n = 1$ ; cf. Figure 4.14. The three spectra are therefore similar in the sense that they contain frequencies predominantly within the linear pass band. As the strength of disorder is increased, the amplitudes at different frequency components decrease, most significantly within the stop band. Overall, there is less energy transmitted to the end of the structure as disorder strength increases. This is consistent with the decrease in  $E_N$  from Figure 4.13.

Once we realize that frequency components of the transmitted waves lie within and near the pass band, we can explain, albeit *qualitatively*, certain aspects of disorder effects from a linear perspective as well. Firstly, we expect from linear theory that within the stop band disorder localizes energy near the source of excitation and that less energy is transmitted through the structure as the strength of disorder increases. This is consistent with the average energy profiles in Figure 4.13(a). It also explains why within the stop band disorder has a more significant influence on the response of the structure above the transmission threshold than below it. Below

the threshold, the structure behaves linearly and is therefore barely influenced by disorder. Above the threshold, on the other hand, the transmitted waves lie within the pass band, where disorder affects the results most significantly.

Secondly, we showed for a linear system that the transmitted energy covers a relatively wider frequency range as disorder increases (see Figure 4.5). The data in Figure 4.15(a) is not conclusive in this regard though. To investigate this point further, we have computed the average squared spectra for each ensemble: for each realization within an ensemble, the absolute value of the frequency spectrum is squared, then the arithmetic mean over all realizations is used as the average squared spectrum of the ensemble – notice that energy is related to squared amplitudes. We have shown the squared spectra in Figure 4.15(b) for frequency components close to the pass band. We see that as disorder increases, there is less energy in the transmitted waves. Also, energy transmission occurs over a slightly wider frequency range for stronger disorder strengths. This widening of the transmission band is similar to linear systems, but less pronounced. Notice, however, that this widening occurs at very low amplitudes and can therefore pose challenges to experiments.

### 4.3.5 Prediction of Transmitted Energies Based on Linear Theory

As we discussed in Sections 4.3.3 and 4.3.4, the average behavior of the transmitted waves above the threshold is reminiscent of the average linear behavior of disordered structures. In this light, we ask whether the average transmitted energies above the threshold can be predicted based on linear theory. We introduce the transmitted energy ratio as

$$e = e(D/C) \equiv \frac{\langle E_N(D/C) \rangle}{\langle E_1(D/C) \rangle} \quad (4.7)$$

At a given strength of disorder,  $e$  describes the ratio of average transmitted energy to energy in the driven unit. We show the normalized transmitted energy ratios  $e/e(0)$  for both the linear and nonlinear structures in Figure 4.16. For each system, the transmitted energy ratio is normalized to its value for an ordered structure,  $e(0)$ . For the linear system, we considered the frequency range between 0 and 2 for energy calculation; widening this frequency range did not change the results.

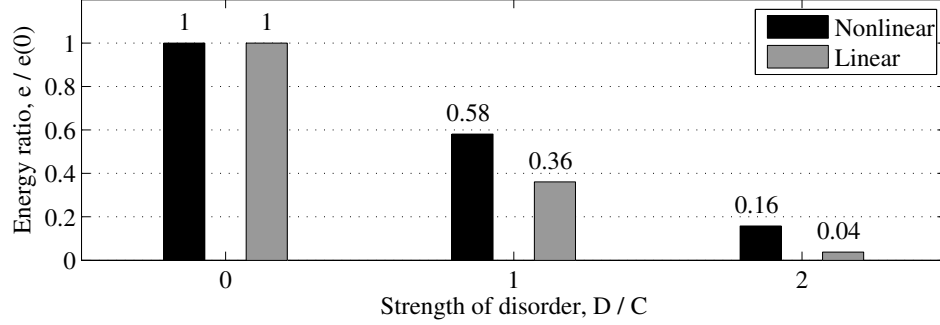


**Figure 4.16:** Normalized transmitted energy ratios,  $e/e(0)$ , for different values of disorder. The numerical value of each bar is shown above it. These results indicate that linear theory cannot be used for making quantitative predictions of disorder effects above the threshold.

Although linear theory can be used to make qualitative predictions of the average behavior of the response above the supratransmission threshold, the results in Figure 4.16 suggest that they are not appropriate for making quantitative predictions.

## 4.4 Prediction of the Onset of Supratransmission in Disordered Structures

### 4.4.1 Analytical Estimate of the Force Threshold

We make two assumptions to develop a theoretical framework for predicting the onset of transmission. Results from direct numerical simulations suggest that, to some extent, the periodic structure (i) behaves linearly below the threshold; i.e. for  $F < F_{th}$ , (ii) behaves nonlinearly predominantly at the first unit. These effects are observed because of the weak coupling between units. Based on these simplifications, we linearize the system for  $n \geq 2$ ; i.e. treat the nonlinearity locally. Moreover, we only keep the cubic term of  $F_M$  at  $n = 1$ ; this is done to keep the analysis tractable by pencil and paper. We call this model the *semi-linear* system. A similar approach, in terms of treating the nonlinearity locally, is used in [9] in the time domain for modeling the response of drill strings. The analysis presented here is performed in the frequency domain and consequently applies only to the

steady-state response of the system.

In the linear part of the semi-linear model ( $2 \leq n \leq N$ ), we use a transfer-matrix formulation to find the response of the system. We then use a harmonic approximation of the nonlinear response and find an expression for the onset of instability. We only present the final results from this analysis here. Refer to Appendices B.1 and B.2 for derivations.

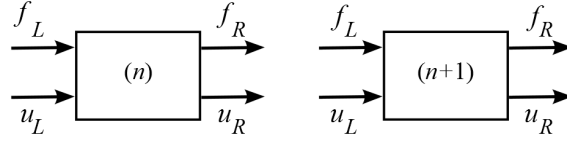


**Figure 4.17:** The schematics of two adjacent units in a mono-coupled system.

Figure 4.17 shows a schematic representation of two adjacent units in the assembled periodic structure. On either side of each unit (left and right), there is a displacement and force. We want to relate the force and displacement on the left side of the second unit ( $n = 2$ ) to the force and displacement on the right side of the last unit ( $n = N$ ). Between adjacent units, we can write

$$\begin{Bmatrix} u_R \\ f_R \end{Bmatrix}^{(n+1)} = [T^{(n+1)}] \begin{Bmatrix} u_R \\ f_R \end{Bmatrix}^{(n)} \quad (4.8)$$

where  $[T^{(n+1)}]$  depends on the properties of the  $(n+1)$ -th unit. The (complex-valued) amplitudes of the displacement and force on the left side of each unit are denoted by  $u_L$  and  $f_L$ , where a time dependence of  $\exp(i\Omega t)$  is assumed. For each linear unit, we have

$$[T^{(n)}] = \begin{bmatrix} 1 + \sigma_n/k_c & 1/k_c \\ \sigma_n & 1 \end{bmatrix} \quad (4.9)$$

where

$$\sigma_n \equiv \omega_n^2 + 2i\zeta\Omega - \Omega^2 \quad (4.10)$$

Moving along the finite chain from the last unit all the way back to the first unit we

can write

$$\begin{Bmatrix} u_R \\ f_R \end{Bmatrix}^{(N)} = \mathbf{T}_{\text{total}} \begin{Bmatrix} u_R \\ f_R \end{Bmatrix}^{(1)} = \begin{bmatrix} T_{11} & T_{12} \\ T_{21} & T_{22} \end{bmatrix} \begin{Bmatrix} u_R \\ f_R \end{Bmatrix}^{(1)} \quad (4.11)$$

where  $\mathbf{T}_{\text{total}} = [T]^{N-1}$  for the ordered system and  $\mathbf{T}_{\text{total}} = [T^{(N)}] \times \dots \times [T^{(2)}]$  in the disordered case. Moving from the right to left side of the nonlinear unit, as explained in Appendix B.2, the forcing amplitude at the onset of transmission,  $F_{th}$ , can be written as

$$F_{th}^2 = 18\alpha^2 \left( p \pm \sqrt{q^3} \right) \quad (4.12)$$

where  $p$  and  $q$  depend on the components of  $\mathbf{T}_{\text{total}}$  and  $[T^{(1)}]$ . Supratransmission occurs when the right-hand side of (4.12) is real and positive. In particular, we need  $q > 0$ ; this gives the critical frequency at which the enhanced nonlinear transmission starts. Threshold curves predicted by (4.12) are *exact* for a periodic structure (ordered or disordered) that has a cubic nonlinearity at  $n = 1$  and is otherwise linear. We have verified this by comparing analytical predictions to exact numerical computation of the threshold curves. The two results match very well. We have not included this comparison for brevity.

Although our derivation was based on a periodic structure with on-site nonlinearity, we expect it to be valid for structures with inter-site nonlinearity as well, provided that ‘strain variables’ (relative displacements of adjacent units) are used. The analysis here is very similar to the analyses performed in Sections 2.5.1 and 3.4. The main difference between the present derivation and the analyses in previous chapters is that the former can include any number of linear units. Indeed, one can retrieve the results from (2.26) and (3.4) by, respectively, setting  $N = 1$  and  $N = 2$  in the formulation presented above.

Finally, it is worth mentioning that (4.12) traces (within the approximation limits) the locus of the first saddle-node bifurcation of the NLRM. Any other bifurcation of the NLRM will go unnoticed by this formulation. It is possible (though painstaking) to extend the analytical results such that the third saddle-node bifurcation of the NLRM can be traced as well. Nevertheless, this might not be worthwhile because of the complications explained in Section 4.2.

## 4.4.2 Dependence of Threshold Curves on Nonlinearity

The main limitations of the current analysis are in (i) confining the nonlinearity to the first (driven) unit and (ii) ignoring the higher-order nonlinear terms in  $F_M$ . The assumption of local nonlinearity is expected to hold for weak coupling (i.e. small  $C$ ) and away from the linear pass band, in particular. Keeping the cubic term is expected to work for weak nonlinearity (i.e. small  $|u_L^{(1)}|^2$ ). In this section, we keep the strength of coupling unchanged ( $C = 0.05$ ) and explore how the two aspects of nonlinearity mentioned above change the threshold curves in an ordered structure. The influence of coupling strength will be explored in Section 4.4.3. The same conclusions that we draw for an ordered structure apply to individual realizations of disordered structures as well. In an ensemble-average sense, we showed in Section 4.3.2 that transmission thresholds do not change away from the pass band. Thus, we expect the results in this section to carry over to average properties of disordered systems as well.

We compare the threshold curves in the following four nonlinear systems:

1. Full nonlinearity, global: the system defined in (2.3).
2. Cubic nonlinearity, global: the system defined in (2.3),  $F_{M,n}$  truncated at cubic term.
3. Full nonlinearity, local: the system defined in (2.3), nonlinear terms of  $F_{M,n}$  ignored for  $2 \leq n \leq N$ .
4. Cubic nonlinearity, local: the system defined in (2.3),  $F_{M,n}$  truncated at cubic term, nonlinear terms of  $F_{M,n}$  ignored for  $2 \leq n \leq N$ .

We consider both softening and hardening systems. We choose system parameters such that the nonlinear terms in the softening and hardening systems have the same magnitude but opposite signs. The results presented in this section are obtained using numerical continuation.

Figure 4.18 shows the threshold curves for the four nonlinear systems for a softening system with cubic coefficient  $k_3 = -0.2$ . Comparing systems with global nonlinearity to those with local nonlinearity, we see that treating the nonlinearity locally results in a slight overestimation of the threshold force. Nevertheless,

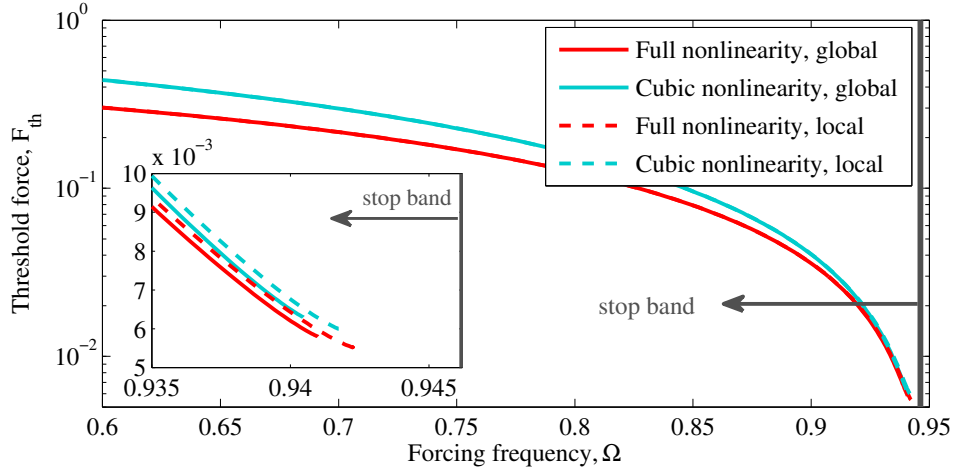


**Figure 4.18:** Threshold curves for different nonlinear forces in a softening structures with  $k_3 = -0.2$ . Solid curves correspond to systems in which all units are nonlinear (global nonlinearity), dashed curves to systems in which only the first unit is nonlinear (local nonlinearity). Red curves are used when the nonlinear term  $F_M$  is used as defined in (2.4). Cyan curves are used when  $F_M$  is truncated at its cubic term. The edge of the pass band is denoted by the horizontal arrows. The inset shows frequencies close to the pass band edge.

this difference is only noticeable at frequencies where the threshold curve starts, which is very close to the pass band (this point is a cusp in the  $F - \Omega$  plane – see Figure 4.6). The reason for the good agreement between locally- and globally-nonlinear systems is that the coupling between units is very weak ( $C \ll 1$ ). As  $\Omega$  moves farther into the stop band, we see that a larger force  $F_{th}$  is required to trigger instability. As a result of this, the amplitude of vibrations in the driven unit (i.e.  $|u_L^{(1)}|$ ) becomes larger at the onset of instability. This makes the contribution from higher-order nonlinear terms more significant; therefore, the approximation in truncating  $F_{M,n}$  at its cubic term becomes less accurate. This is why the difference between threshold curves with full nonlinearity and cubic nonlinearity increases as we move away from the pass band. The same reasoning explains why the system with cubic nonlinearity overestimates the threshold force.

Truncating the nonlinearity at its cubic term or restricting it to  $n = 1$  has the

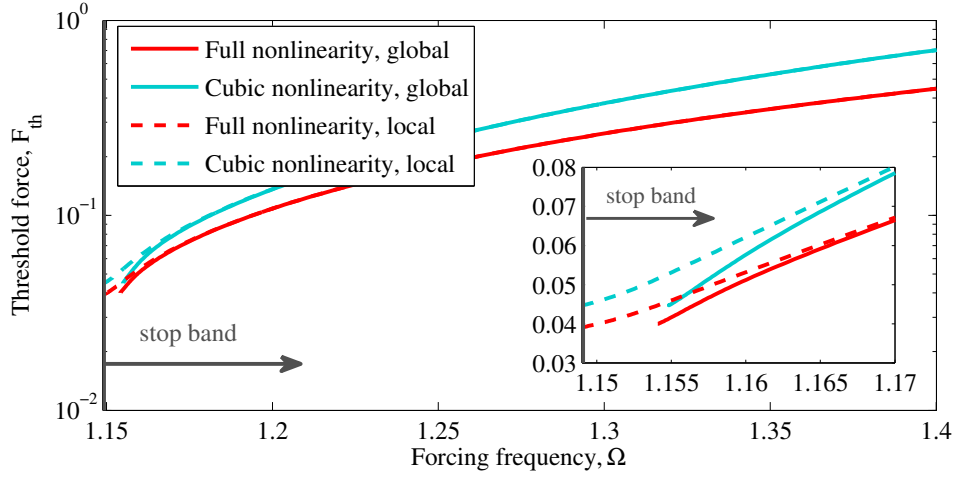


**Figure 4.19:** Threshold curves for different nonlinear forces in a hardening structures with  $k_3 = +0.2$ . Solid curves correspond to systems in which all units are nonlinear (global nonlinearity), dashed curves to systems in which only the first unit is nonlinear (local nonlinearity). Red curves are used when the nonlinear term  $F_M$  is used as defined in (2.4). Cyan curves are used when  $F_M$  is truncated at its cubic term. The edge of the pass band is denoted by the horizontal arrows. The inset shows frequencies close to the pass band edge.

same qualitative effect on threshold curves in hardening systems as it does in softening systems. We can see this in Figure 4.19, which shows the four threshold curves for a hardening system with cubic coefficient  $k_3 = 0.2$ . Apart from these similarities, we see two main differences between threshold curves in hardening and softening systems. Firstly, restricting nonlinearity to the first unit extends the threshold curve to the pass band for a hardening system (compare solid curves to dashed curves in Figure 4.19). To explain this, we recall from Section 4.3.1 that threshold curves trace the locus of saddle-node bifurcations, and from Section 3.6 that the solutions within the pass band usually lose stability through a Neimark-Sacker bifurcation. When the threshold curve of a locally-nonlinear system continues inside the pass band, it means that the corresponding linear solutions lose their stability via saddle-node bifurcation. Thus, treating the nonlinearity locally can predict an incorrect instability mechanism for a globally-nonlinear system close to

(and within) the pass band. Further discussion of the exact bifurcation structure in the vicinity of the pass band, and its dependence on damping, is beyond the scope of this work. This is also the frequency range where supratransmission is of less interest, as discussed in Section 4.2.

Secondly, approximating the nonlinear term as cubic gives a more accurate estimation of the threshold curves in the softening system than the hardening system. We can see this by comparing threshold curves in Figures 4.18 and 4.19. For a given distance from pass band, notice that the values of threshold force  $F_{th}$  are higher in the hardening system than the corresponding ones in the softening system. Thus, just before the onset of instability, the amplitudes of motion are higher in the hardening system. As a result, the higher-order nonlinear terms are more important in determining the onset of transmission in the hardening structure than in the softening one. We have confirmed this by computing the threshold curves for systems in which  $F_{M,n}$  is truncated at its quintic term (not shown). The threshold curves for the systems with quintic nonlinearity were much closer to the threshold curves of the fully nonlinear system.

### 4.4.3 Dependence of Locally-Nonlinear Behavior on Coupling

As already stated, the basis for treating the nonlinearity locally is weak strength of coupling between units. This approximation is expected to lose accuracy as the strength of coupling increases. To investigate this, we compute the threshold curves at different values of  $C$  for two hardening structures with full nonlinearity; i.e. having the complete nonlinear form of  $F_{M,n}$  from (2.4). In one of them nonlinearity is treated locally, while in the other one all units are nonlinear (globally nonlinear). We compare these threshold curves in Figure 4.20 as a function of the distance from pass band,  $\Delta\Omega$ . This is because increasing  $C$  moves the pass band edge to higher frequencies. Thus, we define

$$\Delta\Omega \equiv \Omega - \omega_N \quad (4.13)$$

where  $\omega_N = \omega_N(C)$  is the largest linear natural frequency of the structure.

We see in Figure 4.20 that the threshold curves extend to the pass band for the locally nonlinear structures (see the discussion in Section 4.4.2). There is therefore

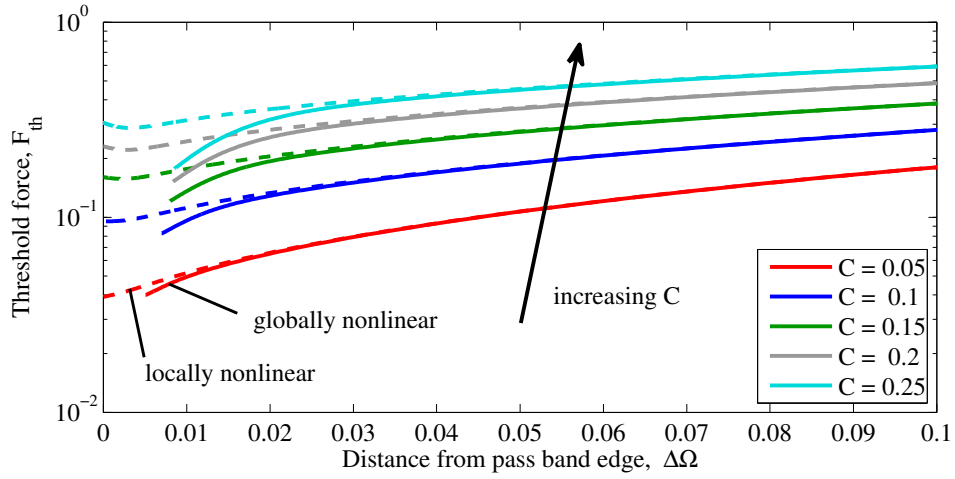


**Figure 4.20:** The influence of coupling strength on threshold curves for the system with full nonlinearity. Solid curves correspond to the globally nonlinear case and dashed curves to the locally nonlinear case. The horizontal axis shows the distance from pass band edge, where  $\Delta\Omega$  is defined in (4.13). The arrow indicates the direction of increasing coupling strength. As the strength of coupling increases, restricting the nonlinear forces to  $n = 1$  is inaccurate over a larger frequency range. The red curves ( $C = 0.05$ ) are reproduced from Figure 4.19.

a frequency range in the vicinity of the pass band where using a locally-nonlinear model predicts an incorrect instability mechanism; this frequency range increases with the strength of coupling. Furthermore, the assumption of local nonlinearity becomes more inaccurate as  $C$  increases, and overestimates the threshold curves over a larger frequency range. For frequencies far from the pass band, restricting nonlinearity to the driven unit gives an accurate prediction of the onset of supra-transmission. The reason is that, in this frequency range, the linear response is highly localized to the driven unit and dispersion (Bragg scattering) dominates over nonlinear forces. As  $C$  increases, the assumption of local nonlinearity is accurate over a smaller frequency range.

## 4.5 Concluding Remarks

We studied the interaction among the effects of dispersion, dissipation, disorder and nonlinearity in the context of supratransmission. We considered a damped nonlinear periodic structure of finite length with weakly coupled units. Disorder was introduced as small variations in the on-site stiffness parameters of the structure, drawn from a uniform statistical distribution.

We showed that although individual realizations of a disordered structure have different onsets of supratransmission, the threshold curve is robust to disorder when averaged over an entire ensemble. For harmonic excitation away from the pass band edge, increasing the strength of disorder has negligible influence on transmitted energies below the onset of supratransmission. In contrast, we found average transmitted energies to decrease with disorder above the transmission threshold. This happens because the average frequency spectra of the nonlinearly transmitted waves lie within the linear pass band of the structure. This is the frequency range where disorder is known to localize the response to the driven unit (Anderson localization). Overall, as the forcing frequency moves away from the pass band, dispersion effects become dominant and the influence of disorder decreases.

We provided approximate analytical expressions for predicting the onset of supratransmission in weakly coupled structures. This formulation is exact for a disordered periodic structure that has cubic nonlinearity in its driven unit and is linear otherwise. We further studied the range of validity of the analysis by studying the dependence of threshold curves on nonlinearity and strength of coupling. For forcing frequencies away from the edge of a pass band, where the linear solution is highly localized, we found that the nonlinear forces are confined to the driven unit. In this frequency range, truncating the nonlinear forces at their cubic terms results in overestimation of the onset of supratransmission. However, using the complete form of the nonlinear forces gives a very accurate prediction of the threshold curves. Closer to the pass band edge, the linear response is no longer highly localized and the nonlinearity spreads to other units. Strong coupling invalidates our analysis, but is of less interest in the context of disordered periodic structures (Anderson localization).

We highlighted a non-trivial influence of damping and disorder on the onset

of supratransmission. Damping may bring about other stable periodic solutions at the first turning point of the NLRM. In this scenario, supratransmission does not occur at the first turning point of the NLRM, as normally expected. We showed that disorder may either facilitate or inhibit this feature, depending on the realization and strength of disorder. We further observed that supratransmission could still take place at a subsequent (the third) turning point of the NLRM.

## Chapter 5

# Conclusion

When a nonlinear periodic structure is harmonically forced at one end with a forcing frequency within its stop band, wave transmission can still occur if the forcing amplitude is beyond a certain threshold. This is a generic instability-driven transmission phenomenon in discrete nonlinear periodic structures, known as supratransmission.

This thesis has addressed the nonlinear phenomenon of supratransmission in a discrete periodic structure using computational and analytical techniques. We reported several novel findings in this context, specifically targeted to periodic structures that are relevant in engineering applications: periodic structures with damping, finite length and disorder (small deviations from exact periodicity spread throughout the structure). The knowledge generated in this thesis contributes to the understanding of high-amplitude energy transmission characteristics of periodic structures, and to design of new devices and materials with almost-periodic micro-architecture to operate in the nonlinear regime.

We summarize our findings in Section 5.1 and provide a synopsis of our analyses. In Section 5.2, we discuss the limitations of the methodologies used in this thesis. We provide suggestions for future research in this area in Section 5.3.

## 5.1 Summary of Contributions

We proposed a macro-mechanical periodic structure that consists of coupled suspended cantilever beams (Figure 2.1). Within each unit cell, the linear restoring force of the beam is combined locally with a strong nonlinear magnetic force to produce on-site nonlinearity. The magnetic force can be tuned, thus providing control over the strength of nonlinearity, as well as its type (softening or hardening). We carried out our entire investigations based on a mathematical model of this setup that was developed in Section 2.1.

Using this platform, we performed a systematic study of the supratransmission phenomenon. The nonlinear periodic structures considered throughout the thesis have finite length, light damping and weak coupling forces between adjacent units. We summarize our contributions under three main categories:

### I. Underlying mechanism

We studied supratransmission using direct numerical simulations and numerical continuation techniques (Sections 2.3 and 2.4). We identified the instability mechanism underlying supratransmission as a saddle-node bifurcation in the nonlinear response manifold (NLRM) of the damped, finite structure. This is the same mechanism responsible for supratransmission in infinite-dimensional Hamiltonian systems. Using continuation methods, the NLRM is constructed numerically and *threshold curves* are computed as the loci of the first saddle-node bifurcation points as a function of the forcing frequency.

The supratransmission phenomenon may be explained, *in a qualitative fashion*, as the resonance of the driving force with the shifted pass bands of the periodic structure. The behavior of the threshold curve also supports this explanation: as the forcing frequency moves farther from the pass band, a higher force amplitude is required for the onset of supratransmission. We showed in Section 2.4.2 that the true mechanism underlying supratransmission is indeed the instability of periodic solutions via a saddle-node bifurcation. We concluded that the resonance of the driving force with the shifted pass band is not an accurate predictor of supratransmission from either a phenomenological or quantitative perspective.

For forcing amplitudes below the supratransmission threshold, the response of

the structure lies within the basin of attraction of a limit cycle (a periodic attractor). This solution branch continues to the trivial (static) equilibrium of the structure. At the onset of supratransmission, the response of the system jumps from this basin of attraction to that of a non-periodic (either a quasi-periodic or chaotic) attractor. This change in the basin of attraction is accompanied by a large increase (orders of magnitude) in the transmitted energy; i.e. supratransmission. If another periodic attractor (limit cycle) existed at the saddle-node bifurcation point, then the response would have jumped to that solution branch instead, though the increase in the transmitted energy would be significantly smaller in comparison.

The occurrence of supratransmission has two main manifestations in the post-threshold response of the structure: (1) the response of the first unit has a broadband frequency spectrum, (2) the response of the last unit has a band-limited frequency spectrum, concentrated at the pass bands of the linear structure. From this perspective, supratransmission can be described as a band-limited transmission mechanism.

## **II. Influence of system parameters (ordered structures)**

We studied the influence of several system parameters on the supratransmission phenomenon in ordered structures (Chapter 3). A synopsis of these parametric studies is provided here:

- **Forcing frequency**

The forcing frequency plays a significant role in supratransmission. As the forcing frequency moves away from the pass band, dispersion effects become more dominant and a higher force amplitude is required for the onset of supratransmission.

The increase in transmitted energies is higher for forcing frequencies that are farther from the edge of a pass band.

- **Type and strength of nonlinearity**

The type of nonlinearity determines on which side of a pass band supratransmission may occur. This is below the pass band in the case of softening nonlinearity

and above it when the nonlinear force is hardening.

Increasing the strength of nonlinear forces decreases the force required for the onset of supratransmission.

- **Number of units**

For weakly coupled structures, increasing the number of units increases the force threshold at the onset of supratransmission.

For both types of nonlinearity, the influence of the number of units on supratransmission is significant only for driving frequencies very close to the pass band edge.

- **Damping**

Generally speaking, damping increases the force required for the onset of supratransmission. Apart from this, we have identified two other effects that are brought about by damping.

(i) Damping may eliminate supratransmission within a frequency range in the vicinity of the linear pass band. This occurs because damping can modify the topology of an NLRM such that it no longer possesses a saddle-node bifurcation. Damping also introduces a threshold on the minimum force amplitude required for supratransmission to occur. This threshold is zero in undamped structures and increases with damping. Also, increasing the damping ratio widens the frequency range over which supratransmission is prohibited by damping.

(ii) Damping may delay the onset of supratransmission compared to the expected force threshold of a damped structure (coinciding with the first turning point of the NLRM, TP1). This could happen provided that damping stabilizes other branches of periodic solutions above TP1. In this case, supratransmission cannot take place at TP1 because the response gets trapped to another limit cycle instead of moving to the basin of attraction of a non-periodic attractor. Supratransmission may still take place in this scenario, but at a subsequent bifurcation of the NLRM (e.g. the third turning point).

- **Strength of coupling**

Increasing the strength of coupling increases the minimum force required for the onset of supratransmission at all driving frequencies.

For damped structures with weak coupling, the strength of coupling does not alter the location of the critical frequency at the onset of supratransmission (with respect to the edge of a pass band).

### **III. Analytical prediction of the onset of supratransmission**

Using numerical simulations, we observed that nonlinear forces are confined to the driven unit for weakly coupled systems. Relying on this observation, and truncating the nonlinear forces at the cubic terms, we were able to provide three approximate closed-form analytical estimates for predicting the onset of supratransmission for weakly coupled periodic structures. These expressions vary in their degree of complexity and range of applicability. Nevertheless, they all rely on estimating the locus of the first saddle-node bifurcation of the NLRM of the system. The first two analyses are developed based on the equations governing the evolution of the envelope of harmonic waves through the structure. The third analysis is developed based on a nonlinear analysis of the first unit coupled with a transfer-matrix formulation to account for the (linear) dynamics of the rest of the periodic structure.

The first analysis (Section 2.5) is based on the local nonlinear dynamics of the driven unit, decoupled from the rest of the periodic structure. Accordingly, this formulation cannot capture the dependence of supratransmission on the strength of coupling. The results of this analysis are valid for very weak values of coupling, near the anti-continuum limit. Nevertheless, this formulation can be used to provide qualitative explanations of certain features of supratransmission; examples include the influence of nonlinearity and damping (Sections 3.1 and 3.3).

The second analysis (Section 3.4) is an improvement of the first one, incorporating the strength of coupling into the predictions. This analysis is based on the local nonlinear dynamics of the driven unit coupled to another linearized unit (the rest of the structure is truncated after the second unit). The expression obtained from the second analysis can estimate the influence of coupling on threshold curves, but cannot be used in a disordered structure. The second formulation

is valid over a wider range of coupling strengths than the first formulation, but it is still limited to weak strengths of coupling.

The third analysis (Section 4.4) is performed for a periodic structure of arbitrary length, with the nonlinear forces confined to the driven unit and truncated at the cubic term. Thus, it can be used for estimating the onset of supratransmission in ordered and disordered periodic structures. We explored the range of validity of this formulation by studying the dependence of threshold curves on nonlinearity and strength of coupling. We find that our analytical predictions overestimate the onset of supratransmission, particularly at frequencies close to the pass band.

All three analytical approaches rely on weak strength of coupling to ensure that the nonlinear forces can be confined to the driven unit. Strong coupling invalidates this assumption, but is of less interest in the context of disordered periodic structures.

Although our analyses were based on a periodic structure with on-site nonlinearity, we expect them to be generally valid for structures with inter-site nonlinearity as well, provided that ‘strain variables’ (relative displacements of adjacent units) are used.

#### **IV. Interaction between supratransmission and Anderson localization**

We studied the interaction between supratransmission and Anderson localization in a weakly coupled disordered periodic structure with damping and finite length. Disorder was introduced as small random perturbations in the stiffness parameters of the structure, drawn from a uniform statistical distribution.

We showed that supratransmission persists in the presence of disorder, with individual realizations of a disordered structure having different force thresholds. The influence of disorder decreases in general as the forcing frequency moves away from the pass band edge, reminiscent of dispersion effects subsuming Anderson localization in linear periodic structures.

Averaging over an entire ensemble of disordered structures, we found that the threshold curve is robust to disorder. In other words, the average force threshold required to trigger supratransmission remains unchanged. In contrast, the average transmitted energy above the supratransmission threshold decreases with the

strength of disorder. This happens because the average frequency spectra of the nonlinearly transmitted waves lie within the linear pass band of the structure.

## 5.2 Limitations

Naturally, the methodology adopted in a study includes certain limitations. We highlight the following factors as the main limitations of this work.

### Mathematical modeling

The mathematical modeling of the periodic structure in Figure 2.1 was based on the assumption that the motion of each beam is described by its fundamental mode shape. This is a reasonable assumption as long as (a) the forcing frequencies are close to the first pass band of the structure (b) the second pass band is far from this frequency range. In the presence of nonlinear forces, however, it is possible to excite higher frequencies through internal and combination resonances [98]. In this situation, the mathematical model developed in Section 2.1.1 would need to be updated. Ultimately, experimental results can determine whether these effects are significant.

Another important assumption made in developing the equations of motion was the modeling of the magnetic forces,  $F_{M,n}$  in (2.2). Within each unit cell, we treated the permanent magnet and electromagnets as magnetic poles and used Coulomb's law to model the magnetic interaction forces between them. In practice, this force would need to be modeled based on experimental system identification; refer to [59, 100] for comprehensive reviews of relevant experimental methodologies.

Throughout this work, dissipative effects were modeled using mass-proportional linear viscous damping forces. This is a very common assumption in physical modeling of periodic structures (even in granular crystals [110]). However, it is conceivable that damping in the structure can be non-proportional, for example due to electrodynamic damping introduced through connecting a shaker to the structure. Again, this aspect would need to be explored experimentally [107].

## **Weak coupling**

For periodic structures with damping and finite length, Anderson localization becomes relevant at weak strengths of coupling – recall the discussion in Section 4.1. Accordingly, we restricted the scope of this thesis to weakly coupled periodic structures. In the absence of disorder, however, this requirement may be relaxed.

Although supratransmission relies on the existence of a stop band, it is not restricted to weakly coupled structures. In fact, the initial studies on supratransmission [39, 40, 60, 62] were performed closer to the continuum limit. Weakly coupled structures were eventually considered, possibly due to the existence of discrete breathers and specifically the connection between supratransmission and mobile breathers in some parameter ranges [82]. Although supratransmission has been studied for moderate and strong strengths of coupling, these studies mostly pertain to undamped periodic structures of infinite extent. The effects of damping and finite length on supratransmission in (ordered) periodic structures remain unexplored in this range of coupling strengths.

## **Analytical approach**

The analytical predictions of the onset of supratransmission were developed based on estimating the loci of the first turning points (saddle-node bifurcations) of the NLRM. Consequently, any other bifurcation of an NLRM will go unnoticed by these formulations. For undamped structures, there exists no precedence of supratransmission occurring through a different mechanism. In damped structures, however, we showed that damping may stabilize another periodic branch at the first turning point of the NLRM, thereby delaying the onset of supratransmission until subsequent bifurcations of the NLRM.

It is possible to extend the existing analytical approach to locate the third turning point of the NLRM as well. This becomes possible by truncating the nonlinear force at the quintic term instead of the cubic term. Note, however, that it might be possible for the periodic solutions to lose their stability between the first and third turning points through a Neimark-Sacker bifurcation. We are not aware of a methodology that can be used to tackle this scenario analytically.

In our analyses, we restricted the nonlinear forces to the driven unit. Relaxing

this assumption makes the analytical approach intractable.

### **Disorder effects**

Throughout Chapter 4, we used a uniform statistical distribution for realization of disordered structures. Furthermore, we mostly focused on the average properties of an ensemble. A comprehensive statistical analysis of the threshold curves and transmitted energies remains to be performed. This analysis could determine, among other things, the relations between the probability density functions and standard deviations of the disorder parameter and threshold curves. This information is important from a practical point of view because the statistical mode of an ensemble may be significantly different from its mean value depending on the corresponding probability distribution function – this was not the situation encountered for the case studied in this thesis.

In this work, we introduced disorder to the on-site stiffness parameter. From a phenomenological point of view, disorder-borne localization still occurs if disorder is introduced through other parameters of the system [65, 108]. Nevertheless, it will be useful to obtain a *quantitative* comparison of disorder effects based on different disorder parameters. Possible additional disorder parameters include coupling stiffness, on-site and inter-site damping and on-site modal mass parameters.

## **5.3 Future Directions**

In addition to the limitations outlined in Section 5.2, a number of other avenues can be explored for future research on this topic.

### **Experimental realization of supratransmission**

An impactful continuation of this thesis is experimental realization of supratransmission in the periodic structure proposed in Section 2.1. This experimental setup can be readily used to investigate the influence of the type and strength of non-linearity on supratransmission, as well as to investigate the associated hysteresis phenomenon. It may also be used to realize disordered periodic structures by varying the currents passing through the electromagnets in different units.

### **Band-limited excitation**

In supratransmission, external excitation is provided through a harmonic force. This is equivalent to a very sharp frequency spectrum (a Dirac delta function, strictly speaking). In engineering practice, it is not uncommon to encounter a situation where the frequency spectrum of an excitation comprises a narrow band of frequencies. For a given wave form with its bandwidth entirely within the stop band, it would be expected that a phenomenon similar to supratransmission would occur beyond a certain forcing amplitude; i.e. a sudden increase in the transmitted energies with the frequency spectra of transmitted waves lying within the pass band.

### **Multi-coupled structures**

The periodic structure we studied in this thesis is a *mono-coupled* structure, meaning that the coupling between adjacent units occurs through *one* coordinate (degree of freedom) of the system. Wave propagation in *multi-coupled* periodic structures is more complicated. Multi-coupled structures carry different types of traveling waves, which can convert to each other as they propagate through the structure [15, 88]. Although the consequences of such wave conversions have been addressed in the linear operating range, their nonlinear counterpart has not received much attention.

### **Strong propagation regime**

The strong propagation regime that was briefly introduced in Section 3.7 has received very little attention in the literature. Further numerical investigation of this phenomenon could be of interest. The pressing practical question here is to determine whether the strong propagation regime exists in the presence of damping.

Some of the above studies are ongoing and others will need to be pursued in the future.

# Bibliography

- [1] M. Abramowitz and I. A. Stegun. *Handbook of Mathematical Functions*. Number 55. Courier Dover Publications, 1972. → pages 40, 120
- [2] V. Achilleos, G. Theocharis, and C. Skokos. Energy transport in one-dimensional disordered granular solids. *Physical Review E*, 93: 022903, 2016. → pages 10
- [3] P. W. Anderson. Absence of diffusion in certain random lattices. *Physical Review*, 109(5):1492, 1958. → pages 62
- [4] N. Ashcroft and N. Mermin. *Solid State Physics*. HRW international editions. Holt, Rinehart and Winston, USA, 1976. → pages 3
- [5] S. Aubry. Discrete breathers: Localization and transfer of energy in discrete Hamiltonian nonlinear systems. *Physica D: Nonlinear Phenomena*, 216(1):1–30, 2006. → pages 33
- [6] W.-J. Beyn, A. Champneys, E. Doedel, W. Govaerts, Y. A. Kuznetsov, and B. Sandstede. Numerical continuation, and computation of normal forms. In B. Fiedler, editor, *Handbook of Dynamical Systems*, pages 149 – 219. Elsevier Science, 2002. → pages 115
- [7] N. Boechler, G. Theocharis, and C. Daraio. Bifurcation-based acoustic switching and rectification. *Nature Materials*, 10(9):665–668, 2011. → pages 9
- [8] L. Brillouin. *Wave Propagation in Periodic Structures*. Dover Publications, U.S.A., 1953. → pages 1, 3
- [9] T. Butlin and R. Langley. An efficient model of drillstring dynamics. *Journal of Sound and Vibration*, 356:100–123, 2015. → pages 83

- [10] D. K. Campbell, S. Flach, and Y. S. Kivshar. Localizing energy through nonlinearity and discreteness. *Physics Today*, 57(1):43–49, 2004. → pages 6, 33
- [11] M. Carrara, M. Cacan, M. Leamy, M. Ruzzene, and A. Erturk. Dramatic enhancement of structure-borne wave energy harvesting using an elliptical acoustic mirror. *Applied Physics Letters*, 100(20):204105, 2012. → pages 2
- [12] M. P. Castanier and C. Pierre. Individual and interactive mechanisms for localization and dissipation in a mono-coupled nearly-periodic structure. *Journal of Sound and Vibration*, 168(3):479–505, 1993. → pages 62, 65
- [13] P. D. Cha and C. R. Morganti. Numerical statistical investigation on the dynamics of finitely long, nearly periodic chains. *AIAA Journal*, 32(11):2269–2275, 1994. → pages 62
- [14] G. Chakraborty and A. Mallik. Dynamics of a weakly non-linear periodic chain. *International Journal of Non-Linear Mechanics*, 36(2):375–389, 2001. → pages 8, 36
- [15] W. J. Chen. *Vibration localization and wave conversion phenomena in a multi-coupled, nearly periodic, disordered truss beam*. PhD thesis, University of Michigan, 1993. → pages 102
- [16] D. Chevriaux, R. Khomeriki, and J. Léon. Theory of a Josephson junction parallel array detector sensitive to very weak signals. *Physical Review B*, 73(21):214516, 2006. → pages 9
- [17] H. Cho, M.-F. Yu, A. F. Vakakis, L. A. Bergman, and D. M. McFarland. Tunable, broadband nonlinear nanomechanical resonator. *Nano Letters*, 10(5):1793–1798, 2010. → pages 9
- [18] H. Cho, B. Jeong, M.-F. Yu, A. F. Vakakis, D. M. McFarland, and L. A. Bergman. Nonlinear hardening and softening resonances in micromechanical cantilever-nanotube systems originated from nanoscale geometric nonlinearities. *International Journal of Solids and Structures*, 49(15):2059–2065, 2012. → pages 9
- [19] R. V. Craster and S. Guenneau. *Acoustic Metamaterials: Negative Refraction, Imaging, Lensing and Cloaking*, volume 166. Springer Science & Business Media, 2012. → pages 2
- [20] S. A. Cummer, J. Christensen, and A. Alù. Controlling sound with acoustic metamaterials. *Nature Reviews Materials*, 1:16001, 2016. → pages 2

- [21] H. Dankowicz and F. Schilder. *Recipes for Continuation*, volume 11. Society for Industrial and Applied Mathematics, U.S.A., 2013. → pages 117
- [22] T. Dauxois and M. Peyrard. *Physics of Solitons*. Cambridge University Press, U.K., 2006. → pages 6
- [23] J. P. Den Hartog. *Mechanical Vibrations*. Dover Publications, U.S.A., second edition, 1985. → pages 13
- [24] P. A. Deymier. *Acoustic Metamaterials and Phononic Crystals*, volume 173. Springer Science & Business Media, 2013. → pages 2
- [25] A. Dick, B. Balachandran, and C. Mote Jr. Intrinsic localized modes in microresonator arrays and their relationship to nonlinear vibration modes. *Nonlinear Dynamics*, 54(1-2):13–29, 2008. → pages 7
- [26] E. J. Doedel and B. E. Oldeman. *AUTO-07P: Continuation and bifurcation software for ordinary differential equations*. Concordia University, Canada, 2012. → pages 33, 117
- [27] I. El-Kady, R. Olsson, and J. Fleming. Phononic band-gap crystals for radio frequency communications. *Applied Physics Letters*, 92(23):3504, 2008. → pages 2
- [28] E. Emaci, D. Kim, and A. F. Vakakis. Impurity modes in disordered non-linear lattices. *International Journal of Non-Linear Mechanics*, 32(1): 21–30, 1997. → pages 10
- [29] J. Emad, A. F. Vakakis, and N. Miller. Experimental nonlinear localization in a periodically forced repetitive system of coupled magnetoelastic beams. *Physica D: Nonlinear Phenomena*, 137(1):192–201, 2000. → pages 7
- [30] D. Ewins. Vibration characteristics of bladed disc assemblies. *Journal of Mechanical Engineering Science*, 15(3):165–186, 1973. → pages 3
- [31] B.-F. Feng and T. Kawahara. Discrete breathers in two-dimensional nonlinear lattices. *Wave Motion*, 45(1):68–82, 2007. → pages 6
- [32] S. Flach and A. V. Gorbach. Discrete breathers: Advances in theory and applications. *Physics Reports*, 467(1):1–116, 2008. → pages 7
- [33] N. Fleck, V. Deshpande, and M. Ashby. Micro-architected materials: Past, present and future. *Proceedings of the Royal Society of London A*:

*Mathematical, Physical and Engineering Sciences*, 466(2121):2495–2516, 2010. → pages 1

- [34] N. M. Frandsen, O. R. Bilal, J. S. Jensen, and M. I. Hussein. Inertial amplification of continuous structures: Large band gaps from small masses. *Journal of Applied Physics*, 119(12):124902, 2016. → pages 2
- [35] V. Freilikher, B. Liansky, I. Yurkevich, A. Maradudin, and A. McGurn. Enhanced transmission due to disorder. *Physical Review E*, 51(6):6301, 1995. → pages 68
- [36] H. Furstenberg and H. Kesten. Products of random matrices. *The Annals of Mathematical Statistics*, pages 457–469, 1960. → pages 65
- [37] R. Ganesh and S. Gonella. Spectro-spatial wave features as detectors and classifiers of nonlinearity in periodic chains. *Wave Motion*, 50(4):821–835, 2013. → pages 8
- [38] R. Ganesh and S. Gonella. Invariants of nonlinearity in the phononic characteristics of granular chains. *Physical Review E*, 90(2):023205, 2014. → pages 8
- [39] F. Geniet and J. Léon. Energy transmission in the forbidden band gap of a nonlinear chain. *Physical Review Letters*, 89(13):134102, 2002. → pages 9, 45, 100
- [40] F. Geniet and J. Léon. Nonlinear supratransmission. *Journal of Physics: Condensed Matter*, 15(17):2933, 2003. → pages 9, 17, 100
- [41] W. Govaerts, Y. A. Kuznetsov, and A. Dhooge. Numerical continuation of bifurcations of limit cycles in matlab. *SIAM Journal on Scientific Computing*, 27(1):231–252, 2005. → pages 117
- [42] M. R. Haberman and M. D. Guild. Acoustic metamaterials. *Physics Today*, 69(6):42–48, 2016. → pages 2
- [43] M. A. Hasan and S. Nemat-Nasser. Universal relations for solitary waves in granular crystals under shocks with finite rise and decay times. *Physical Review E*, 93(4):042905, 2016. → pages 8
- [44] S. He and J. Maynard. Detailed measurements of inelastic scattering in Anderson localization. *Physical Review Letters*, 57(25):3171, 1986. → pages 11

- [45] D. Hennig and G. P. Tsironis. Wave transmission in nonlinear lattices. *Physics Reports*, 307(5):333–432, 1999. → pages 7
- [46] D. Herbert and R. Jones. Localized states in disordered systems. *Journal of Physics C: Solid State Physics*, 4(10):1145, 1971. → pages 65
- [47] C. Hodges. Confinement of vibration by structural irregularity. *Journal of Sound and Vibration*, 82(3):411–424, 1982. → pages 62, 63, 67
- [48] C. Hodges and J. Woodhouse. Confinement of vibration by one-dimensional disorder, I: Theory of ensemble averaging. *Journal of Sound and Vibration*, 130(2):237–251, 1989. → pages 62
- [49] C. H. Hodges and J. Woodhouse. Vibration isolation from irregularity in a nearly periodic structure: Theory and measurements. *The Journal of the Acoustical Society of America*, 74(3):894–905, 1983. → pages 3, 64, 65, 67
- [50] P. Holmes and D. Rand. The bifurcations of Duffing’s equation: An application of catastrophe theory. *Journal of Sound and Vibration*, 44(2): 237–253, 1976. → pages 40, 120
- [51] C. Hoogeboom, Y. Man, N. Boechler, G. Theocharis, P. Kevrekidis, I. Kevrekidis, and C. Daraio. Hysteresis loops and multi-stability: From periodic orbits to chaotic dynamics (and back) in diatomic granular crystals. *Europhysics Letters*, 101(4):44003, 2013. → pages 9, 55
- [52] V. A. Hopkins, J. Keat, G. D. Meegan, T. Zhang, and J. Maynard. Observation of the predicted behavior of nonlinear pulse propagation in disordered media. *Physical Review Letters*, 76(7):1102, 1996. → pages 10
- [53] V. A. Hopkins, L. Kryzac, and J. Maynard. Experimental studies of nonlinear continuous waves and pulses in disordered media showing Anderson localization. *Physical Review B*, 58(17):11377, 1998. → pages 11
- [54] M. I. Hussein and M. J. Frazier. Band structure of phononic crystals with general damping. *Journal of Applied Physics*, 108(9):093506, 2010. → pages 4, 23
- [55] M. I. Hussein, M. J. Leamy, and M. Ruzzene. Dynamics of phononic materials and structures: Historical origins, recent progress, and future outlook. *Applied Mechanics Reviews*, 66(4):040802, 2014. → pages 2, 8

- [56] T. Ikeda, Y. Harata, and K. Nishimura. Intrinsic localized modes of harmonic oscillations in pendulum arrays subjected to horizontal excitation. *Journal of Computational and Nonlinear Dynamics*, 10(2):021007, 2015. → pages 7
- [57] M. Johansson, G. Kopidakis, S. Lepri, and S. Aubry. Transmission thresholds in time-periodically driven nonlinear disordered systems. *Europhysics Letters*, 86(1):10009, 2009. → pages 11, 12, 74
- [58] R. A. Johnson. *Mechanical Filters in Electronics*. John Wiley & Sons, 1983. → pages 2
- [59] G. Kerschen, K. Worden, A. F. Vakakis, and J.-C. Golinval. Past, present and future of nonlinear system identification in structural dynamics. *Mechanical Systems and Signal Processing*, 20(3):505–592, 2006. → pages 99
- [60] R. Khomeriki. Nonlinear band gap transmission in optical waveguide arrays. *Physical review letters*, 92(6):063905, 2004. → pages 100
- [61] R. Khomeriki, S. Lepri, and S. Ruffo. Pattern formation and localization in the forced-damped Fermi-Pasta-Ulam lattice. *Physical Review E*, 64(5):056606, 2001. → pages 9
- [62] R. Khomeriki, S. Lepri, and S. Ruffo. Nonlinear supratransmission and bistability in the Fermi-Pasta-Ulam model. *Physical Review E*, 70(6):066626, 2004. → pages 9, 39, 55, 100
- [63] M. Kimura and T. Hikihara. Coupled cantilever array with tunable on-site nonlinearity and observation of localized oscillations. *Physics Letters A*, 373(14):1257–1260, 2009. → pages 7, 13, 21
- [64] M. E. King and P. A. Layne. Dynamics of nonlinear cyclic systems with structural irregularity. *Nonlinear Dynamics*, 15(3):225–244, 1998. → pages 10
- [65] G. J. Kissel. *Localization in Disordered Periodic Structures*. PhD thesis, Massachusetts Institute of Technology, 1988. → pages 63, 101
- [66] K. T. V. Koon, J. Léon, P. Marquie, and P. Tchofo-Dinda. Cutoff solitons and bistability of the discrete inductance-capacitance electrical line: Theory and experiments. *Physical Review E*, 75(6):066604, 2007. → pages 9, 39, 55

- [67] G. Kopidakis and S. Aubry. Intraband discrete breathers in disordered nonlinear systems. II. Localization. *Physica D: Nonlinear Phenomena*, 139(3):247–275, 2000. → pages 33
- [68] B. Kramer and A. MacKinnon. Localization: Theory and experiment. *Reports on Progress in Physics*, 56(12):1469, 1993. → pages 67
- [69] B. Krauskopf, H. Osinga, and J. Galan-Vioque. *Numerical Continuation Methods for Dynamical Systems: Path Following and Boundary Value Problems*. Springer-Verlag, Netherlands, 2007. → pages 115
- [70] Y. Kuznetsov. *Elements of Applied Bifurcation Theory*. Springer-Verlag, U.S.A., 2004. → pages 28, 33, 58
- [71] A. Lagendijk, B. van Tiggelen, and D. S. Wiersma. Fifty years of Anderson localization. *Physics Today*, 62(8):24, 2009. → pages 62
- [72] R. Langley, N. Bardell, and H. Ruivo. The response of two-dimensional periodic structures to harmonic point loading: A theoretical and experimental study of a beam grillage. *Journal of Sound and Vibration*, 207(4):521–535, 1997. → pages 2
- [73] T. Lapyeva, M. Ivanchenko, and S. Flach. Nonlinear lattice waves in heterogeneous media. *Journal of Physics A: Mathematical and Theoretical*, 47(49):493001, 2014. → pages 10
- [74] B. S. Lazarov and J. S. Jensen. Low-frequency band gaps in chains with attached non-linear oscillators. *International Journal of Non-Linear Mechanics*, 42(10):1186–1193, 2007. → pages 8
- [75] Z. Liu, X. Zhang, Y. Mao, Y. Zhu, Z. Yang, C. Chan, and P. Sheng. Locally resonant sonic materials. *Science*, 289(5485):1734–1736, 2000. → pages 2
- [76] M.-H. Lu, L. Feng, and Y.-F. Chen. Phononic crystals and acoustic metamaterials. *Materials Today*, 12(12):34–42, 2009. → pages 2
- [77] T. Lu and F. Xin. *Vibro-acoustics of Lightweight Sandwich Structures*. Springer, 2014. → pages 3
- [78] J. Lydon, G. Theocharis, and C. Daraio. Nonlinear resonances and energy transfer in finite granular chains. *Physical Review E*, 91(2):023208, 2015. → pages 8
- [79] G. Ma and P. Sheng. Acoustic metamaterials: From local resonances to broad horizons. *Science advances*, 2(2):e1501595, 2016. → pages 2

- [80] J. Macías-Díaz and A. Puri. On the propagation of binary signals in damped mechanical systems of oscillators. *Physica D: Nonlinear Phenomena*, 228(2):112–121, 2007. → pages 9
- [81] P. Maniadis and S. Flach. Mechanism of discrete breather excitation in driven micro-mechanical cantilever arrays. *Europhysics Letters*, 74(3):452, 2006. → pages 48
- [82] P. Maniadis, G. Kopidakis, and S. Aubry. Energy dissipation threshold and self-induced transparency in systems with discrete breathers. *Physica D: Nonlinear Phenomena*, 216(1):121–135, 2006. → pages 8, 9, 10, 33, 39, 45, 48, 54, 58, 72, 73, 74, 100
- [83] J. M. Manimala and C. Sun. Numerical investigation of amplitude-dependent dynamic response in acoustic metamaterials with nonlinear oscillators. *The Journal of the Acoustical Society of America*, 139(6):3365–3372, 2016. → pages 8
- [84] A. J. Martínez, P. Kevrekidis, and M. A. Porter. Superdiffusive transport and energy localization in disordered granular crystals. *Physical Review E*, 93:022902, 2016. → pages 10
- [85] A. J. Martínez, H. Yasuda, E. Kim, P. Kevrekidis, M. A. Porter, and J. Yang. Scattering of waves by impurities in precompressed granular chains. *Physical Review E*, 93(5):052224, 2016. → pages 10
- [86] J. Maynard. Wave propagation in arrays of scatterers. Tutorial: Part 2. *Acoustics Today*, 6(1):13–21, 2010. → pages 62
- [87] D. Mead. Wave propagation and natural modes in periodic systems: I. Mono-coupled systems. *Journal of Sound and Vibration*, 40(1):1 – 18, 1975. ISSN 0022-460X. → pages 25
- [88] D. Mead. Wave propagation and natural modes in periodic systems: II. Multi-coupled systems, with and without damping. *Journal of Sound and Vibration*, 40(1):19 – 39, 1975. ISSN 0022-460X. → pages 102
- [89] D. Mead. Waves and modes in finite beams: Application of the phase-closure principle. *Journal of Sound and Vibration*, 171(5):695–702, 1994. → pages 4
- [90] D. Mead. Wave propagation in continuous periodic structures: Research contributions from Southampton, 1964–1995. *Journal of Sound and Vibration*, 190(3):495–524, 1996. → pages 3

- [91] D. Mead and S. Lee. Receptance methods and the dynamics of disordered one-dimensional lattices. *Journal of Sound and Vibration*, 92(3):427–445, 1984. → pages 65
- [92] E. W. Montroll and R. B. Potts. Effect of defects on lattice vibrations. *Physical Review*, 100(2):525, 1955. → pages 4
- [93] F. Moon and P. J. Holmes. A magnetoelastic strange attractor. *Journal of Sound and Vibration*, 65(2):275–296, 1979. → pages 13
- [94] M. Mulansky and A. Pikovsky. Energy spreading in strongly nonlinear disordered lattices. *New Journal of Physics*, 15(5):053015, 2013. → pages 10
- [95] A. Naess and T. Moan. *Stochastic Dynamics of Marine Structures*. Cambridge University Press, U.S.A., 2012. → pages 5
- [96] R. Narisetti, M. Ruzzene, and M. Leamy. A perturbation approach for analyzing dispersion and group velocities in two-dimensional nonlinear periodic lattices. *Journal of Vibration and Acoustics*, 133(6):061020, 2011. → pages 8
- [97] R. K. Narisetti, M. J. Leamy, and M. Ruzzene. A perturbation approach for predicting wave propagation in one-dimensional nonlinear periodic structures. *Journal of Vibration and Acoustics*, 132(3):031001, 2010. → pages 8, 26
- [98] A. H. Nayfeh. *Nonlinear Interactions*. Wiley, U.S.A., 2000. → pages 8, 99
- [99] A. H. Nayfeh and D. T. Mook. *Nonlinear Oscillations*. John Wiley & Sons, U.S.A., 1979. → pages 37, 38
- [100] J. Noël and G. Kerschen. Nonlinear system identification in structural dynamics: 10 more years of progress. *Mechanical Systems and Signal Processing*, 2016. → pages 99
- [101] A. N. Norris. Acoustic cloaking. *Acoustics Today*, 11(1):38–46, 2015. → pages 2
- [102] B. J. Olson, S. W. Shaw, C. Shi, C. Pierre, and R. G. Parker. Circulant matrices and their application to vibration analysis. *Applied Mechanics Reviews*, 66(4):040803, 2014. → pages 3

- [103] Z. Peng, Z. Lang, F. Chu, and G. Meng. Locating nonlinear components in periodic structures using nonlinear effects. *Structural Health Monitoring*, 9(5):401–411, 2010. → pages 10
- [104] Y. Pennec, J. O. Vasseur, B. Djafari-Rouhani, L. Dobrzyński, and P. A. Deymier. Two-dimensional phononic crystals: Examples and applications. *Surface Science Reports*, 65(8):229–291, 2010. → pages 2
- [105] A. S. Phani and M. I. Hussein. Analysis of damped Bloch waves by the Rayleigh perturbation method. *Journal of Vibration and Acoustics*, 135(4):041014, 2013. → pages 4
- [106] A. S. Phani and J. Woodhouse. Viscous damping identification in linear vibration. *Journal of Sound and Vibration*, 303(3):475–500, 2007. → pages 62
- [107] A. S. Phani and J. Woodhouse. Experimental identification of viscous damping in linear vibration. *Journal of Sound and Vibration*, 319(3):832–849, 2009. → pages 62, 99
- [108] C. Pierre. Weak and strong vibration localization in disordered structures: A statistical investigation. *Journal of Sound and Vibration*, 139(1):111–132, 1990. → pages 62, 63, 65, 101
- [109] L. Ponson, N. Boechler, Y. M. Lai, M. A. Porter, P. Kevrekidis, and C. Daraio. Nonlinear waves in disordered diatomic granular chains. *Physical Review E*, 82(2):021301, 2010. → pages 10
- [110] M. A. Porter, P. G. Kevrekidis, and C. Daraio. Granular crystals. *Physics Today*, 68(11):44–50, 2015. → pages 7, 99
- [111] L. Rayleigh. On the maintenance of vibrations by forces of double frequency, and on the propagation of waves through a medium endowed with a periodic structure. *Philosophical Magazine*, 24(147):145–159, 1887. → pages 3
- [112] M. Remoissenet. *Waves Called Solitons: Concepts and Experiments*. Springer Science & Business Media, Germany, 2003. → pages 6
- [113] J. F. Rhoads, S. W. Shaw, and K. L. Turner. Nonlinear dynamics and its applications in micro- and nanoresonators. *Journal of Dynamic Systems, Measurement, and Control*, 132(3):034001, 2010. → pages 5

- [114] O. Richoux, C. Depollier, and J. Hardy. Propagation of mechanical waves in a one-dimensional nonlinear disordered lattice. *Physical Review E*, 73(2):026611, 2006. → pages 11
- [115] V. Rothos and A. Vakakis. Dynamic interactions of traveling waves propagating in a linear chain with an local essentially nonlinear attachment. *Wave Motion*, 46(3):174–188, 2009. → pages 9
- [116] M. Sato, B. Hubbard, and A. Sievers. Colloquium: Nonlinear energy localization and its manipulation in micromechanical oscillator arrays. *Reviews of Modern Physics*, 78(1):137, 2006. → pages 5, 6, 7, 17
- [117] M. Sayar, M. Demirel, and A. Atilgan. Dynamics of disordered structures: Effect of non-linearity on the localization. *Journal of Sound and Vibration*, 205(3):372–379, 1997. → pages 10
- [118] T. A. Schaedler, A. J. Jacobsen, A. Torrents, A. E. Sorensen, J. Lian, J. R. Greer, L. Valdevit, and W. B. Carter. Ultralight metallic microlattices. *Science*, 334(6058):962–965, 2011. → pages 1
- [119] G. Sen Gupta. Natural flexural waves and the normal modes of periodically-supported beams and plates. *Journal of Sound and Vibration*, 13(1):89–101, 1970. → pages 4, 25
- [120] C. A. Steeves, S. L. d. S. e Lucato, M. He, E. Antinucci, J. W. Hutchinson, and A. G. Evans. Concepts for structurally robust materials that combine low thermal expansion with high stiffness. *Journal of the Mechanics and Physics of Solids*, 55(9):1803–1822, 2007. → pages 1
- [121] J. J. Stoker. *Nonlinear Vibrations in Mechanical and Electrical Systems*. Wiley, New York, 1950. → pages 37
- [122] H. Susanto. Boundary driven waveguide arrays: Supratransmission and saddle-node bifurcation. *SIAM Journal on Applied Mathematics*, 69(1):111–125, 2008. → pages 8, 9, 45
- [123] R. B. Thakur, L. English, and A. Sievers. Driven intrinsic localized modes in a coupled pendulum array. *Journal of Physics D: Applied Physics*, 41(1):015503, 2007. → pages 7
- [124] M. Thota, R. Harne, and K. Wang. Harnessing intrinsic localized modes to identify impurities in nonlinear periodic systems. *Journal of Applied Physics*, 117(7):074505, 2015. → pages 7

- [125] S. Tietsche and A. Pikovsky. Chaotic destruction of Anderson localization in a nonlinear lattice. *Europhysics Letters*, 84(1):10006, 2008. → pages 11, 12
- [126] A. Vakakis, M. King, and A. Pearlstein. Forced localization in a periodic chain of non-linear oscillators. *International Journal of Non-Linear Mechanics*, 29(3):429–447, 1994. → pages 39
- [127] A. F. Vakakis. Relaxation oscillations, subharmonic orbits and chaos in the dynamics of a linear lattice with a local essentially nonlinear attachment. *Nonlinear Dynamics*, 61(3):443–463, 2010. → pages 9
- [128] A. F. Vakakis and M. E. King. Nonlinear wave transmission in a monocoupled elastic periodic system. *The Journal of the Acoustical Society of America*, 98(3):1534–1546, 1995. → pages 8, 26, 36
- [129] L. N. Virgin. *Vibration of Axially-Loaded Structures*. Cambridge University Press, 2007. → pages 5
- [130] H. N. Wadley. Multifunctional periodic cellular metals. *Philosophical Transactions of the Royal Society of London A: Mathematical, Physical and Engineering Sciences*, 364(1838):31–68, 2006. → pages 1
- [131] C. Yilmaz, G. Hulbert, and N. Kikuchi. Phononic band gaps induced by inertial amplification in periodic media. *Physical Review B*, 76(5):054309, 2007. → pages 2
- [132] B. Yousefzadeh and A. S. Phani. Nonlinear energy transmission in a finite dissipative periodic structure. In *International Symposium on Optomechatronic Technologies*, pages 7–11, Seattle, WA, 2014. IEEE. → pages iv
- [133] B. Yousefzadeh and A. S. Phani. Energy transmission in finite nonlinear periodic structures from excitations within the stop band. *Journal of Sound and Vibration*, 354:180–195, 2015. → pages iv
- [134] B. Yousefzadeh and A. S. Phani. Supratransmission in a disordered nonlinear periodic structure. *Journal of Sound and Vibration*, 380:242–266, 2016. → pages iv

## Appendix A

# Numerical Continuation

Numerical continuation is a computational technique that makes it possible to follow the evolution of the solutions of systems of ordinary differential equations as a function of a system parameter. This approach was used throughout the thesis for studying the evolution of the steady state solutions of the structures as a functions of forcing amplitude or forcing frequency. In this chapter, we present a very brief overview of the basic formulation for numerical continuation of periodic orbits. For comprehensive explanations of numerical continuation techniques, refer to [6, 69].

Our first task is to set up the governing equations that are second-order in time as a set of first-order autonomous dynamical system. The first-order formulation may be obtained by writing the equations of motion in the state space, with displacements and velocities as the states. The conversion from a non-autonomous system to an autonomous one (i.e. removing the explicit dependence on time on the right-hand side of the state-space equations) is commonly done by either of two methods: (i) introducing time as an additional state, (ii) replacing the time-dependent (harmonic) forcing term with an autonomous system that has a stable limit cycle and coupling this to the original system. The first method adds one extra degree of freedom to the dynamical system, while the second approach adds two extra degrees of freedom.

Following this procedure, the governing equations take the following form:

$$\dot{x}(t) = f(x(t), \alpha) \quad (\text{A.1})$$

where the vector  $x(t)$  contains all the states. The scalar parameter  $\alpha$  represents the continuation parameter, which could be the forcing amplitude, for example.

We are seeking solutions of (A.1) that are periodic in time with period  $T$ . Because  $T$  is not a known parameter a priori (and would normally vary with  $\alpha$ ), we rescale time as  $t \rightarrow t/T$  so that the interval of periodicity is fixed to unity. With this, the governing equations transform to the following:

$$\dot{x}(t) = Tf(x(t), \alpha) \quad (\text{A.2})$$

in the rescaled time variable.

To continue the (steady-state) periodic solutions, we will transform the initial-value problem in (A.2) to a boundary-value problem. The boundary conditions for this problem is the periodicity condition in the time domain, which can be written as follows:

$$x(0) = x(1) \quad (\text{A.3})$$

Recall that we have rescaled time such that the interval of periodicity in (A.2) is unity.

Given that we are looking for periodic solutions of an autonomous system, we also need to impose a phase condition on  $x$  to ensure uniqueness of the solutions. Without ensuring the uniqueness of solution, any arbitrary shift in a periodic solution would give the same periodic solution. There are various phase conditions that can be used. For example, we can specify zero velocity for one of the units. The advantage of this phase condition is that it is realistic from a physical point of view and realizable in experiments.

Thus, numerical continuation of the periodic orbits of the equations of motion transforms to solving the boundary-value problem defined in (A.2) and (A.3), subject to a phase condition to ensure uniqueness of solutions.

When using numerical continuation, we need to start with a known solution of the system. At each continuation step  $k$ , we are seeking the solution  $(x_k, T_k, \alpha_k)$

based on the known solution at the previous step,  $(x_{k-1}, T_{k-1}, \alpha_{k-1})$ . Also, the solutions along a periodic branch need to be suitably discretized. This aspect of continuation can be readily dealt with through available software packages such as AUTO [26], Matcont [41] and COCO [21]. We have used AUTO for numerical continuation computations in this thesis, which uses the orthogonal collocation method.

## Appendix B

# Derivations

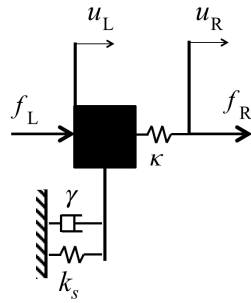
### B.1 Derivation of the Transfer Matrix Formulation

Figure B.1 shows a schematic of a unit cell. The unit cell consists of a unit mass, a coupling spring ( $k_c$ ), a grounding spring ( $k_s$ ), and a damper ( $2\zeta$ ). Force equilibrium at the left and right ends of the  $n$ -th unit, respectively, give the following relations

$$\sigma_n u_L^{(n)} + k_c(u_L^{(n)} - u_R^{(n)}) = f_L^{(n)} \quad (\text{B.1a})$$

$$k_c(u_R^{(n)} - u_L^{(n)}) = f_R^{(n)} \quad (\text{B.1b})$$

where  $\sigma_n$  is defined in (4.10). From compatibility and force equilibrium between



**Figure B.1:** The schematic of a unit cell. We have  $k_s = \omega_n^2$  for linear units, while  $k_s = \omega_n^2 + 3/4k_3|u_L^{(n)}|^2$  for nonlinear units.

adjacent units we have

$$u_L^{(n+1)} = u_R^{(n)} \quad (\text{B.2a})$$

$$f_L^{(n+1)} = -f_R^{(n)} \quad (\text{B.2b})$$

We can rearrange (B.1) to have the ‘left’ variables in terms of the ‘right’ variables. Then, using (B.2), we have

$$u_R^{(n)} = (1 + \sigma_n/k_c)u_R^{(n-1)} + f_R^{(n-1)}/k_c \quad (\text{B.3a})$$

$$f_R^{(n)} = \sigma_n u_R^{(n-1)} + f_R^{(n-1)} \quad (\text{B.3b})$$

which gives the transfer matrix in (4.9).

## B.2 Derivation of the Onset of Supratransmission

Applying Newton’s second law to the right and left nodes of the nonlinear unit at  $n = 1$ , respectively, results in the following equations

$$f_R^{(1)} = k_c(u_R^{(1)} - u_L^{(1)}) \quad (\text{B.4a})$$

$$f_L^{(1)} = (\sigma_1 + \beta)u_L^{(1)} + k_c(u_L^{(1)} - u_R^{(1)}) \quad (\text{B.4b})$$

where we have defined

$$\beta = \beta(u_L) \equiv 3/4 k_3 |u_L|^2 \quad (\text{B.5})$$

We rearrange the terms to get

$$u_R^{(1)} = (1 + (\sigma_1 + \beta)/k_c)u_L^{(1)} - f_L^{(1)}/k_c \quad (\text{B.6a})$$

$$f_R^{(1)} = (\sigma_1 + \beta)u_L^{(1)} - f_L^{(1)} \quad (\text{B.6b})$$

using (B.6) in combination with (4.11), we can relate the response on the right of  $n = N$  to the response on the left of  $n = 1$ . The external force applied to the structure corresponds to  $f_L^{(1)} = F$  and, without loss of generality, we take  $F$  to be real-valued. To enforce the free boundary on the right end of the structure we require  $f_R^{(N)} = 0$ . This, after substituting  $u_R^{(1)}$  and  $f_R^{(1)}$  from (B.6) into (4.11), results

in the following

$$(T_{21}(1 + (\sigma + \beta)/k_c) + T_{22}(\sigma + \beta))u_L^{(1)} = (T_{21}/k_c + T_{22})f_L^{(1)} \quad (\text{B.7})$$

which can be used to find the onset of transmission for the semi-linear system.

Setting

$$\rho \equiv |u_L^{(1)}|^2 \quad (\text{B.8})$$

we can obtain the following cubic equation for  $\rho$

$$a_3\rho^3 + a_2\rho^2 + a_1\rho + a_0 = 0 \quad (\text{B.9})$$

where

$$a_3 = (9/16)k_3^2 |T_{21}/k_c + T_{22}|^2 > 0 \quad (\text{B.10a})$$

$$a_2 = (3/2)k_3 \text{Re}\{(T_{21}/k_c + T_{22})^\dagger (\sigma(T_{21}/k_c + T_{22}) + T_{21})\} \quad (\text{B.10b})$$

$$a_1 = |(1 + \sigma/k_c)T_{21} + T_{22}|^2 \quad (\text{B.10c})$$

$$a_0 = -F^2 |T_{21}/k_c + T_{22}|^2 < 0 \quad (\text{B.10d})$$

Here, the superscript  $\dagger$  denotes complex conjugate.

Equation (B.9) is a cubic polynomial with real coefficients and, depending on the relation between its coefficients, may have three real roots or only one. The onset of transmission is where there are three real roots with two of them being equal (i.e. multiple real roots). Such points correspond to saddle-node bifurcations of the Duffing equation [50]. We first re-write (B.9) as follows

$$\rho^3 + c_2\rho^2 + c_1\rho + c_0 = 0 \quad (\text{B.11})$$

Now we restrict the coefficients of (B.11) such that it has at least two equal real roots by setting [1]

$$c_0 = -2 \left( p \pm \sqrt{q^3} \right) \quad (\text{B.12})$$

where

$$p = c_2^3/27 - c_1c_2/6 \quad (\text{B.13a})$$

$$q = c_2^2/9 - c_1/3 \quad (\text{B.13b})$$

Using  $c_0 = -(4F/3k_3)^2$ , the critical forcing amplitude at the onset of threshold,  $F_{th}$ , can be written as shown in (4.12).

In the above analysis, we assumed the structure to have free boundaries at both ends. A very similar formulation applies if the boundary on either end of structure is fixed. In this case, the formula in (4.12) remains valid but the coefficients  $a_n$  in (B.10) need to be updated. For a fixed boundary on the driven end of the structure (left side), we have  $f_L^{(1)} = F - k_c u_L^{(1)}$ . To model a fixed boundary on the right end of the structure, the free boundary condition  $f_R^{(N)} = 0$  should be replaced with  $u_R^{(N)} = 0$ .